DISS. ETH NO. 22204

IN VIVO IMAGING OF HYPOXIA SIGNALING PATHWAY IN A GLIOBLASTOMA MOUSE MODEL

A thesis submitted to attain the degree of

DOCTOR OF SCIENCES of ETH ZURICH
(Dr. sc. ETH Zurich)

presented by

SANDRA BÜRGI MONTEMAYOR TREVIÑO

Master of Science UZH in Biologie Humanbiologie,
Universität Zürich

born on *04.04.1983*
citizen of Gachnang, Switzerland

accepted on the recommendation of

Prof. Dr. Markus Rudin, examiner
Prof Dr. Michael Weller, co-examiner
Prof. Dr. Wilhelm Krek, co-examiner

2014

THE FIRST PRINCIPLE IS THAT YOU MUST NOT FOOL YOURSELF - AND YOU ARE THE EASIEST PERSON TO FOOL. SO YOU HAVE TO BE VERY CAREFUL ABOUT THAT. AFTER YOU'VE NOT FOOLED YOURSELF, IT'S EASY NOT TO FOOL OTHER SCIENTISTS. YOU JUST HAVE TO BE HONEST IN A CONVENTIONAL WAY AFTER THAT.

Richard P. Feynman

SUMMARY ..... **III**
ZUSAMMENFASSUNG ..... **VI**
ABBREVIATIONS ..... **IX**
1 INTRODUCTION **1**
1.1 MALIGNANT GLIOMAS 2
1.1.1 The four prognostic grades of glioma tumors *3*
1.1.2 Characteristics of glioblastoma *3*
1.1.3 Diagnosis and treatment *6*
1.1.4 Brain tumor animal model *9*
1.1.5 Glioblastoma cell lines *11*
1.2 HYPOXIA AND HIF PATHWAY IN TUMOR 12
1.2.1 HIF and tumor angiogenesis *17*
1.2.2 HIF and glycolytic energy metabolism *20*
1.2.3 HIF and pH homeostasis *21*
1.2.4 HIF and metastasis *22*
1.2.5 HIF and cell death and survival *22*
1.2.6 Oxygen independent HIF regulation *27*
1.2.7 Therapy approaches targeting HIF pathway *29*
1.3 NON-INVASIVE METHODS FOR STRUCTURAL, FUNCTIONAL AND MOLECULAR IMAGING 30
1.3.1 Magnetic resonance imaging *30*
1.3.2 PET imaging *33*
1.3.3 Non-invasive optical imaging *34*
1.4 AIM OF THE PRESENT STUDY 40
2 MATERIALS AND METHODS **42**
2.1 CELLS 42
2.2 PRODUCTION OF STABLY TRANSFECTED CELL LINES 42
2.3 LUCIFERASE ACTIVITY ASSAY 43
2.4 PROLIFERATION ASSAY 44
2.5 IMMUNOBLOT ASSAY 44
2.6 MOUSE MODEL AND GLIOBLASTOMA CELL IMPLANTATION 45
2.7 *IN VIVO* BIOLUMINESCENCE IMAGING 46
2.8 MAGNETIC RESONANCE IMAGING 46
2.9 TUMOR VOLUME DETERMINATION 47
2.10 IMMUNOFLUORESCENCE ON TISSUE SECTIONS 47
2.11 STATISTICAL ANALYSIS 48

3 RESULTS 49

3.1 ENDOGENOUS HIF REGULATION IN THE THREE TESTED GLIOBLASTOMA CELL LINES 49

3.2 HIF REGULATION BEHAVIOR OF TRANSFECTED GLIOBLASTOMA CELL LINES *IN VITRO* 50

3.3 PROLIFERATION ASSAY *IN VITRO* 53

3.4 EVALUATION OF THE HIF PATHWAY REGULATION *IN VIVO* FOR THREE TRANSFECTED GLIOBLASTOMA CELL LINES 55

3.5 COMPARISON OF INTRATUMORAL PROTEIN EXPRESSION BY IMMUNOFLUORESCENCE ANALYSIS 63

4 DISCUSSION 68

4.1 LUCIFERASE REPORTER GENE ASSAY AS A GOOD METHOD TO INVESTIGATE THE HIF PATHWAY DURING TUMOR GROWTH 69

4.2 DIFFERENCES IN THE ESTABLISHMENT OF THE REPORTER GENE ASSAY BETWEEN THE GLIOMA CELL LINES *IN VITRO* 70

4.3 EVALUATION OF HIF SIGNALING IN TUMOR GROWTH PROGRESSION IN VIVO 72

4.4 *IN VIVO* HIF SIGNALING IN RELATION TO ITS *EX VIVO* ANALYSIS 75

4.5 COMPARISON BETWEEN DIFFERENT ANATOMICAL TUMOR LOCATIONS 79

4.6 OUTLOOK 80

4.7 CONCLUSION 82

5 REFERENCES 83

6 ACKNOWLEDGMENT 103

Summary

Glioblastomas are one of the most common primary brain tumors in adults. Statistically patients find themselves with a median life expectation of 12 to 15 months after diagnosis, even with standard treatment which consists of tumor surgical resection, radio- and chemotherapy. Two of the main hallmarks of glioblastomas are diffuse infiltrative growth and the formation of necrotic and hypoxic regions within the tumor mass. Intratumoral hypoxia is a common phenomenon of tumors and has been shown to be associated with tumor growth and its resistance to radio- and chemotherapy. This resistance originates in the decreased blood supply to hypoxic regions, which results in reduced delivery of the chemotherapeutic agents and oxygen, both of which are required for efficient therapy. It is therefore of high interest to enhance the understanding of hypoxia triggered processes, in particular signaling induced by the nuclear transcription factor HIF (hypoxia inducible factor).

The objective of this thesis was to investigate the HIF pathway regulation in relation to the tumor growth in glioblastomas using a non-invasive longitudinal imaging approach. HIF activity was assessed by means of a reporter gene assay using the bioluminescent enzyme firefly luciferase (Luc). Three glioblastoma tumor cell lines (LN229, U87, and GL261) were stably transfected with a Luc construct under the control of a promoter comprising a hypoxia response element (HRE), which is induced in the presence of HIF. A constitutively expressed SV40-Luc construct was used as control. Luc oxidizes its substrate D-luciferin and thereby generates a bioluminescent signal. The *in vitro* bioluminescence evaluation showed an induction of the bioluminescent signal in HRE-Luc transfected cells upon mimicking hypoxic settings as compared to normoxia. In contrast, the bioluminescent signal was not different for the two conditions in SV40-luc transfected control cells. An *in vitro* proliferation assay was performed to test the growth behavior of the transfected cells in comparison to the native cells. No difference in proliferation was observed for LN229 cells, while there was a difference for U87 and GL261 cells.

To evaluate hypoxia signaling under *in vivo* conditions, studies were performed for all three cell lines with tumor cells injected subcutaneously into the flank of nude mice. Tumor volume and the emitted bioluminescent signal were monitored at regular intervals during cancer growth. While LN229 and U87 tumors developed measurable tumor masses *in vivo*, GL261 tumors showed a robust growth behavior. The normalized

bioluminescence signal of GL261/HRE-Luc tumors indicated a significant transient induction of the reporter enzyme with a maximum at day 14 after implantation followed by a signal decrease toward the end of the experiment. In contrast, the control tumor GL261/SV40-Luc showed a stable bioluminescent signal output throughout the course of the experiment. This suggests a transient induction of the HIF signaling during tumor development. In comparison to the subcutaneous tumors, GL261 tumors orthotopically implanted into the mouse striatum showed a weaker induction of the GL261/HRE-Luc construct indicative of a lesser degree of hypoxia.

Histological *ex vivo* analysis of the isolated tumor tissue revealed large hypoxic as well as necrotic areas in subcutaneous GL261 tumors and only weak patchy hypoxic areas in 50% of the analyzed orthotopic tumors. The observed transient bioluminescence signal induction in subcutaneous GL261/HRE-Luc tumors decreasing toward the end of the experiment despite persistent high levels of hypoxia might be explained either by a HIF induced feedback mechanism or by the effect of the increasing necrosis toward the end of the experiment. The histological analysis of the HIF downstream products demonstrated that GLUT1 and CA9 were largely colocalized in hypoxic regions in subcutaneous tumors whereas in orthotopic tumors they were expressed in non-hypoxic tumor areas as well, suggesting that non-hypoxia dependent factors might contribute to HIF regulation in orthotopic brain tumors. For example processes reducing the availability of cofactors required for proteasomal HIF degradation would induce HIF activity even under normoxic conditions.

In conclusion the studies conducted during this thesis have shown that HIF regulation during glioblastoma tumor development can be monitored in a longitudinal manner using a luciferase reporter gene readout, that HIF signaling is transiently induced in subcutaneous and to a lesser extent in orthotopic GL261 tumors, and that there are significant differences in hypoxia and hypoxia signaling between the two implantation sites. Orthotopic tumors were found to be less hypoxic, probably due to their embedding in a heavily vascularized host region, and showed evidence of non-hypoxic activation of HIF signaling. While reporter gene based imaging assays are valuable tools for experimental studies to reveal detailed insights in biological processes in living organisms, they cannot be translated into the clinics. Translatable imaging approaches would rather use exogenous probes for HIF downstream targets using reporter systems compatible with fluorescence imaging, MRI or PET. In addition to this

it would be of high interest for future studies to target the HIF pathway in relation to the tumor microenvironment and to study the tumor-host interaction thereby.

Zusammenfassung

Glioblastomen gehören zu den häufigsten primären Hirntumoren bei Erwachsenen. Nach der Diagnose haben diese Patienten eine statistische Lebenserwartung von 12 bis 15 Monaten, auch mit Therapie. Die Standardtherapie beinhaltet die chirurgische Entfernung der Tumormasse, gefolgt von Strahlen- und Chemotherapie. Zwei Hauptmerkmale von Glioblastomen sind ein diffus infiltrierendes Wachstumsverhalten und die Bildung von nektrotischen und hypoxischen Regionen im Tumorgewebe. Intratumorale Hypoxie ist ein ausgeprägtes Phänomen bei Tumoren und es wurde gezeigt, dass es mit der Tumorentwicklung und der Resistenz zu Strahlen- und Chemotherapie assoziiert ist. Diese Therapieresistenz ist zurückzuführen auf einer verminderten Durchblutung in hypoxischen Regionen, was zu einer reduzierten Lieferung von Chemotherapiemitteln und zu einem vermindertem Sauerstoffgehalt führt. Diese sind jedoch für die Effizienz der Behandlung unerlässlich. Daher besteht ein grosses Interesse, das Verständnis des Hypoxie-induzierten Prozesses in Glioblastomen zu verbessern, insbesondere den Signalweg, der durch den nukleären Faktor HIF (Hypoxie-induzierter Faktor) reguliert wird.

Diese Doktorarbeit wurde mit dem Ziel durchgeführt, die Regulation des HIF Signalweges im Zusammenhang mit dem Tumorwachstumsprozess in Glioblastomen mit Hilfe eines nicht-invasiven, zeitlich verlaufenden *Imaging* Verfahrens zu untersuchen. Um die HIF Aktivität zu messen wurde ein Reporter Gene Ansatz mit dem biolumineszenten Enzym Firefly Luciferase (Luc) verwendet. Dafür wurden drei Glioblastoma Zelllinien (LN229, U87 und GL261) mit einem Luciferase Konstrukt stabil transfiziert, das unter der Kontrolle des HIF regulierten Motifes *Hypoxia response element* (HRE) aktiviert wird, und einem ständig aktiviertem SV40-Luciferase Konstrukt als Kontrolle. Luc oxidiert sein Substrate D-Luciferin und generiert dabei ein biolumineszentes Signal. Die *in vitro* Biolumineszenz Untersuchung zeigte für die HRE-Luc transfizierten Zellen einen Anstieg des Biolumineszenzsignals unter simulierten hypoxischen Bedingungen im Vergleich zu normoxischen Bedingungen. Im Gegensatz dazu war das Biolumineszenzsignal in SV40-Luc transfizierten Kontrollzellen gleichbleibend zwischen diesen beiden Bedingungen. Ein *in vitro* Proliferations-Test wurde durchgeführt um das Wachstumsverhalten der transfizierten mit den ursprünglichen Zellen zu vergleichen. Zwischen den transfizierten und untransfizierten

LN229 Zellen konnte kein Unterschied in der Proliferation gemessen werden. Ein Unterschied wurde allerdings bei den U87 und GL261 Zellen gemessen.

Um den Hypoxie Signalweg unter *in vivo* Bedingungen zu untersuchen wurden Experimente mit allen drei Zelllinien durchgeführt. Dafür wurden die Zellen subkutan in die Flanken von Nacktmäusen injiziert. Das Tumorvolumen und das von den Tumoren abgestrahlte Biolumineszenzsignal wurde in regelmässigen Intervallen im Laufe des Tumorwachstums gemessen. Während wir bei den LN229 und U87 Tumoren *in vivo* eine messbare Tumormasse feststellen, zeigten die GL261 Tumore ein solides Wachstumsverhalten. Das normalisierte Biolumineszenzsignal der GL261/HRE-Luc Tumore zeigte einen signifikanten vorübergehenden Anstieg des Reporter Enzyms, mit einem Maximum am Tag 14 nach der Implantation. Danach folgte ein Rückgang bis zum Ende des Experimentes. Die Kontrolltumore GL261/SV40-Luc zeigten dagegen eine stabil bleibende Signalproduktion im Verlauf des Experimentes. Das deutet auf eine transiente Aktivierung des HIF Signalweges während der Tumorentwicklung hin. Bei den orthotop implantierten GL261 Tumoren in das Striatum der Maus, zeigten die GL261/HRE-Luc Tumore einen schwächeren Anstieg verglichen mit den subkutanen Tumoren, was auf ein geringeres Mass an Hypoxie hinweist.

Die histologische *ex vivo* Analyse des isolierten Tumorgewebes zeigte grosse hypoxische, als auch nekrotische Regionen in subkutanen GL261 Tumoren und nur schwache fleckenhafte hypoxische Regionen in 50% der orthotopischen Tumoren. Der transiente Anstieg des Biolumineszenzsignals in subkutanen GL261/HRE-Luc Tumoren mit einer Reduktion gegen Ende des Experimentes trotz anhaltend hohem Grad an Hypoxie, könnte mit einem HIF-induzierten Feedback Mechanismus oder dem Einfluss der angestiegenen Nekrose gegen Ende des Experimentes erklärt werden. Die histologische Analyse der von HIF kontrollierten Proteinen zeigte, dass GLUT1 und CA9 weitgehend mit hypoxischen Regionen in subkutanen Tumoren kolokalisiert sind, während sie in orthotopen Tumoren auch in nicht-hypoxischen Regionen exprimiert wurden. Das deutet darauf hin, dass die HIF Regulation in orthotopen Tumoren noch zusätzlich von Hypoxie unabhängigen Faktoren aktiviert wird. Zum Beispiel würde die HIF Aktivität auch unter normoxischen Bedingungen gesteigert werden durch Prozesse, welche die Verfügbarkeit von Kofaktoren reduzieren, die für den proteasomalen Abbau von HIF benötigt werden.

Zusammenfassend haben die Experimente dieser Doktorarbeit gezeigt, dass die HIF Regulation während der Glioblastoma Tumorentwicklung mit Hilfe eines zeitlich verlaufenden Ansatz kombiniert mit einer Luciferase Reporter Gen Messung untersucht werden kann. Wir zeigten einen vorübergehenden Anstieg des HIF Signalweges in subkutanen und zu einem geringeren Masse in orthotopischen GL261 Tumoren. Weiter konnten wir signifikante Unterschiede in der Hypoxie und dem Hypoxie Signalweg zwischen den zwei Implantationsstellen zeigen. Die orthotopen Tumore waren weniger hypoxisch, möglicherweise begründet durch ihre Einbettung in eine stark vaskularisierte Region. Zudem deuteten die orthotopen Tumore auf Hypoxie-unabhängige Aktivierung des HIF Signalweges hin. Während diese Reporter Gen basierenden Ansätze eine nützliche Technologie für experimentelle Studien darstellen, die einen detaillierten Einblick in die biologischen Prozesse von lebenden Organismen ermöglichen, können sie jedoch nicht in klinischen Studien übertragen werden. Übertragbare *Imaging* Verfahren könnten eher exogene Proben für HIF Zielgene verwenden die mit fluoreszierender *Imaging* Proben, MRI oder PET kompatibel sind. Zusätzlich wäre es von grossem Interesse für zukünftige Studien, den HIF Signalweg im Zusammenhang mit der Tumor-Mikroumgebung Interaktion zu analysieren.

Abbreviations

AKT:	protein kinase B
Ang:	angiopoietin
ARNT:	aryl hydrocarbon receptor nuclear translocator
ATP:	adenosine triphosphate
BBB:	blood brain barrier
BCL2:	B-cell lymphoma 2
bHLH:	basic-helix-loop-helix
BNIP3:	Bcl-2/adenovirus E1B 19-kDa interacting protein 3
BNIP3L:	Bcl-2/adenovirus E1B 19-kDa interacting protein 3 like
CA9:	carbonic anhydrase 9
CBP:	CREB binding protein
CT:	computed tomography
C-TAD:	C-terminal transactivation domain
CXCR4:	C-X-C chemokine receptor 4
DMOG:	dimethyloxalylglycine
DMSO:	dimethyl sulfoxide
EGFR:	epidermal growth factor receptor
FIH:	factor inhibiting HIF
FITC:	fluorescein isothiocyanate
GFAP:	glial fibrillary acidic protein
GLUT:	glucose transporter
HBSS:	Hanks balanced salt solution
HIF:	hypoxia inducible factor
HRE:	hypoxia responsive element
LDH-A:	lactate dehydrogenase a
LOH:	loss of heterozygosity
Luc:	luciferase
MDM2:	mouse double minute 2
MGMT:	O^6-methylguanine-DNA methyltransferase
MMP:	matrix metalloproteinases
MRI:	magnetic resonance imaging
MRS:	magnetic resonance spectroscopy
MSOT:	multi-spectral optoacoustic tomography
mTOR:	mammalian target of rapamycin
NAA:	*N*-acetylaspartate
N-TAD:	N-terminal transactivation domain
ODDD:	oxygen-dependent degradation domain
OXPHOS:	oxidative phosphorylation
PAS:	PER-ARNT-SIM
PBS:	phosphate buffered saline
PET:	positron emission tomography
PDK:	pyruvate dehydrogenase kinase
PHD:	prolyl hydroxylase domain protein
PI3K:	phosphatidylinositol-3-kinase
PTEN:	phosphatase and tensin homolog
ROS:	reactive oxygen species
SDF-1:	stromal cell-derived factor 1
TCA:	tricarboxylic acid
VEGF:	vascular endothelial growth factor
VHL:	von Hippel-Lindau protein

1 Introduction

8.2 million people worldwide died from cancer in 2012, as published by the World Health Organization (WHO) [1]. Cancer is already the main cause of death in high-income countries, and as developing nations continue their fast-paced economic development, cancer is expected to become the leading cause of death worldwide in the next decades [2]. In figures, cancer incidence is expected to increase by more than 75% in high HDI (Human Development Index) countries, and by more than 90% in low and middle HDI countries in the year 2030 [2]. These figures are far above the expected increment in world population by the UN, which is only of 9.5% (7 Billion in 2013, vs. 8.3 Billion in 2030).

In a single human cell many DNA damages take place every day as a result of reactive molecules that are produced by metabolic or hydrolytic mechanisms [4]. In general, these DNA damages are taken care of the intrinsic DNA repair machinery. However, it might happen that the repair mechanisms miss a damaged DNA site. In this case the damage can activate the programmed cell death (apoptosis) mechanism, which has the purpose of arresting the cell cycle and prepare the cell to die in ordinate manner. Failed apoptosis upon DNA damage may result in a tumor cell. This single cell may then proliferate leading to the formation of a tumor [3, 4]. Hanahan and Weinberg have proposed six main biological characteristics as hallmarks of cancer that are widely accepted [5]. These phenotypic hallmarks appear during the development of (human) tumors. The original six hallmarks are: (I) Sustained proliferative signaling allows tumor cells to chronically proliferate as a result of gene alterations, involving signaling pathways that normally positively induce the proliferation behavior. (II) Evasion of growth suppressors and thus the influence of the negative regulation of proliferation control mechanisms. Due to genetic alterations tumor suppressor genes lose the ability to stop the cell cycle progression via cell cycle arrests. (III) Resistance to cell death thereby preventing elimination of tumor cells upon stress signals. A mechanism of tumor cells to avoid apoptosis is by loss of function of tumor suppressor genes that are able to recognize DNA damages. (IV) Acquisition of replicative immortality is an important distinction from normal healthy cells. Telomere shortening dictates the residual time of replication in normal cells. To achieve immortality, cells have to circumvent the implications of telomere shortening. (V) The formation of a vascular system (angiogenesis) is necessary to ensure the supply of the increasing tumor mass

with nutrients and oxygen and the disposal of metabolic residues. Tumors induce angiogenesis by secretion of proangiogenic factors that trigger the development of vascular sprouts and ultimately new vessels from the host vascular bed. (VI) Invasion of the host tissue and the formation of distant metastasis allow tumors to expand their size into healthy tissue resulting in higher malignancy. This step is induced by genetic alterations in genes that are responsible for cell-to-cell and cell-to-extracellular matrix (ECM) adhesion. Recently this list of tumor hallmarks has been expanded by adding two characteristics: genomic instability and tumor-promoting inflammation, which enable tumorigenesis. Additionally two phenomenological hallmarks, the deregulating cellular energetic and the avoidance of immune destruction have been added as well [5]. Many of these phenotypic characteristics that differentiate tumor cells from normal cells such as angiogenesis, metabolic changes, or metastasis were triggered by the environment of the tumor cell and especially by the appearance of hypoxia as it is discussed in section 1.2 HIF pathways and hypoxia in tumors.

1.1 Malignant gliomas

Gliomas are primary brain tumors arising in the central nervous system from glial progenitor cells. These glial progenitor cells were found to be located in the subventricular zone, are multipotent, self-renewing and able to differentiate into astrocytes and oligodendrocytes [6]. However the mechanisms underlying development of gliomas are not yet completely understood. Gliomas often contain both astrocytes and oligodendrocytes. Genetic and cellular variations across gliomas are probably caused by secondary alterations within tumor subclones or may originate from multipotent tumor cells [6, 7]. It has been hypothesized that cancer stem cells could arise from normal stem cells or glial progenitor cells and that only these cancer stem cells have the potential to develop into a tumor. Human stem cells from the central nervous system have been shown to express CD133 (also known as prominin 1 which is used as (cancer) stem cell marker). Such multipotent self-renewing cells that express the cell-surface marker CD133 have been isolated from glioblastomas. In transplantation experiments it could be shown that as few as approximately 100 CD133+ glioblastoma cells were sufficient to establish a tumor, whereas injection of 50'000-100'000 CD133- glioblastoma cells failed to develop a tumor [3, 6, 8]. This illustrates the critical role of cancer stem cells for the development of the glioblastoma.

1.1.1 The four prognostic grades of glioma tumors

Malignant gliomas are both invasive and heterogeneous. The WHO classifies tumors of the central nervous system into four prognostic grades, each associated with a different degree of aggressiveness. This classification is based mainly on the histological characteristics. Grade I is characterized by low proliferative activity and a high chance to cure upon surgical resection (pilocytic astrocytoma). Grade II is characterized by low proliferative yet infiltrative potential. These tumors show a significant probability to progress toward higher tumor grades (diffuse astrocytoma and oligodendroglioma). Grade III is characterized by atypic cellular nuclei and increased mitotic activity (anaplastic astrocytoma and anaplastic oligodendroglioma). Finally grade IV is characterized by high malignancy, high proliferation activity, with a tendency of forming necrotic domains and a high likelihood of fatal outcome (glioblastoma). Glioblastomas can be divided into two subtypes: the primary glioblastoma that arises de novo and the secondary glioblastomas that originates from lower grade glioma forms (Fig. 1) [9, 10].

1.1.2 Characteristics of glioblastoma

The location of gliomas occurrence was analyzed in over 640 patient data sets and was shown to most frequently take place in the frontal lobe (~43%), followed by the temporal lobe (~28%), the parietal lobe (~25%), and the occipital lobe (~3%). Their anatomical location may influence both prognosis and treatment options [11, 12]. Primary glioblastomas are more often found in older patients in contrast to secondary glioblastomas that are more prominent in younger patients. The mean age of primary glioblastomas patients is reported from 50 to 62 years [13, 14]. What triggers the development of glioblastoma is not yet known. Besides the common risk factors for tumorigenesis such as exposure to chemical hazards, electromagnetic radiation or viral infection it has been only shown that the exposure to therapeutic x-radiation could be related to brain tumor occurrence [15, 16]. Furthermore, it has been shown that polymorphism of genes involved in waste removal, DNA repair and regulation of the cell cycle is related with the development of glioblastomas [10, 16]. Indeed genetic alterations are a hallmark of all kind of cancers including glioblastomas. In primary glioblastoma the following mutations are typically observed [7, 10, 13, 17]: activating mutations and amplification of the epidermal growth factor receptor (EGFR) resulting

in increased levels and activity of EGFR even in absence of its ligand; loss of heterozygosity (LOH) of chromosome 10q, which can influence PTEN (phosphatase and tensin homolog); mutation of the PTEN on chromosome 10 itself, which typically mostly results in loss of function and thereby in an increase of AKT (protein kinase B) activity; deletion in INK4A, which leads to inhibition of cell cycle arrest (and apoptosis) controlled by the $p16^{INK4A}$ and RB (retinoblastoma) pathway or the $p14^{ARF}$ and p53 tumor suppressor gene respectively; mutation and overexpression of phospatidylinositol-3-kinase (PI3K); and overexpression of vascular endothelial growth factor (VEGF) (Fig. 1).

Glioblastomas show an aggressive development indicated by fast proliferation and diffuse infiltration of surrounding healthy tissue [18]. Glioblastomas are among the most highly vascularized tumors in humans [19, 20]. At the beginning of the tumor growth glioblastoma cells often migrate along vascular vessels of the host tissue, a parasitic behavior called co-option. This process leads to a destabilization of the blood vessels resulting in degeneration and decreased perfusion, which in turn leads to local hypoxia and reduced nutrient supply so that tumor cells eventually die [21, 22]. Hypoxia, on the other hand triggers a signaling cascade that among other effects leads to the expression of growth factors that initiate and promote angiogenesis. VEGF is probably the best characterized angiogenesis promoting factor [21].

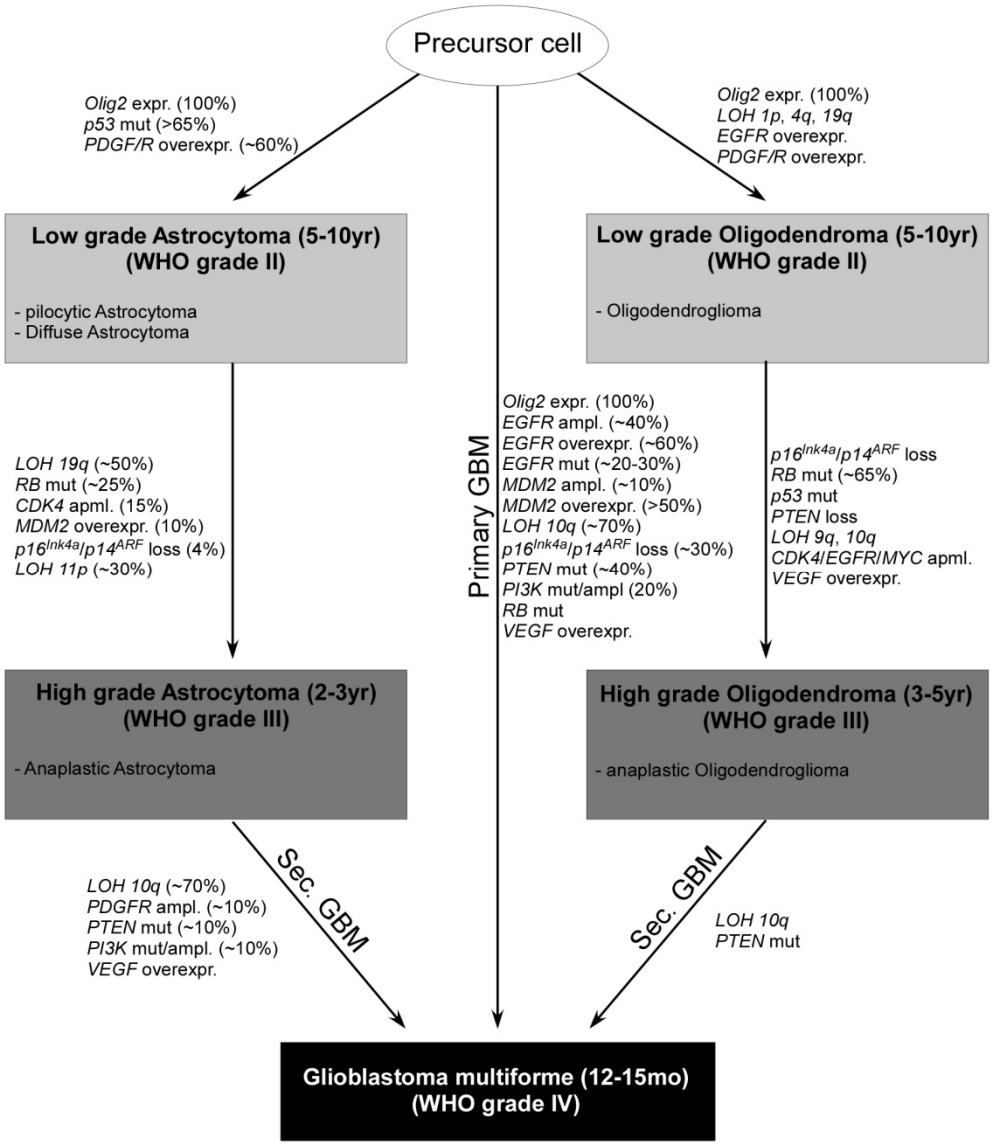

Figure 1. Possible genetic pathways in the development of malignant gliomas. Here are shown the genetic and chromosomal alterations that are involved in the development in primary glioblastomas or secondary glioblastomas over the process of astrocytomas and oligodendromas. Different kinds of gliomas are labeled with the corresponding prognostic grade according to the WHO and the median length of patients life span. Oligodendrocyte transcription factor 2 (Olig 2) is expressed in all gliomas and vascular endothelial growth factor (VEGF) is overexpressed in all high grade gliomas. EGFR stands for epidermal growth factor receptor, LOH for loss of heterozygosity, MDM2 for murine double minute 2, PDGF for platelet-derived growth factor, PDGFR for platelet-derived growth factor receptor, PI3K for phosphatidylinositol 3-kinase, PTEN for phosphatase and tensin homolog, RB for retinoblastoma, and CDK4 for cyclin dependent kinase 4. Adapted from Wen and Kesari 2008 [10] and Smith and Jenkins 2000 [23].

1.1.3 Diagnosis and treatment

Radiological diagnosis of brain tumors is based on magnetic resonance imaging (MRI) and X-ray computed tomography (CT), whereby the CT method might fail to detect structural lesions due to insufficient soft tissue contrast [24]. Today, MRI is the gold standard for diagnosis of malignant glioma and for monitoring treatment follow-up. T1- and T2-weighted MRI are used to determine the size and location of tumors with reference to the brain anatomy (Fig. 2). Furthermore, diffusion-weighted imaging (DWI) and diffusion-tensor imaging (DTI) may help in differentiating gliomas from brain metastasis and in classifying glioma tumor grade. These MRI methods assess the diffusibility of tissue water, which depends on the cellularity of tissue (extracellular versus intracellular volumes, cell membranes) and hence allows identifying proliferating structures [25]. Magnetic resonance spectroscopy (MRS) probes the chemical environment of hydrogen nuclei, which allows identifying the molecular species contributing to the signal, i.e. it yields a neuro/tumor-chemical profile. Due to limitations in sensitivity metabolites have to be in the millimolar concentration range to be reliable detected. The chemical specificity of MRS enables the differentiation of healthy tissue as well as viable and necrotic tumor tissue. The metabolite profile in gliomas shows high *N*-phosphocholine (choline) peaks as markers for membrane turnover, a low *N*-acetylaspartate (NAA) peak (marker for neuronal cellularity), elevated lactate signals as marker of high glycolytic activity and a high lipid peak [25]. MRI and MRS readouts may be complemented by positron-emission tomography (PET), which also provides metabolic information, in particular on glucose metabolism, but also offers the possibility of studying molecular events such as receptor expression on tumor cells [10, 27]. A major PET application is the measurement of glucose utilization using the substrate [^{18}F]-2-fluoro-2-deoxy-glucose [^{18}F]-FDG, a tracer that is transported across the blood brain barrier (BBB) via the glucose transporter 1 (GLUT1) into the brain tissue, phosphorylated by hexokinase and thereby trapped in the cells (Fig. 2). Due to the high glycolytic activity of high grade gliomas (Warburg effect [26]) these cells exert high FDG uptake [27]. Another interesting PET tracer is [^{18}F]-fluoromisonidazole ([^{18}F]-FMISO) that is trapped in hypoxic cells and thereby allows identifying hypoxic areas within the tumors (glioblastomas). This is relevant as it has been shown in clinical studies that the degree of hypoxia correlates positively with tumor development and resistance to radiotherapy [27].

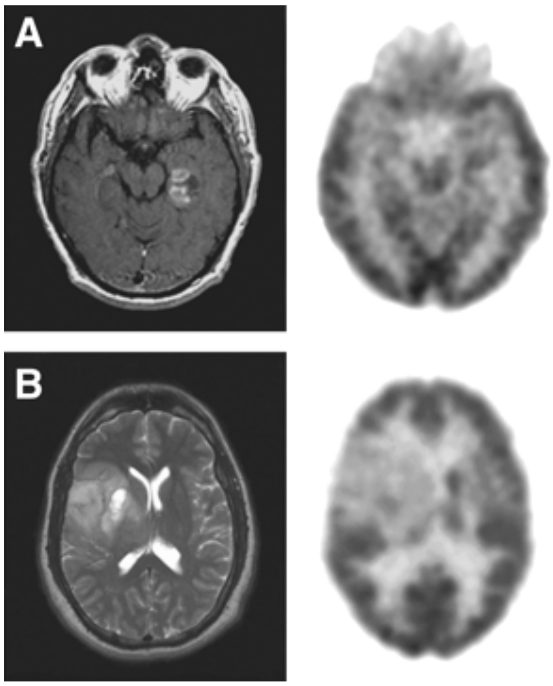

Figure 2. MRI (left) and ^{18}F-FDG-PET imaging (right) of newly diagnosed gliomas. A. glioblastoma, **B.** grade II Oligodendroglioma. Adapted from Chen et al. 2006 [28].

Patients with malignant gliomas show a variety of clinical symptoms, which depend on the location and size of the tumor, triggered among other reasons from the increasing pressure of the growing tumor mass impairing the function of normal brain tissue. Symptoms include headache, seizures, hemiparesis, impaired vision, aphasia, confusion, memory loss and personality changes (Table 1) [10, 24]. The average life span of a glioblastoma patient is 12 to 15 months following diagnosis [10].

Table 1. Percental incidence of symptoms of low grade and malignant gliomas. D'Angelo et al. 2003 [29].

Symptoms	Tumor Type	
	Low grade glioma	Malignant glioma
	percent with symptoms	
Headache	40	50
Seizure	65-95	15-25
Hemiparesis	5-15	30-50
Mental-status abnormalities	10	40-60

The standard therapy for glioblastoma is surgical resection if possible, followed by radio- and chemotherapy [10, 30]. Prognostic factors that are associated with a negative outcome are age, the degree of necrosis and the Karnofsky Performance Scale (KPS), which is a performance status indicating the patient's self-sufficiency and quality of life degrees. This index is used by physicians to evaluate the benefit of chemotherapy in patients with malignant tumors [31]. By far the most effective prolongation of the life span is achieved by surgical resection. Patients with a resection of 98% or more of the tumor mass showed an increase in their life span compared to patients with a resection below this value of the tumor mass [31]. Following surgical resection, radiotherapy is commonly applied. It has been shown that exposing the tissue to cumulated doses of radiation of 50 to 60 Gy (gray, is the unit for measuring ionizing radiation dosage, 1 Gy corresponding to the absorption of one Joule of energy in the form of ionizing radiation per kilogram of matter), typically split into 30 sessions of 2 Gy, resulted in a further increase of life span of glioblastoma patient as compared to surgical resection only [32]. The addition of chemotherapy to treatment remains controversial, because it led only to a slight increase in the life span of glioblastoma patients when combined with radiation therapy [33]. Improved beneficial effect of the chemotherapy using the agent temozolomide were observed in tumors characterized by a methylated MGMT (O^6-methylguanine-DNA methyltransferase) promoter [34]. MGMT is an important repair gene, which is responsible for genome stability by rectifying the methylated guanine residues in the DNA. Failure to repair these errors has been shown to lead to increased susceptibility to tumors upon exposure to alkylating (carcinogenic) chemicals in mice [35]. Tumors with silenced or impaired MGMT activity display reduced DNA repairing thus improving susceptibility to temozolomide treatment. Temozolomide, an alkylating chemotherapeutic agent works by creating deathly genomic errors through guanine residues alkylation. These differences were observed from up the ninth month of follow-up after treatment [34]. Therefore studies are focusing in a treatment combination of temozolomide with inhibitors of MGMT (e.g. O6-benzylguanine) or of other gene repair enzymes (e.g. poly-(ADP-ribose)-polymerase) [10]. Aside from surgery, radio- and chemotherapy are the current standard of care for glioblastomas [10, 30]. Unfortunately the latter two have the disadvantage of not reaching their full potential: on one side successful radiation therapy depends on oxygen which is scarce in the characteristical intratumoral hypoxic areas of glioblastoma; on the other side the hypoxic areas show not only a limited

oxygen content but also perfusion, meaning that chemotherapeutic have a limited access to tumor tissue [36-38]. The relatively weak effect of radiation- and chemotherapy on hypoxic areas of glioblastomas, as well as of many other tumors, makes surviving cancer cells highly resistant to these treatments [39-41]. Notwithstanding this weakness, radio- and chemotherapy represent at this moment the most promising therapies after surgical resection in terms of life expectancy [10, 30, 33].

Radiation induced DNA damage is triggered by ionization, either directly or through the formation of reactive oxygen species (ROS) such as oxygen free radicals and highly reactive peroxides. In hypoxic areas the absence of ROS greatly reduces DNA damage by radiation and thus the effectiveness of the therapy [41]. In addition diminished blood perfusion to hypoxic areas reduces the efficiency of drug delivery [21, 42, 43]. Glioblastomas are among the most vascularized tumors [19, 20]. However, the architecture of neovasculature in tumors is in general chaotic and local perfusion may be impaired as reflected by the occurrence of hypoxic areas. Nevertheless, targeting angiogenesis appears an attractive approach [19-21]. The administration of bevacizumab (Avastin), an antibody inhibiting pro-angiogenesis factor VEGF, showed encouraging promising results in some clinical trials in prolonging survival life span [33, 44]. Significant effort has been invested in the development of therapies for treating glioblastoma patients; unfortunately none of them has led to a cure so far. The benefit of prolongation in the lifespan is measurable in months and all tumors will sooner or later overcome therapy effects and relapse. Therefore sustained efforts for developing glioblastoma therapies are required involving novel therapeutic strategies. Currently, several novel approaches are being explored including immune and gene therapy, novel antigenic agents and targeting of growth promoting pathways [33].

1.1.4 Brain tumor animal model

Animal models of (human) brain tumors are essential for investigating the molecular mechanisms behind tumor development and for evaluating treatment approaches. There are three main types of mouse models: (i) those with chemically induced tumors, (ii) those based on implantation of tumor cells (xenograft) and (iii) those genetically engineered based mouse models with spontaneous tumor development [45]. Huszthy et al. [45] explain all three models with advantages and disadvantages as follows. The

propensity of tumor formation by carcinogenic chemicals varies with dose and exposure period but also on other factors which results in large variations from mouse to mouse with regard to onset time, location of tumors and total tumor burden. An advantage of this model is that mice have an intact immune system, an aspect lacking in many other models. Nevertheless the high degree of variability renders this model unpractical for experimental studies, in particular when evaluating novel therapeutic strategies. In the xenograft model tumor cells collected from tumor biopsies are implanted in the brain of immune deficient mice either as solution containing isolated cells or as spheroids. Implantation of tumor cells derived from monolayer cell cultures shows consistent growth behavior and therefore forms tumors rather reproducibly. The cultured cells show clonal selection and differ genotypically and phenotypically from the originally isolated glioblastoma cells. Finally, genetically engineered models are useful to investigate the role of specific genes crucial to tumor development such as those eliminating specific tumor suppressor genes or those related to upregulation of oncogenes. For genetically engineered mouse models, gene regulating systems based on controlled transcriptional activation such as those with promoters tet (tetracycline-induced) or cre (Cre-recombinase-induced) can be introduced into mice in combination with oncogenes or tumor suppressor genes. This allows regulating through the switch-on mechanism the time point, intensity, and duration of the expression of the genes of interest. However the time point of the tumor genesis is not controllable [45, 46].

None of the currently available animal models of brain tumor does fully emulate human glioblastoma, however they can be used to represent specific aspects of the disease and thus constitute an important platform to investigate the tumors [45]. Furthermore, it has been shown that they show some drawbacks such as the glioma models derived from cultured tumor cells often losing their specific diffuse infiltrative behavior [18]. An optimal animal model for glioblastoma should mimic its pivotal characteristics to a large extend, including histopathology, tumor biology, genetics and invasive properties [46].

1.1.5 Glioblastoma cell lines

In the context of this PhD project we have used the xenograft approach. The three glioblastoma cell lines we used for the *in vitro* and *in vivo* studies are introduced in more detail in the subsequent section:

1) LN229 is a human glioblastoma cell line that was isolated from the right frontal-parieto-occipital lope of a 60 year old female patient [47]. LN229 cells contain mutations of the tumor suppressor genes p53, p16 and p14, but not of PTEN [47, 48]. LN229 cells were found to express increased levels of activated AKT (phosphorylated AKT, pAKT) and of its downstream targets which is in line with the excessive proliferative behavior of these cells [49]. Furthermore it has been reported that this cell line is particularly suitable to study apoptosis [50].

2) Xenografts grown from implanted U87 human glioblastoma cells are widely used models. The cells were isolated from the right temporal lobe of a 44 year old male patient [47, 51]. U87 tumors are non-infiltrating with an impaired and leaky tumor vasculature [30, 52, 53]. Therefore, the U87 line is a cell line frequently used for studying tumor angiogenesis and the efficacy of antiangiogenic therapy [30, 53]. Contrary to many glioblastoma, U87 tumors show only limited necrosis within the tumor mass. Around these necrotic areas an increased hypoxia inducible factor 1α (HIF-1α) expression can be observed [52, 53]. Several genetic alterations were observed such as a mutation of the PTEN gene and a deletion of the tumor suppressor genes p16 and p14 [47, 53]. In fact, the cyclin-dependent kinase (CDK) inhibitory function of p16 has been shown to be absent in 50% of gliomas [54]. U87 cell contains a wild type of tumor suppressor gene p53 and can be used therefore as a control for p53 deficient glioblastoma cells [48, 52]. Characteristical for glioblastomas is the upregulated PI3/AKT pathway caused by an increased expression of AKT in form of AKT phosphorylation [49, 52]. U87 tumor tissue stains negatively for GFAP (glial fibrillary acidic protein) [52, 53].

3) GL261 is a frequently used murine glioblastoma cell line that was originally obtained from a chemically induced tumor, following the injection of the carcinogen compound methylcholanthrene into the right cerebral hemisphere of C57BL/6 male mice. The induced intracranial tumor was isolated and implanted repeatedly subcutaneously into mice of the same mouse strain before a stable cell culture was established [55]. The GL261 tumor model mimics many characteristics of human glioblastomas and is therefore considered a reliable animal model [46]. It was observed that the GL261

tumors show diffusely infiltrating and invasive character in brain tissue with cells invading the brain tissue within a range of some millimeters [46, 56]. The similarities of the GL261 model to human glioblastoma include aggressive and infiltrative growth pattern, necrotic areas, hypoxic areas mostly located in the pseudopalisading area at the border of necrosis, and areas of angiogenesis [46]. Although gliomas shown upregulation of the PI3K/AKT pathway a further increase this expression can be based by the observed PTEN mutation in GL261 [46, 57]. GL261 cells contain some major point mutation analogous to human glioblastomas such as a mutation in the tumor suppressor gene p53 and the tumor oncogene K-ras [57, 58]. The expression of glial fibrillary acidic protein (GFAP) in GL261 is controversial and both positive and negative staining of GFAP has been reported [46, 59]. As GL261 cells are of murine origin (C57BL/6), implantation in immune competent C57BL/6 mice allows more realistic studies including immune responses [53].

1.2 Hypoxia and HIF pathway in tumor

Hypoxia is an important stimulus for physiological processes such as blood vessel formation during embryonic development [60, 61]. On the other side, hypoxia is a negative factor under many pathophysiological conditions as for example in neurodegeneration of the Alzheimer type, atherosclerosis and consequences thereof, or in cancer [62-64]. As already discussed in section 1.1 tumor hypoxia is a major cause for inefficacy of radio- or chemotherapy. This is attributed to the deficient blood supply of tumors not delivering enough chemotherapeutic agent or oxygen capable of building ROS during radiation. In fact it has been shown that radio and/or chemotherapy render hypoxic tumors even more aggressive [41, 42].

Hypoxia signaling is mediated via the hypoxia inducible factor (HIF), a heterodimeric transcription factor that consists of two counterparts [61]. The first one is a HIF-α subunit whose stability is dependent on the oxygen tension in tissue. Three different isoforms, HIF-1α, HIF-2α and HIF-3α, have been described for the alpha subunits (Fig. 3); their occurrence is cell type dependent [65, 67]. Their counterpart is a HIF-β subunit, whose stability is independent on the oxygen tension. Three different HIF-β subunits are known: aryl hydrocarbon receptor nuclear translocator (ARNT)/HIF-1β, ARNT2, and ARNT3/MOP3, though it has been shown that only the first two are able to dimerize

with the α-subunit and form heterodimeric HIF complexes, with HIF-1β being the main player (Fig. 3) [66, 67]. Structurally all HIF proteins contain a bHLH (basic helix-loop-helix) sequence for specific DNA binding and a PAS (PER-ARNT-SIM) sequence that is needed for the dimerization of the HIF-α and the HIF-β subunit [65, 67, 68]. Beside the bHLH-PAS sequence the HIF-1/2α protein comprises an oxygen-dependent degradation domain (ODDD) and two transactivation domains (TAD), whereby HIF-1α and HIF-2α contain a N- and a C-terminal TAD (N-TAD and C-TAD) and HIF-3α contains only a N-TAD sequence [69-72].

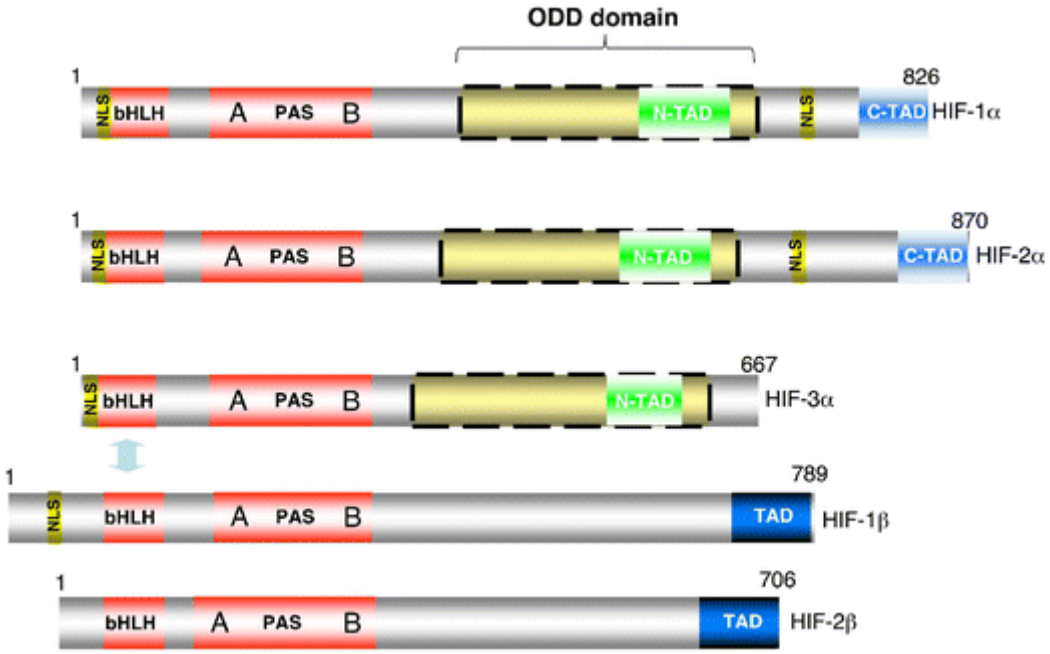

Figure 3. Schematic structure of the three HIF-α and the tow HIF-β subunits. NLS stands for nuclear localization signal, bHLH for basic helix-loop-helix sequence PAS, PER-ARNT-SIM domain (containing of two divisions PAS A and PAS B), ODD domain stands for oxygen-dependent degradation domain, and TAD is the transactivation domain. Adapted from Dayan et al. 2008 [73].

Under normoxic conditions, the HIF-α protein has a half-life of 5 min [65]. Different post-translational modifications influence the HIF-α stability under normoxic conditions. HIF-α stability is regulated by two hydroxylases, the prolyl hydroxylase domain (PHD) and the HIF-inhibiting factor (FIH, factor inhibiting HIF) (Fig. 4A) [74]. Three different PHD isoforms have been shown (PHD1-3) to hydroxylate the proline

residues Pro402 and Pro564 located in the ODDD of the human HIF-1α protein. Hydroxylation facilitates the interaction of HIF-α with the von Hippel-Lindau protein (pVHL). Binding of the pVHL protein to the E3 ubiquitin-protein ligase complex leads to the ubiquitination and subsequent proteasomal degradation of HIF-α (Fig. 4A) [70, 75, 76]. FIH hydroxylates the asparaginyl residue (Asn803 in HIF-1α) located on the C-TAD region (Fig. 4A). This results in an inhibition of the interaction between the HIF-1α and the coactivators p300/CREB binding protein (CBP) that is necessary for the HIF-α dependent target gene expression [74, 77, 78]. Further post-transcriptional modifications of HIF-α have been described: acetylation of Lys532 on the ODDD facilitates the interaction of HIF-α with the pVHL protein leading to the proteasomal degradation of HIF-α [79]. Nitrosylation of Cys520 on the ODDD leads to stabilization of HIF-α while [79] nitrosylation of Cys800 of the C-TAD increases the binding of HIF-α to the p300/CBP [79]. HIF-1α phosphorylation was observed to be induced by the p42/p44 MAP kinase resulting in a larger molecular form of HIF-1α that seems to enhance its transcriptional activity [80].

Under hypoxic conditions the oxygen-dependent dioxygenases PHD and FIH become inactive due to insufficient oxygen levels [74]. The two dioxygenases exert different oxygen affinity, whereby the PHD shows the stronger oxygen affinities and therefore requires a higher oxygen concentration to hydroxylate the proline residues as compared to FIH [81]. This means that with decreasing amounts of tissue oxygen (i.e. at a state of a mild hypoxia) first the PHD becomes inactivated leading to increased HIF-α stabilization; yet, FIH mediated hydroxylation of asparagine residue Asn803 prevents transcriptional activity of HIF. As oxygen levels further decrease FIH also loses its activity [82]. The stabilized and active HIF-α protein enters the cell nucleus where it dimerizes with HIF-1β via the bHLH-PAS A and B interaction and binds to the coactivator p300/CBP (Fig. 4B) [65, 68, 83]. The HIF dimer binds to a specific DNA sequence, the hypoxia-responsive element (HRE), consisting of the motif 5'-RCGTG-3' (R could be replaced by A or G) located in promoter, intron and/or enhancer regions of HIF-target genes (Fig. 4B) [67, 84, 85]. Today, at least 70 genes are characterized as HIF regulated target genes that are involved in angiogenesis, metabolism, pH homeostasis, metastasis, and cell survival/death [84].

HIF-1α and HIF-2α show a high structural and functional similarity (Fig. 3) and it has been shown that both are stabilized under hypoxic conditions and dimerize with HIF-1β to form an active transcription factor. Whereas HIF-1α expression has been observed in most kind of tissues, HIF-2α expression appears to be more specific [65, 72, 86, 87]. The two homologs regulate a common group of target genes. For example while HIF-1α showed to regulate more prominently the expression of carbonic anhydrase (CA9), HIF-2α showed a stronger regulation of the expression of the octamer binding transcription factor 4 (Oct4) [86]. HIF-1α and HIF-2α contain two TAD sequences that individually regulate a specific group of HIF target genes via hydroxylation status of PHD and FIH displaying different oxygen affinities. The N-TAD located within the ODDD is regulated by PHDs, which as we know are sensitive to even mild levels of hypoxia. Therefore genes regulated via N-TAD are up-regulated under mild conditions. C-TAD that is regulated by FIH stays unmodified under this setting. At a more severe degree of hypoxia, both PHD and FIH do not hydroxylate their specific residues on HIF-α any longer leading to the expression of both groups of TAD specific genes [71, 78, 82]. HIF-3α is less well characterized than HIF-1α and HIF-2α but it has been reported that the protein acts as a negative regulator of HIF-1α function [67, 88].

Hypoxia has two contrary effects. On one hand it constitutes a physiological stress for the affected cells which may lead to dysfunction or even cell death but on the other hand it initiates a signaling cascade that prepares the cells to handle this situation by initiating adaptation mechanisms [73, 79]. In the following sections we will have a closer look on this HIF mediated signaling mechanism and its consequences for the cells. A negative gradient in oxygen concentration can be measured in tumor tissue with increasing distance to capillaries. Within a radius of about 300μm from the capillary the oxygen pressure (pO_2) in tissue was reported to decrease from 12mmHg to 0 mmHg in a breast cancer model [91]. In human colon cancer the oxygen gradient was found to be even steeper: a decrease in oxygen pressure from 14mmHg to hypoxic values of ≤5mmHg within a distance of 70-80μm and to anoxic values of 0.0-0.5mmHg at a distance of ≥150μm to the nearest vessel wall was measured [92].

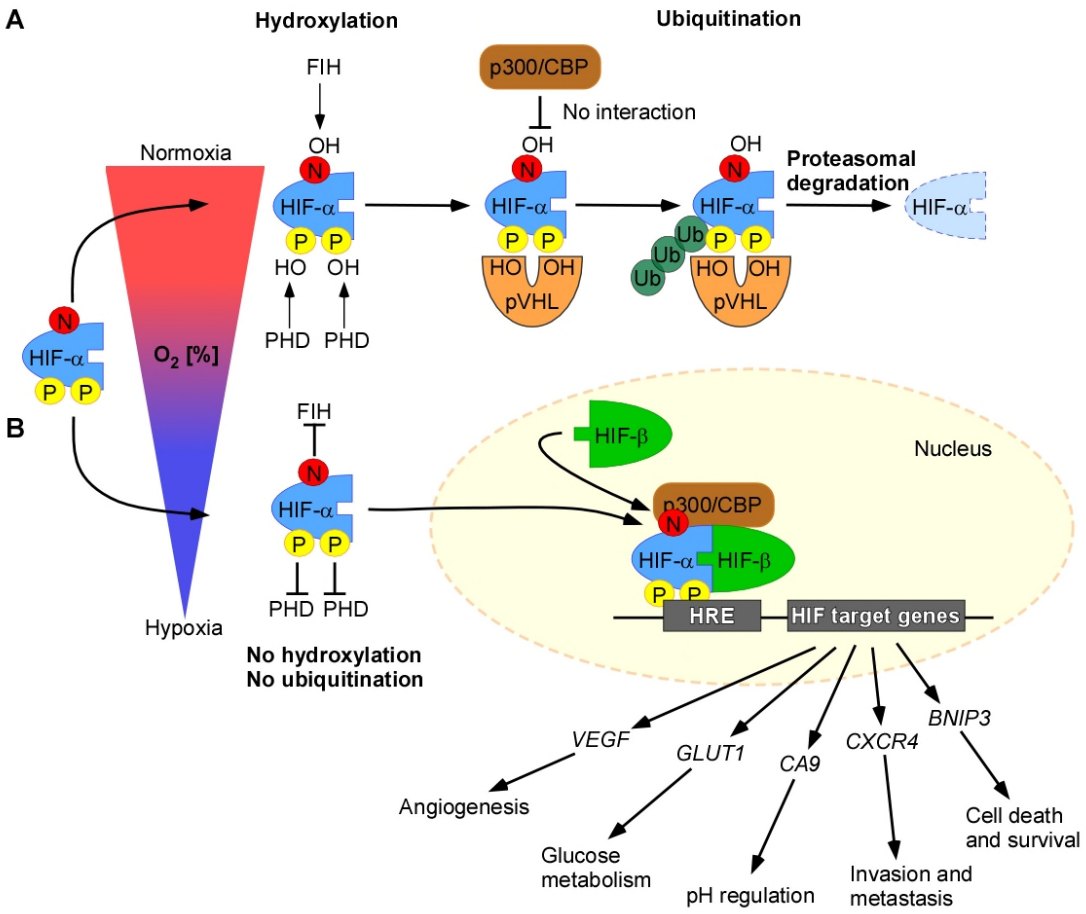

Figure 4. HIF signaling pathway. A. Under normoxic conditions HIF-α protein is hydroxylated by prolyl hydroxylases (PHD) at the proline residues located in the oxygen degradation domain. Factor inhibiting HIF (FIH) hydroxylates an asparagine residue (N) in the C-TAD region resulting in a decreased interaction of HIF-α with the coactivator p300/CBP (CREB-binding protein). The hydroxylated proline residues are recognized by the von Hippel-Lindau protein (pVHL) which is a component of an ubiquitin ligase complex that ubiquitinates (Ub) HIF-α making it for proteasomal degradation. **B.** Under hypoxic conditions hydroxylases PHD and FIH are not active. HIF-α enters the cell nucleus and dimerizes with its cofactor HIF-β, recruits the coactivator p300/CBP and binds to the HIF specific promoter motif hypoxia responsive element (HRE) to regulate the transcription of HIF target genes. These are involved in many physiological processes such as angiogenesis, glucose metabolism, or pH regulation. This happens through the expression of vascular endothelial growth factor (VEGF), glucose transporter 1 (GLUT1), carbonic anhydrase 9 (CA9), C-X-C chemokine receptor 4 (CXCR4), BCL-2/adenovirus E1B 19-kDa interacting protein 3 (BNIP3). Adapted from Carroll and Ashcroft 2005 [89] and Zarember and Malech 2005 [90].

1.2.1 HIF and tumor angiogenesis

When proliferative masses grow fast they face the problem of insufficient oxygen and nutrient supply due to the lack of an adequate vascular system, leading to hypoxic potentially even necrotic tumor regions [73]. One of the principal target genes triggered by hypoxia signaling mediated by HIF is the vascular endothelial growth factor (VEGF), a pro-angiogenic factor that induces and promotes neoangiogenesis, i.e. the formation of a vascular system directed toward the hypoxic area (Fig. 5A) [73, 93]. It was shown that the molecular target of VEGF, the VEGF receptor 2 (VEGF-R2) is highly expressed in endothelial tip cells. Binding of VEGF to these receptors induces vascular sprouts [94]. As HIF induced VEGF is expressed by hypoxic cells and then diffuses through the extracellular space a concentration gradient of VEGF protein will develop guiding the newly formed vessels toward the hypoxic areas to restore the adequate oxygen delivery to these cells [93, 95].

Angiogenesis relies on a balance between positive and negative angiogenic factors [21]. Comparable to VEGF, Angiopoietin-1 (Ang1) is known to be essential for normal vascular development and integrity. Whereas Angiopoietin-2 (Ang2) factor induces destabilization in blood vessels leading to impaired vasculature and prevents vessel maturation resulting in permeable walls. Ang2 has been shown to be HIF inducible (Fig. 5A) [73, 96, 97]. Both Ang1 and Ang2 bind to the Tie2 receptor in endothelial cells whereby Ang2 acts as antagonist resulting in a destabilization of capillary organization. A comparison between different tumor types showed that Ang1 and Ang2 are not uniformly expressed throughout the tumors. However, independently from the actual values it was shown that in cancer tissue the Ang1:Ang2 ratio is in general shifted in favor of Ang2. Such a shift was also observed in glioblastoma tumors [73, 96-98]. It is suggested that for the process of angiogenesis both HIF-1 and HIF-2 are required. HIF-2 is mainly involved in the final stages of vessel formation, as it is required for the remodeling of the newly built blood vessels [72]. The formation of a tumor vascular network, enables the initially hypoxic tissue areas to recruit oxygen and nutrients required for survival and proliferative activity. However the newly formed blood vessels in tumors have been shown to be structurally and functionally abnormal, which leads to inefficient and fluctuating tissue perfusion [21, 43]. Glioblastomas have been reported to have the potential to grow by vessel co-option, i.e. initially tumor cells grow along the pre-existing blood vessels, which given the high capillary density in brain tissue warrants supply by oxygen and nutrients. Yet, this co-option process has been

observed to induce regression of host vessels leading to a reduced tumor perfusion [21, 22]. As the tumor grows beyond the limits given by the diffusion radius of molecular oxygen (typically 200μm) the co-opted host vessels are pushed to the border of the tumor. At regions distant enough from capillaries hypoxic domains will emerge triggering local HIF signaling and the secretion of pro-angiogenic factors [21, 22, 99]. The development of novel vessels will restore oxygen supply to these areas. If the vascularization does not develop in due time persistent hypoxic stress may lead to tissue necrosis. A factor involved in this process is Ang2, which is not detectable in normal brain tissue, but the expression of which is increased in vessels co-opted by brain tumors prior to the increase in the VEGF levels [22, 99].

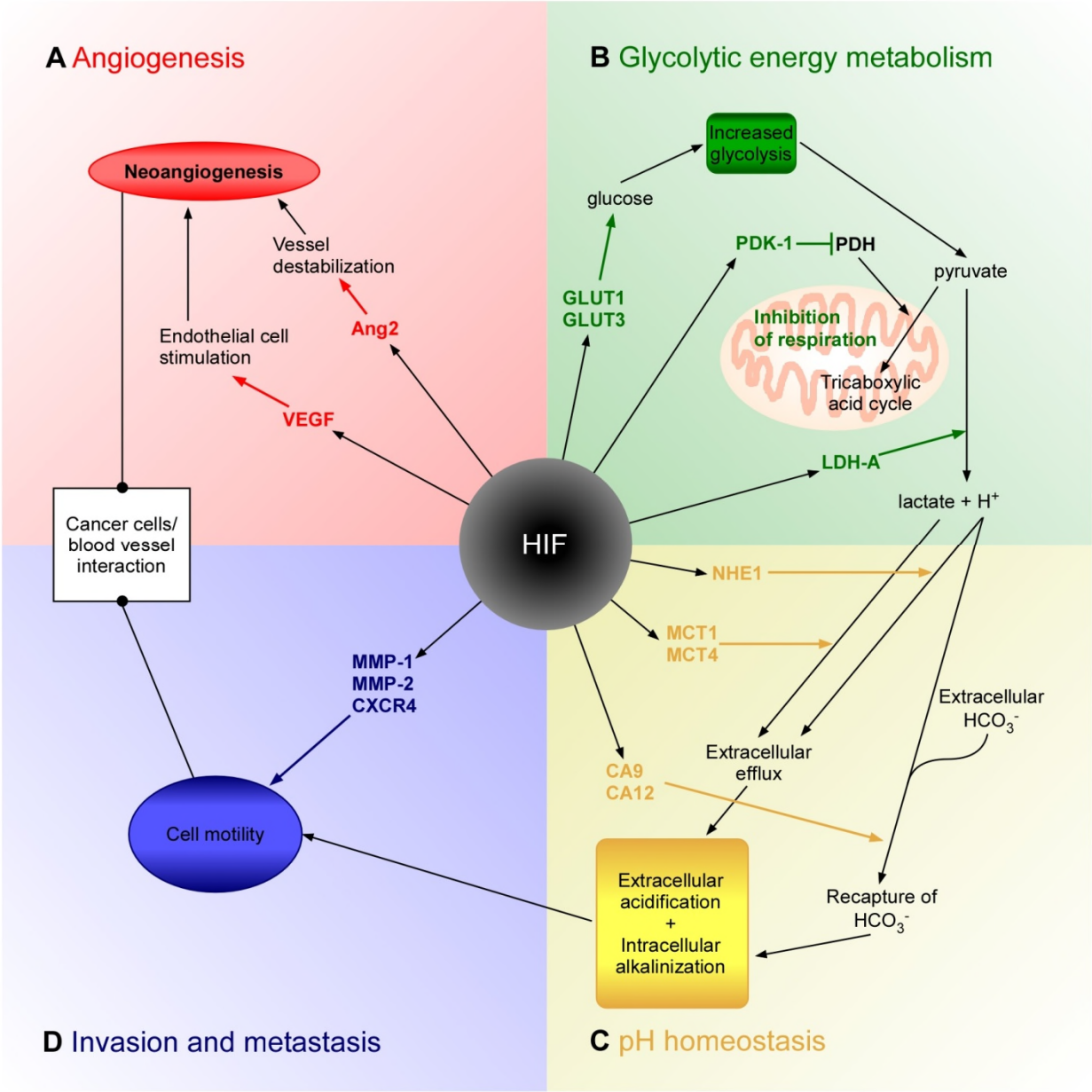

Figure 5. HIF directed modification on physiological processes. A. A selection of HIF target genes involved in Angiogenesis is shown in red; VEGF endothelial growth factor, Ang2 Angiopoitin-2. **B.** A selection of HIF target genes involved in the glycolytic energy metabolism is shown in green; GLUT glucose transporter, PDK-1 pyruvate dehydrogenase kinase-1, PDH pyruvate dehydrogenase, LDH-A lactate dehydrogenase-A. **C.** A selection of HIF target genes involved in the pH homeostasis is shown in yellow; CA carbonic anhydrase, MCT monocarboxylate transporter, NHE Na^+/H^+ exchanger. **D.** A selection of HIF target genes involved in invasion and metastasis is shown in blue; MMP matrix metalloproteases, CXCR4 chemokine receptor. Adapted from Dayan et al. 2008 [73].

1.2.2 HIF and glycolytic energy metabolism

Healthy, normoxic tissue derives its energy by glycolysis followed by oxygen consuming oxidative phosphorylation (OXPHOS) in the mitochondria. This requires the catabolization of glucose pyruvate, which enters the tricarboxylic acid (TCA) cycle inside the mitochondria. The TCA cycle produces usable chemical energy in the form of ATP by consuming pyruvate and oxygen, reducing NAD^+ to NADH through electron transfer and producing carbon dioxide [102]. Normal differentiating cells switch their metabolism to anaerobic glycolysis, which involves metabolism of the pyruvate to lactate, only under hypoxic or even anoxic conditions. Glycolysis is considerably less efficient that OXPHOS producing 2 moles of adenosine-triphosphate (ATP) instead of 38 moles per mole of glucose respectively [73, 101-102]. Warburg demonstrated already in 1924 that in tumor tissues metabolism was shifts to aerobic glycolysis, independent of the tissue oxygen concentration. This non-oxygen dependent glucose metabolism results in the production of excessive amounts of lactate accumulating in the cytoplasm [73, 100-102]. Nowadays it is widely accepted that cancer cells utilize both aerobic glycolysis (Warburg effect) and oxidative phosphorylation for energy production. Under hypoxic conditions, energy production is pushed toward anaerobic glycolysis, which constitutes a HIF mediated cellular response (see below) [101]. However, it has been recently demonstrated that metabolic products of glycolysis, such as lactate, pyruvate, or α-ketoglutarate, may induce stabilization of HIF-1α and thereby activation of HIF signaling even under normoxic conditions [103, 104]. By this effect the glycolytic products may act as activators in a positive feedback loop [103].

Glucose, being the main energy substrate for the brain tissue, is supplied via circulation and is transported into the adjacent tissue via glucose transporter molecules such as glucose transporter GLUT1 [105]. In the tissue it distributes by molecular diffusion, which results in distribution pattern similar to that of oxygen with a negative concentration gradient originating at the feeding vessel [73, 105]. As mentioned above, cells need glucose as source for their energy production. Therefore hypoxic cells that have switched to inefficient anaerobic glycolysis require elevated glucose uptake to cope with the increased substrate demand [73, 102, 106]. This is achieved by upregulating the expression of glucose transporters, in particular GLUT1 and GLUT3, which has been observed in hypoxic and normoxic tumors cells. Glucose upregulation is indirectly mediated by increased activity from glucose transporters via HIF signaling under hypoxic conditions and/or oncogenes such as ras (Fig. 5B) [106, 107]. In addition,

hypoxic cells were shown to induce the expression of pyruvate dehydrogenase kinase-1 (PDK-1), which blocks the uptake of pyruvate by the mitochondria for further catabolism through tricarboxylic acid (TCA) cycle (Fig. 5B) [26, 108]. Therefore the high levels of pyruvate, resulting from the increased glucose uptake, is metabolized in the presence of NADH to form lactate and NAD^+ via the lactate dehydrogenase-a (LDH-A) in the cytoplasm or to form alanine by the enzyme alanine-aminotransferase (ALT) [26, 109].

1.2.3 HIF and pH homeostasis

The increased lactate production resulting from the metabolic switch to glycolysis in hypoxic tissue but also in normoxic cancer cells leads to increasing lactose levels, which are then exported out of the cells resulting in an extracellular acidosis (Fig. 5C) [73, 110]. This is accompanied with poor blood perfusion of hypoxic areas, which prevents the efficient removal of lactate [110]. To maintain pH homeostasis metabolites which cannot be processed inside the cell should be efficiently exported to the extracellular matrix. This requires 1) transport of the polar/charged molecules across the cell membrane into the extracellular space and the blood compartment and 2) transport out from the areas by the circulation system [110]. Transport of lactate across cell membranes is achieved by the monocarboxylate transporter 4 (MCT4), the expression of which is HIF regulated (Fig. 5C) [110, 111]. In addition, the Na^+/H^+ exchanger 1 (NHE1), which is also HIF regulated, transports excess of H^+ resulting from the anaerobic metabolism into the extracellular compartment in order to maintain the intracellular pH homeostasis (Fig. 5C) [73, 112]. The implications of these two transport processes is that in order to maintain intracellular pH there is considerable extracellular acidification [110, 112]. Another important HIF target gene, the transmembrane CA9 acts as a pH buffer by converting the CO_2 that cannot be removed by the vascular system to bicarbonate ions (HCO_3^-). The HCO_3^- produced is subsequently transported into the cells leading to an intracellular alkalinization (Fig. 5C). Furthermore it has been shown that CA9, and to a lesser extend CA12, were correlated to the occurrence of necrotic/hypoxic regions in glioblastomas [73, 110, 113].

1.2.4 HIF and metastasis

During invasion of healthy tissue areas and the formation of distant metastases tumor cells need to penetrate the basement membrane, which is a special matrix structure build of extracellular matrix (ECM) components, called the underlying epithelium [114]. Matrix degradation is achieved with a family of proteins called proteinases, which include the matrix metalloproteinases (MMP), which are zinc dependent endopeptidases. About 30 members of this peptide family are known. The usual MMP content of healthy cells is very low, while tumor cells express increased levels of MMPs [115]. Among them, MMP2 and the membrane type-1 (MT1-MMP) were shown to be expressed in a HIF dependent way and it has been shown that hypoxia stimulates breast carcinoma cell invasion though activation of these two MMPs (Fig. 5D) [116]. In a breast cancer metastasis study it was observed that cancer cells show increased levels of the chemokine receptor (CXCR4), the expression of which facilitates the migration of cancer cells via interaction with their ligand stromal cell-derived factor-1α (SDF-1α) (Fig. 5D) [117]. This highlights an important role of HIF regulated CXCR4 metastasis formation [118]. CXCR4 was demonstrated to be highly expressed in glioblastomas in particular in regions of pronounced angiogenesis, which requires matrix degradation to allow vessel formation, and in necrotic areas [119, 120]. The expression of these MMP and chemokine receptors appears, to be correlated with the grade of tumor malignancy: the fact that these molecular targets are regulated by HIF signaling indicates that hypoxia and HIF levels may be considered indicators of glioblastoma cell migration [119, 120].

1.2.5 HIF and cell death and survival

The physiological environment in hypoxic tumor regions is very challenging. Energy production is reduced by the metabolic switch to glycolysis despite the high proliferative activity that already consumes considerable energy. As a result glucose consumption has to be increased, which leads to massive production of lactate and hence acidosis [73, 102]. Moreover under severe hypoxia conditions tumor cells have two possibilities: either they adapt to the situation or they die [73, 79]. Apoptosis is one of the two outcomes of the cell cycle (the other one being division) and is the mechanism by which cells die in a controlled way to protect the organism from

infections and cancer [121]. Apoptosis is also required during fetal development [122] and during T and B cell maturation [123].

The characteristic morphological features of apoptosis are losing intracellular contact, detachment, cell shrinkage, condensation of chromatin, internucleosomal DNA cleavage and self-fragmentation into apoptotic bodies which are eventually engulfed by phagocytes and adjacent cells [124]. Apoptosis can be induced externally by the activation of surface cell death receptors or via the mitochondrial release of cytochrome c upon specific stimuli or events damaging the cell or causing serious cellular stress [124, 125]. Because of the transcendental importance of apoptosis for higher eukaryotes this process is very tightly controlled intrinsically by a complex balance between proapoptotic and antiapoptotic genes [54] i.e. the expression of pro and antiapoptotic proteins of the BCL2 (B-cell lymphoma 2) family can lead to cytochrome c release [124, 125]. The cytosolic cytochrome c interacts with ATP and the apoptotic protease activating factor 1 (APAF-1) to build the proapoptotic complex apoptosome. This complex leads to the activation of the caspase (death proteases) mediated apoptotic cell death (Fig. 6A) [124, 125]. Tumor cells are able to overcome apoptosis through genetic alterations. For example the antiapoptotic BCL-2 family proteins are preferentially expressed in glioblastomas upon apoptotic stimuli leading to the failure of activation of the caspases [48, 126]. Tumor progression involves mutagenesis that is induced by hypoxic and hypoglycaemic stress. The relationship of HIF to the programmed cell death is debated. It seems that hypoxia alone is not enough to trigger apoptosis and it has been proposed that hypoxia causes programmed cell death in tumor cells suffering from additional stresses such acidosis or nutrient deprivation [127].

The resulting mutations to adapt to their environment can initiate apoptotic cell death in tumors [128, 129]. However, this process requires energy in the form of ATP, yet energy supply is limited in many tumors including glioblastomas, which leads to uncontrollable cell death by necrosis [130]. Therefore for tumor cells to survive and proliferate the protective mechanism of apoptosis and additional hypoxic stresses have to be circumvented with great care without maneuvering themselves into necrosis. Some proapoptotic mutations have been shown to be HIF-1α dependent like p53, p21, and BCL2 [128, 131]. p53 is a tumor suppressor gene that probably is the most frequently mutated gene in cancer [132, 133]. It was shown to be associated with the cell cycle

arrest in the G_1 phase upon radiation or DNA damage and thus protects cells from division and proliferation into a tumor mass. Cells with a non-functional or mutated p53 gene do not show the induced cell cycle arrest in the G_1 phase upon exposure to DNA-damaging agents [131, 134].

HIF-1α is accumulating and HIF-1 is transcriptionally active under hypoxic conditions [82]. It was observed that after a prolonged period of hypoxic conditions the HIF-1α activity decreases with time indicating a negative feedback mechanism for down-regulating HIF-1α protein [135]. The level of p53 was shown to increase under severe hypoxia indicating that under this condition apoptosis was induced to inhibit the tumor progression [79]. This was indicated by p53 induced transcription of proapoptotic genes such as the proapoptotic BCL-2 family member BAX [79]. p53 and HIF-1α were shown to compete for binding to the cofactor p300 under severe hypoxia/anoxia conditions resulting in reduced transcriptional activity of HIF-1. Under a constant severe hypoxia or anoxia the p53 and HIF-1α build a tertiary complex with the p53 negative regulator mouse double minute 2 (MDM2). This leads to HIF-1α degradation by a mechanism that is independent of pVHL [135-137]. Mutation of p53 is observed more frequently in secondary (65%) rather than primary (10%) glioblastomas [126]. PTEN is mutated in many glioblastomas [10]. It inhibits the phosphatidylinositol-3-kinase (PI3K) that in turn activates AKT. This increased AKT activity decreases the apoptotic potential by inducing the antiapoptotic factor Bcl-2 and blocking the proapoptotic factor Bad (Fig. 6A) [138].

BNIP3 (Bcl-2/adenovirus E1B 19-kDa interacting protein 3) and BNIP3L (Bcl-2/adenovirus E1B 19-kDa interacting protein 3 like) are two pro-apoptotic proteins that were shown to be HIF inducible in several human tumors [139]. They induce cell death mechanism independent of cytochrome c. It is characterized by early mitochondrial damage leading to mitochondrial pore opening, a decrease of the mitochondrial electrochemical gradient and to an increase ROS level (Fig. 6B). This cell death showed necrotic cell characteristics [125, 140].

Hypoxia induced apoptosis and necrosis seem to be cell type specific. An over-expression of the antiapoptotic genes BCL2 and BCL-X_L leads to the suppression of apoptosis and a decrease in necrosis [141]. The switch between apoptosis and necrosis is regulated by the presence of ATP. Nitric oxide (NO) has been shown to influence this switch [142]. In malignant glioblastoma cell lines it was observed that cell death upon

hypoxia was rarely observed as long as energy supply was available. Thereafter the cell death by necrosis was seen to be much more prominent than cell death by apoptosis [143].

Necrosis is described as uncontrolled cell death that is triggered by extreme environmental stresses and as hypoxia it is also a hallmark in glioblastomas. Increased necrosis correlates with negative clinical outcome [17, 138]. The necrosis is initiated by decreased levels of ATP and low pH resulting from the change from oxidative phosphorylation to glycolysis [124]. This leads to the condensation of the chromatin. The reduced ATP levels evoke leakage of ion channels allowing uncontrolled diffusion of water and sodium ions into the cytosol leading to cell swelling. This results in extrusion of lysosomal enzymes, proteases and degraded molecules which extravasate into the extracellular space and prompt inflammation [124, 138]. The characteristic features of necrosis are cell swelling, reduced function of the mitochondria, membrane rupture with efflux of cytoplasmic content and cell lysis [124, 138].

The debris resulting from necrosis is toxic to adjacent still viable cells [124]. However, as previously mentioned necrotic areas are a hallmark of glioblastomas and correlate with negative outcome [17]. It is therefore of great interest to gain insights in tumor progression by studying how cancer cells exploit the adaptation machinery of eukaryotes to overcome hypoxia and nutrient deprivation while also exposing themselves to (and taking benefit from) the extreme stress of a necrotic environment.

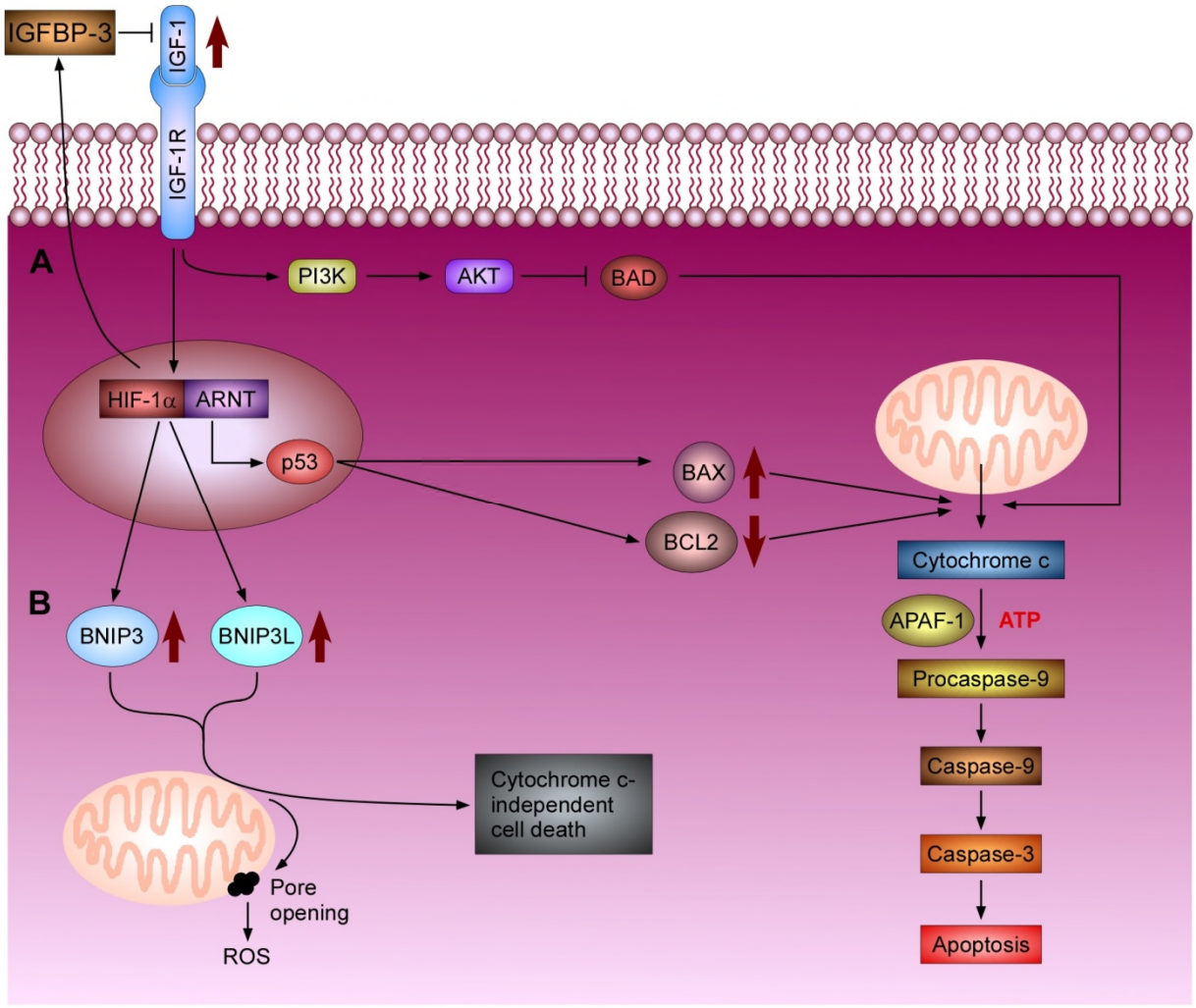

Figure 6. Cell death in relation to HIF activity. A. The HIF-1 interacts with the tumor suppressor gene p53 resulting initiated apoptosis. HIF-1 activates the transcription factor p53, which recruits of many proapoptotic proteins, such as BAX. BAX promotes the release of cytochrome c from the mitochondrial membrane. Cytosolic cytochrome c interacts with the apoptotic protease-activating fator-1 (APAF-1) and ATP, activating procaspase-9 conversion to caspase-9. Caspase-9 then starts the caspase cascade, leading to apoptosis. Apoptosis can be initiated by the proapoptotic protein BAD, which BAX it functions at the mitochondrial membrane for promoting cytochrome c release. BAD can be inhibited by the kinase AKT, which is activated by insulin-like growth factor-1 (IGF-1), which is therefore antiapoptotic. HIF-1 activates transcription of the proapoptotic protein IGF-binding protein 3 (IGFBP-3), which blocks IGF-1 signaling. **B.** HIF also starts expression of BNIP3 and BNIP3L, which induce pore permeability in the mitochondria, increased ROS production and cell death through a mechanism independent from cytochrome c release and caspases. Hypoxia has also been reported to reduce transcription of the antiapoptotic protein BCL-2 in some cell types. Adapted from Harris 2002 [125], and Vande Velde et al. 2000 [140].

1.2.6 Oxygen independent HIF regulation

Although hypoxia is regarded as a main inducer of the HIF pathway regulation, it has been shown that growth factors can influence HIF expression as well [144]. With increasing cell growth and proliferation the oxygen consumption rises correspondingly. Therefore it seems obvious that pathways related to the cell growth and proliferation could also induce HIF [144]. This preemptive HIF activity should warrant optimal oxygen and nutrient supply under growth conditions by activating angiogenesis via the HIF target gene VEGF [144]. In fact, it was shown that growth factors and hormones are able to stimulate the HIF-1α expression and stabilization and thus HIF-1 activity via the PI3K/Akt signaling pathway (Fig. 7 and Table 2) [145-147]. Whereas the p42/p44 MAP kinase pathway was shown not to be involved in the synthesis, stabilization or degradation of HIF-α, it was shown to phosphorylate the HIF-1 protein independently of oxygen, resulting in an enlarged HIF-1 molecular form [80, 147]. HIF activity can also be regulated by mutations of tumor suppressor genes. In renal cell carcinoma (RCC), the VHL protein that enables ubiquitination and degradation of HIF-α, is not functional under normoxic conditions (Table 2). This leads to persistent HIF activity even under sufficient oxygen levels [144, 148]. Another mutation has been reported to be relevant for glioblastomas: that of the glycolytic enzyme isocitrate dehydrogenase 1 (IDH1). Loss of function of IDH1 results in decreased levels of α-ketoglutarate, which is a co-substrate of PHD, the enzyme responsible to mark HIF-1α for degradation even under normoxic conditions (Table 2) [149]. Further genetic alterations such as loss of function of p53 or PTEN may increase the HIF activity, either by inhibiting the ubiquitination and degradation of HIF-1α or by the PI3K pathway activation due to the loss of the inhibitory effects of PTEN (Table 2 and Fig. 7) [144, 150, 151].

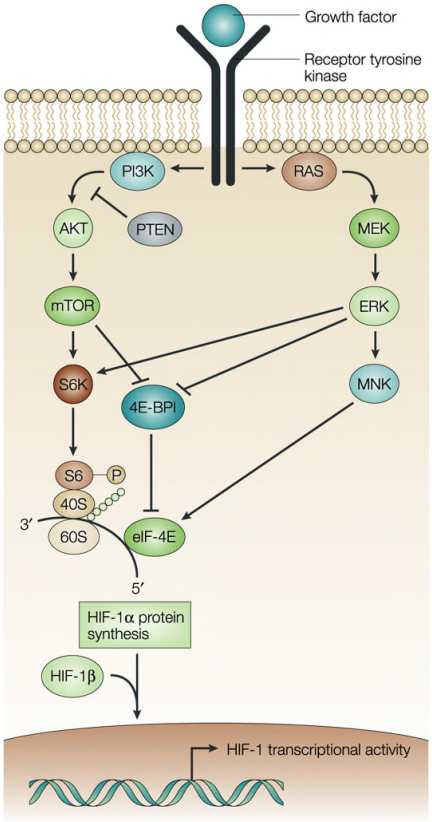

Figure 7. Oxygen independent HIF-1α regulation by growth factor. Growth factors bound to the receptor tyrosine kinase can activate the phosphatidylinositol 3-kinase (PI3K) and the mitogen-activated protein kinase (MAPK) signaling pathways. Other proteins involved are: protein kinase B (AKT), mammalian target of rapamycin (mTOR), MAP/ERK kinase (MEK), extracellular-signal-reduced kinase (ERK), MAPK-interacting kinase (MNK), p70 S6 kinase (S6K), eukaryotic translation initiation factor 4E binding protein (4E-BPI), eukaryotic translation initiation factor 4E (eIF-4E). Semenza 2003 [144].

Table 2. Stimuli and genetic alterations that induce the HIF-1α activity. Adapted from Semenza 2003 [144] and Meijer et al. 2012 [152].

Modification	Examples	Mechanism of HIF-1α induction
Physiological stress	Hypoxia	Decreased ubiquitination
	Oxygen and nitrogen species	Decreased ubiquitination
Growth factor stimulation	EGFR → PI3K/AKT/mTOR activity	Increased synthesis
Genetic alteration	VHL loss of function	Decreased ubiquitination
	p53 loss of function	Decreased ubiquitination
	PTEN loss of function	Increased synthesis
	IHD1 loss of function	Decreased ubiquitination

1.2.7 Therapy approaches targeting HIF pathway

Angiogenesis that is induced by HIF constitutes a crucial step in tumor formation [21, 73]. Therefore angiogenesis appears as a promising target for novel tumor treatments complementing the long established approaches based on DNA interfering drugs. Bevacizumab (Avastin) is an antibody against VEGF that is used already in clinical treatments together with chemotherapy in relapsing glioblastoma in patients [33, 44]. In addition to its antiangiogenic efficacy, an inhibitory effect on the antigenic activity of the tumor stem cell population was demonstrated, resulting in a reduced tumor growth potential [153-155].

Since intratumoral hypoxia correlates with negative outcome by increasing resistance to the most frequently used treatment therapies such as radio- and chemotherapy, it appears logical to target the HIF pathway for alternative therapy approaches [37, 41, 42]. There are two main different strategies to interfere with the HIF pathway, either by direct or indirect HIF-α inhibition [79].

The most obvious way to interfere the HIF pathway is to inhibit HIF-α directly [79]. Several studies were performed using small interfering RNA sequences to investigate the effects of a HIF-1α knock-down on the tumor progression. A significant reduction in glioma tumor migration, proliferation and invasion was detected *in vitro* and *in vivo* in HIF-1α and HIF-2α knock-downs using siRNA's [156-159]. Other strategy for a direct HIF inactivation is the inhibition of HIF-1 DNA binding using molecules such as echinomycin (NSC-13502). This compound specifically inhibits the binding of the HIF-1 protein to the HRE motif on the DNA sequence *in vitro* as demonstrated in U251 human glioma cells [160]. Alternatively, HIF activity can be inhibited by using a compound that increases HIF-1α degradation, such as LW6. This substance promotes the degradation of hydroxylated HIF-1α proteins via upregulation of VHL expression as shown in colorectal carcinoma HCT116 *in vitro* and *in vivo* [161]. HIF may also be inactivated by interfering in the interaction of HIF protein with the coactivators required for function using drugs such as chetomin. Chetomin interferes with the interaction between the C-TAD sequence of HIF-α and the CH1 domain of the HIF coactivator p300 as demonstrated in colorectal carcinomas (HCT116) *in vitro* and *in vivo* [162].

Indirect inhibition of HIF-α is based on influencing the signaling pathways that modulate the HIF-α activity. Many studies have shown that mTOR inhibitor rapamycin

(mTOR: mammalian target of rapamycin) and LY294002 (PI3K inhibitor) reduce the HIF-1α translation via their effect on the PI3K-AKT signaling pathway [145, 147]. Alternatively, the activity of HIF-1α might be reduce by inhibition of topoisomerase-1, an enzyme involved in the DNA winding and unwinding process required for DNA replication [79, 144, 163]. Topotecan is a camptothecin analogue that has an inhibiting effect on topoisomerase 1. Topotecan was shown to negatively affect the HIF-1α translation resulting in a reduced HIF-1α protein accumulation [79, 163].

1.3 Non-invasive methods for structural, functional and molecular imaging

The following section gives a short introduction on imaging methods that can be used for tumor visualization and for investigating physiological and molecular processes (in our context molecules associated to the HIF pathway activity). These methods range in their resolution from several micrometers to several millimeters and from low to cost intensive (Table 3) [188]. Not all of the following listed methods were used in the recent study but they are all important for the tumor imaging based research and it would be of interest to combine them with this project in the future.

1.3.1 Magnetic resonance imaging

Magnetic resonance imaging (MRI) is a non-invasive and versatile three-dimensional imaging method that yields data sets with high spatial resolution exhibiting high intrinsic soft-tissue contrast (Table 3) [24, 188, 164-166]. MRI may yield information on anatomical structures, physiological processes such as tissue perfusion, angiogenesis or tissue oxygenation, as well as on tissue metabolism (using MR spectroscopic techniques) [164-166]. The basic mechanism of MRI is based on nuclear magnetic resonance. Atomic nuclei of hydrogen possess a form of angular momentum called nuclear spin that is associated with a magnetic moment. In the absence of an external magnetic field the nuclear magnet are randomly oriented resulting in zero net magnetization of the samples. Yet, when these nuclear magnets are exposed to a strong magnetic field they align either parallel or antiparallel to the field, with a slight excess taking the parallel orientation, which results in a small net magnetization (Fig. 8). Exposing them to a radio frequency pulse changes the spin alignment of the nuclear atoms, i.e. induces transitions between the two states. By returning back to their

baseline equilibrium state, the absorbed energy is re-emitted, and a so called free induction decay (FID) can be acquired. The energy involved with this process and hence the resonance frequency ω inducing the transition scales with the magnetic field strength B_0, can be defined by:

$$\omega = \gamma \cdot B_0$$

with γ being the gyromagnetic ratio (a nucleus specific property) [165, 166]. In MRI, an image can be encoded according to this principle. In order to spatially localize the origin of the different signals composing the FID, magnetic field gradients are applied in two or three spatial directions. As a consequence, the resonance frequency of the excited protons becomes position dependent. By applying an inverse Fourier transformation on the acquired signal, the different frequencies can be identified and associated to a specific 'line' in the field of view (FOV), along the applied gradient. This gradient is called 'frequency encoding gradient' and is applied during the acquisition of the signal. Signals originating from different positions along this line can be localized by applying a phase encoding gradient. This gradient is applied for a short period of time before the acquisition of the signal. During a short period of time, the resonance frequency of the nuclei along this gradient will be changed. When the gradient is switched off, all the nuclei again precess with the same frequency, but with a different phase, according to their position in the FOV. Therefore, along this so called 'phase encoding gradient', specific signals can be associated to a certain position in the FOV according to their phase. Applying a phase encoding gradient and a frequency encoding gradient in two different spatial directions confers a unique signature to each signal originating from any position in space (depending on the pre-defined spatial resolution). Thereafter, a 2D image can be reconstructed. In order to spatially encode signals in 3 directions, an additional phase encoding gradient is used [165, 166].

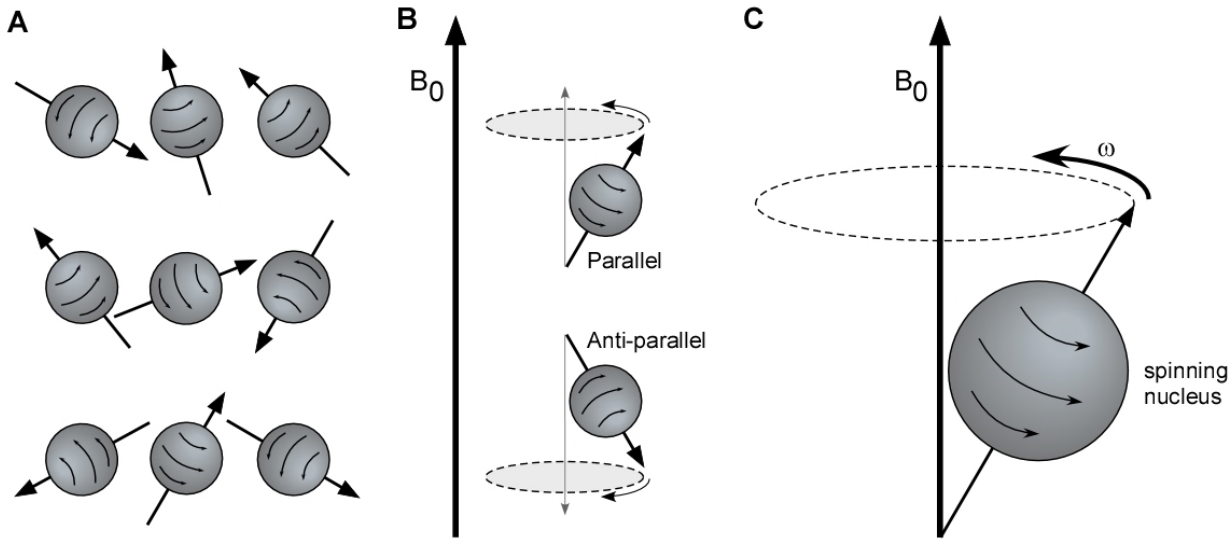

Figure 8. Principle of magnetic resonance imaging. A. Each nucleus rotates around its own axis (spin) in random orientation. **B.** In the presence of an external magnetic field B_0 nuclei align their orientation in respect to the magnetic field. Two different energy states are possible for their orientation: parallel to B_0, which has a low energy level or antiparallel to B_0, which has a higher energy level. **C.** A spinning nucleus process around the magnetic field B_0 with a resonance frequency ω. Adapted from Storey 2006 [165] and Huettel et al. 2006 [167].

The resonance frequency of a proton is slightly different between hydrogen protons of water and those of fat or other organic compounds (metabolites) due to the differences in the chemical environment (chemical shift). These compound specific frequencies constitute a chemical fingerprint and are exploited in MR spectroscopy [165, 166]. Apart from the resonance frequency the MR signal is characterized by lifetime parameters that capture the return of the system to the equilibrium as well as other stochastic processes in the system. Therefore these relaxation processes are described by more than one parameter: T1 describing the return of the system to equilibrium, and T2 describing the stochastic interaction of the ensemble of nuclear magnets. It turns out that these parameters are tissue specific and hence constitute an intrinsic source of contrast in MRI. By adjusting the timing variables of pulse excitation images with different degrees of contrast may be generated (e.g. T1- or T2-weighted contrast) [165, 166, 168]. Contrast may be enhanced by administration of contrast enhancing agents such as gadolinium (Gd) complexes. The contrast agent reaches the tissue through transport via the blood vessels. Contrast enhanced MRI allows to estimate tumor volume of brain cancer as the intrinsic contrast is in many cases not sufficient for a

clear distinction between proliferative and normal tissue [166, 169]. Dynamic contrast enhanced MRI (DCE MRI) is a method that measures the uptake of the contrast agent over a period of time, giving information about the tumor perfusion and, if the contrast agents leaks out of the vasculature, on vascular permeability [164, 166, 170]. Such measurements allow assessing the integrity of the blood vessels. Newly formed blood vessels as found in tumor angiogenic regions are leaky and permeability is accordingly higher than in tissues displaying little angiogenesis or in normal tissues with more mature blood vessels. For example it has been shown that glioblastomas show significantly higher permeability values than low grade gliomas [171].

1.3.2 PET imaging

Positron emission tomography (PET) is a three dimensional nuclear imaging technique that allows to measure biochemical and physiological processes within the body (Table 3) [27, 168, 188]. The mechanism of PET imaging is based on the nuclear decay of radioactive elements such as ^{11}C, ^{13}N, ^{15}O, and ^{18}F, which stabilize by emission of a positron. Positrons are positively changed electrons, i.e. antimatter particles which have a short lifetime in matter. They are captured by electrons. In the annihilation process of prositrons and electrons the mass of the particle is converted into energy in the form of two γ-rays that can be measured by detectors that are located around the subject (Fig. 9) [172]. PET, like MRI, is an expensive technique with a lower spatial resolution but significantly higher sensitivity that makes it ideal for investigating molecular processes. A restriction of PET is the short half-life of the radionucleotides and correspondingly the resulting tracers [168, 172]. The half-life of fluorine-18 is 110 min, which is longer than some other radionucleotides used to label organic molecules, which constitutes an advantage [172]. For example [^{18}F]-2-fluoro-2-dexoglucose ([^{18}F]-FDG) is a frequently used PET tracer for measuring tissue glucose utilization. FDG mimics glucose: it is taken up by tissue via glucose transporters and then phosphorylated by hexokinase. Further processing does not occur due to the absence of the hydroxyl group at the 2-position; hence phosphorylated FDG is trapped in the cell and the measured activity is considered a surrogate for glucose consumption. FDG is widely used in tumor studies due to the high glucose consumption of cancers as a consequence of the shift to aerobic glycolysis, as previously mentioned. [^{18}F]-FDG can also pass the blood brain barrier. This tracer is highly up-taken by high grade glioma but not by low grade

tumors, hence it allows the rating of the glioma grade [27, 172, 173]. Another well established fluorine-based PET tracer is [^{18}F]-fluoromisonidazole ([^{18}F]-MISO) that allows monitoring hypoxic areas within tumors including glioblastoma [27, 172].

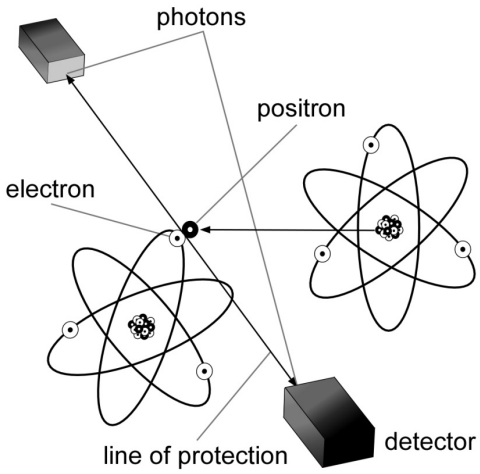

Figure 9. Process of positron annihilation in PET. Through the positron annihilation process two photons are built that travel in the opposite direction and can be measured by a detector. Adapted from Blokland et al. 2002 [172].

1.3.3 Non-invasive optical imaging

Optical imaging techniques such as bioluminescence or fluorescence imaging enable the investigation of molecular mechanisms and are widely used in preclinical studies. These techniques are based on photons of specific wavelength that transverse the tissue [174]. Short wavelength light is highly absorbed by tissue substrates such as hemoglobin or water and has the potential to travel only through a few millimeters of tissue (Fig. 10) [174, 175]. Red shifted luciferase or fluorophore proteins allow a deeper tissue penetration as their wavelengths are not absorbed by the surrounding tissue [174-176].

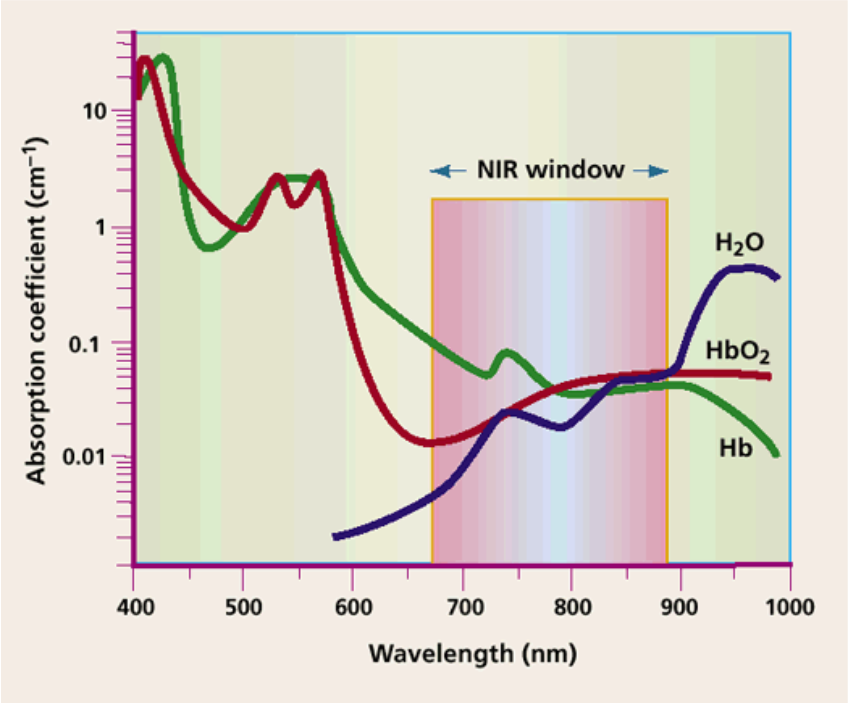

Figure 10. Tissue absorbance. The near-infrared (NIR) window is an optimal range *for in vivo* imaging approaches. Within this frequency the tissue absorption is minimal. Absorption of hemoglobin (Hb) is high <650nm and >900nm for water. Adapted from Weissleder 2001 [177].

a) Bioluminescence imaging of genes of interest such as HIF in tumor mouse model

Bioluminescence is a natural phenomenon observed in several organisms such as bacteria and firefly species. These organisms manage to transform chemical energy into light which they use for example to attract potential mating partners [178]. Almost all known bioluminescence systems are based on a luciferase enzyme. Luciferase catalyzes the reaction of molecular oxygen with luciferins and the resulting excited state intermediate returns to a state of lower energy leading to photon emission [178].

In vivo bioluminescence imaging is a widely used reporter gene technique for preclinical studies that allows observing the regulation of a specific gene in a non-invasive, longitudinal way [174]. This is particular attractive as bioluminescence is not observed in mammalian tissue and hence there is no intrinsic background signal to be dealt with as e.g. when using fluorescence techniques [174, 176, 178]. Bioluminescence imaging offers several advantages: the method is relatively inexpensive, typically the photon flux is high enough to allow for short scanning times of about 1 to 5 minutes,

the field of view of the cameras used allows for simultaneous measurement of multiple mice, which enhances the efficiency of the method; data analysis is relatively simple and involves the determination of photon flux in a specific region of in terest (Table 3) [176, 179]. On the other hand there are also some disadvantages such as the two-dimensional imaging acquisition and a low spatial resolution of the order of a few mm (depending on the depth of the signal source within tissue) due to photon scattering by biological tissue [176, 179]. In order to use bioluminescence imaging cells have to be previously prepared by introducing a luciferase gene under the control of a gene of interest or a specific promoter sequence (Fig. 11B) [174].

Bioluminescence imaging relies on the processing of the substrate (D-luciferin for firefly luciferase, coelenterazine for Renilla luciferase) by the respective luciferase, which is an oxygenase. The reaction requiring the cosubstrates O_2 and ATP (latter only for firefly luciferase) yields an oxygenated product in an excited state that relaxes through photon emission, which is measured by a charged-coupled device (CCD) camera [174, 180]. The photon count constitutes a measure of the expression of a target gene that is coupled to the levels of luciferase expression [176]. Bioluminescence imaging requires cells that were engineered in a way that the reporter gene luciferase is expressed under the control of a specific constitutive or inducible gene promoter (Fig. 11A) [176, 180, 181]. This *in vivo* imaging reporter gene assay allows non-invasive real time imaging, which can be repeatedly performed over time to monitor changes in gene expression in a longitudinal manner. Therefore a comparatively small numbers of experimental animals may be sufficient for obtaining statistically relevant results [180, 181].

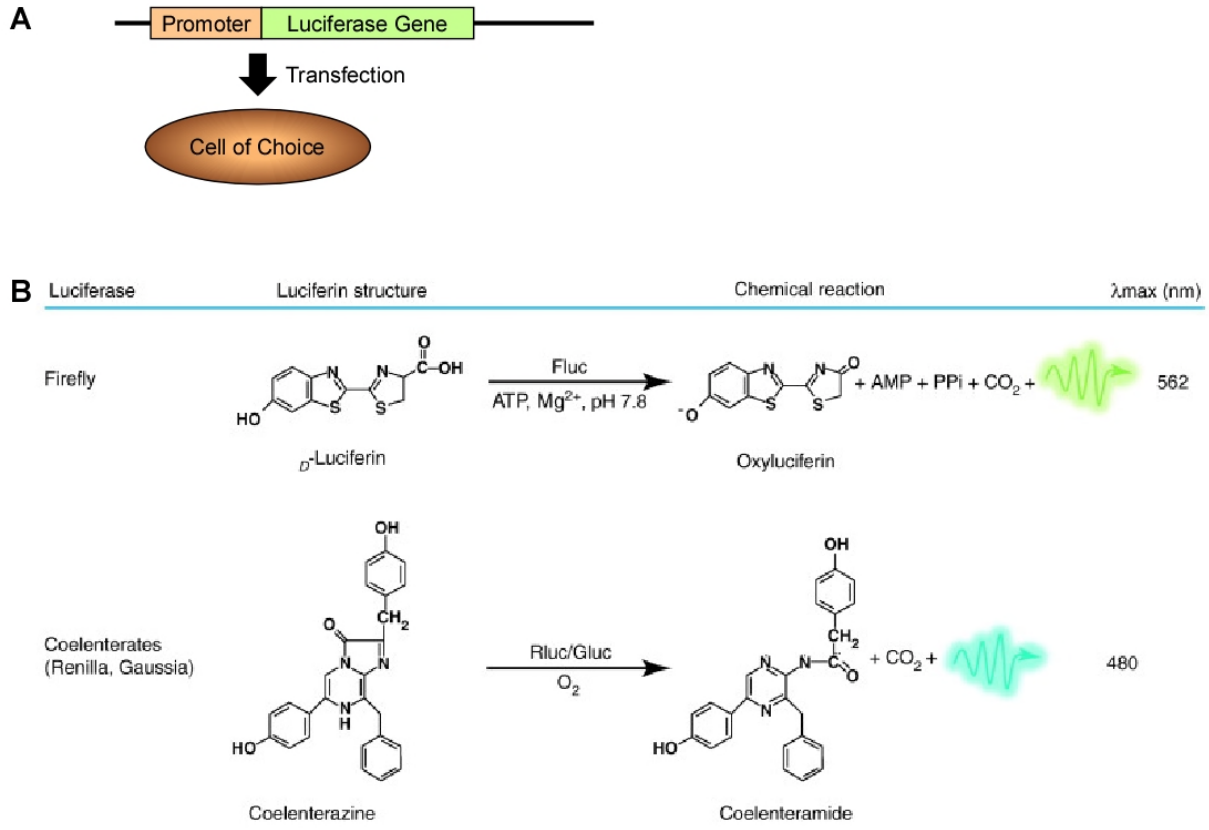

Figure 11. Bioluminescence Imaging. A. Bioluminescence expression construct containing a luciferase gene that is expressed under the control of a promoter. The construct is transfected into a cell of interest. **B.** Bioluminescence reaction of luciferase of Firefly luciferase (Fluc) and Renilla luciferase (RLuc) respectively Gaussia luciferase (Gluc). The catalytic reaction depends on specific cofactors and leads to a luciferase specific peak in light emission (λ_{max}). Adapted from Sato et al. 2004 [180] and Badr and Tannous 2011 [182].

Firefly (*Photinus pyralis*) luciferase (fluc) is one of the most often used bioluminescence genes for reporter gene assays. The intraperitoneal injection of its substrate D-luciferin in experimental animal is sufficient because luciferin distributes rapidly throughout the whole animal, even across the blood brain barrier. A peak in signal intensity is reached approximately 10 to 12 minutes after injection and within a period of 60 minutes the signal decreases slowly [174, 176, 180, 182]. The green light emission of firefly luciferase peaks at about 562nm (Fig. 11B) [174, 180, 182]. Another widely used bioluminescence gene is originating from the sea pansy (*Renilla reniformis*) and compared to firefly luciferase (61kDa) is a small molecule with 36kDa. The catalyzing reaction of *Renilla luciferase* gene (rluc) results in a blue light emission peaking at about 482nm (Fig. 11B) [174, 180, 182]. Because the bioluminescence signal is based on an

enzymatic reaction where the substrate has to be administered, the reaction only take place on the locations where transfected luciferase is present and the system shows a weak background signal, which is predominantly due to photon scattering [174, 176, 180, 183]. The sensitivity of bioluminescence imaging depends on factors such as: the total cell count, the expression intensity of the reporter gene, the presence or absence of cofactors (O_2 and ATP), the time between substrate application and the measurement, as well as the spatial location of the bioluminescence signal source within the body [180]. *In vivo* bioluminescence imaging can be used to investigate genetic regulation, tumor progression, metastasis, treatment response, and tumor recurrence [174, 176]. The luciferase signal has been shown to correlate well with the tumor size in subcutaneous as well as in orthotopic brain tumors. Nevertheless, an increasing tumor size and necrosis can interfere in the correlation between the bioluminescence signal and the tumor volume [179, 180, 183]. Several studies with bioluminescence imaging have been performed to study processes related to tumor hypoxia and HIF signaling [190, 191]. Although oxygen is an essential co-substrate for the bioluminescence reaction the dependence on tissue oxygen levels appears to be uncritically, this is because the low luciferin concentration necessary to emit photons founds enough cosubstrates, even in hypoxic tissues. Even under severe hypoxic conditions with oxygen tension of 0.2%, a bioluminescence signal output of approximately 50% of its normoxia value could still be detected [184].

b) Fluorescence imaging

Fluorescence imaging is an alternative optical imaging method to bioluminescence. The mechanism of fluorescent imaging is based on the excitation of a fluorescent molecule (protein, fluorescent dye, quantum dot) at a specific wavelength and then on the measurement the relaxation of the fluorophore by emission at a red-shifted wavelength [168]. Large battery of fluorescence proteins have been designed covering a large spectrum of wavelengths. The different fluorophores containing specific brightness characteristics and photostabilities can be used as well for multiple labeling [185, 186]. Chromophores in biological organisms, such as hemoglobin or collagen, can absorb light of short wavelengths and relax by so-called autofluorescence. This short wavelength light has the potential to penetrate tissue only a few millimeters [174]. Near-infrared (NIR) fluorescence has a wavelength spectrum from approximately 650

to 1000nm (Fig. 10). At these wavelengths the biological chromophores are absorbing light very weakly, which means positively improves the utility of NIR fluorescence due to autofluorescence is the lowest and measurements of a few centimeters depth are possible [174, 175].

Table 3. Overview about different imaging techniques. Weissleder and Pittet 2008 [188].

Technique	Resol.	Penetr. Depth	Time	Quant.	Imaging agents	Target	Cost	Main-small-animal use	Clinical use
Magnetic resonance imaging (**MRI**)	10-100µm	No limit	Min/ hours	Yes	Paramagnetic chelates, Magnetic particles	Anat. Physiol .Mol.	High	Versatile imaging modality with high soft-tissue contrast	Yes
X-ray computed tomography (**CT**) imaging	50µm	No limit	min	Yes	Iodinated molecules	Anat. Physiol .	Med.	Imaging lungs and bones	Yes
Ultrasound imaging	50µm	cm	Sec/ min	Yes	Microbubbles	Anat. Physiol .	Low	Vascular and interventional imaging	Yes
Positron emission tomography (**PET**) imaging	1-2mm	No limit	Min/ hours	Yes	^{18}F, ^{64}Cu- or ^{11}C labeled compounds	Physiol .Mol.	High	Versatile imaging modality with many tracers	Yes
Single photon emission tomography (**SPECT**) imaging	1-2mm	No limit	Min/ hours	Yes	^{99m}Tc- or ^{111}In-labelled compounds	Physiol .Mol.	Med.	Imaging labeled antibodies, proteins and peptides	Yes
Fluorescence reflectance imaging (**FRI**)	2-3mm	<1cm	Sec/ min	No	Photoproteins, Fluorochromes	Physiol .Mol.	Low	Rapid screening of molecular events in surface-based disease	Yes
Fluorescence mediated tomography (**FMT**)	1mm	cm	Min/ hours	Yes	Near-infrared fluorochromes	Physiol .Mol.	Med.	Quantitative imaging of fluorochrome reporters	In dev.
Bioluminescence Imaging (**BLI**)	Several mm	cm	min	No	Luciferins	Mol.	Med.	Gene expression, cell and bacterium tracking	No
Intravital microscopy (confocal, multiphoton)	1µm	<400µm	Sec/ hours	No	Photoproteins, fluorochromes	Anat. Physiol .Mol.	High	All of the above at higher resolution but limited depth and coverage	In dev.

HResolution (Resol.), Penetration (Penetr.), Quantitative (Quant.), In development (In dev.), Medium (Med.), Cost indication are relative.

In vivo imaging using fluorescent proteins as signal sources can be used to build reporter gene assay approaches analogous to those in bioluminescence imaging investigating molecular events or treatment responses. Frequently, such assays are established pursuing a multimodal strategy to simultaneously image different processes, e.g. tumor growth and HIF pathway activity [174, 175, 181, 187]. Different to bioluminescence imaging, fluorescence imaging can further be used to follow the fate of administered exogenous fluorescent agents that can be injected and detected by binding to a target molecule. This is a promising application for clinical treatment

modalities in patients, as fluorescent *in vivo* imaging is a fast and economic method to image molecular or cellular events [174, 175]. The disadvantages of this technique include the background signal present due to autofluorescence, as well as the potentially weak photostability of the agents that might result in a fast photobleaching and hence loss of the signal [168, 185].

1.4 Aim of the present study

Intratumoral hypoxia is a critical factor in tumor development triggering key processes such as: angiogenesis, enhanced glycolytic metabolism, enhanced probability of tissue invasion and the formation of metastases [73]. Hence hypoxia is typically associated with increased malignancy and poor prognosis for the patient [37]. In addition hypoxic tumor tissue and surrounding regions are treatment resistant because of restricted therapy delivery efficiency (poor perfusion). Resistance against radio- and chemotherapy in hypoxic tumors is further increased due to the lack of enough oxygen to build tissue damaging oxygen derived ROS [41, 42]. Therefore, assessing hypoxia and hypoxia signaling during tumor growth is essential in the search for alternative treatment strategies. A critical aspect in the development of hypoxia is the microenvironment in which a tumor develops. For example it has been shown in murine mammary carcinoma models that the architecture of the tumor vasculature and, as a result, tumor perfusion and the probability of developing hypoxic domains critically depends on the implantation site (subcutaneous, mammary fat pad, brain) [189]. Hence comparing hypoxia signaling for different tumor locations may bring important insights into the influence of the microenvironment on glioblastoma outcome.

The specific objectives of this PhD thesis were:

1. **To develop imaging strategies which monitor HIF signaling in the experimental glioma model.**

   Investigating the HIF pathway is a challenge as it is difficult to target an intracellular effect by exogenous probes. Analogous to the colon cancer model where a transient HIF pathway induction along the tumor growing process could be shown [190], in this work several glioma cell lines will be evaluated for this purpose. The luciferase reporter gene assay has been successfully

established to investigate the HIF pathway in a non-invasive manner, longitudinally during the tumor growth process in different models such as in subcutaneous colon cancer allografts as well as in orthotopic glioblastoma tumor models [190, 191].

2. **To monitor HIF activity as a function of time in subcutaneously and orthotopically implanted tumors and link HIF to downstream processes such as GLUT1/CA9 expression or angiogenesis**

   For the *in vivo* testing stably transfected tumor cells will be implanted at two different anatomical locations (subcutaneous and orthotopic) to compare the impact of the implantation site on the degree of tumor hypoxia, HIF signaling and the induction of HIF downstream products. Further we will investigate, whether the HIF down-regulation observed in the colon cancer model under conditions of persistent hypoxia [190], is also found in glioblastomas, i.e. whether glioblastoma also shows a temporo/special disconnection between hypoxia and hypoxia signaling.

2 Materials and Methods

2.1 Cells

The experiments were performed with human glioblastoma cells LN229 and U87, and murine glioblastoma cells GL261 that were all kindly provided by the group of Prof. Michael Weller from the Department of Neurology at the University Hospital Zurich and with the VHL-deficient renal carcinoma cell line RCC4 [148]. Cells were cultured at 37°C and 5% CO_2 in Dulbecco's modified Eagle's medium high-glucose containing 4.5mg/ml glucose (DMEM, PAA) with 10% heat-inactivated fetal calf serum (FCS) and without additional antibiotics.

2.2 Production of stably transfected cell lines

LN229, U87 and GL261 glioblastoma cells were stable transfected with a pGL3 promoter vector (SV40-luciferase) (Promega) and a pGL(P2P)95bp (HRE-luciferase) construct kindly provided by D. Stiehl, Institute of Physiology, University Zurich, Switzerland. The luciferase gene in the pGL(P2P)95bp vector is regulated by a truncated PHD2 promoter as described previously (Fig. 12A) [190]. pGL(P2P)95bp or pGL3 were both transfected together with a neomycin resistance gene containing the pcDNA3.1 (Invitrogen) vector in a 10:1 ratio using polyethylenimine (Polysciences). For GL261/HRE-Luc, the transfection was done through electroporation with an Eppendorf multiporator by using linearized pGL(P2P)95bp and pcDNA3.1 vectors in ratio 10:1. 24h after the transfection the selection process was started by using culture medium in presence of antibiotic 1mM geneticin (G418, Cayman Chemical) in dimethyl sulfoxide (DMSO, Sigma-Aldrich). When cells restart to grow, after the cell dependent selection phase, they were plated into a 96-well plate (0.5 cells per well) for single cell colony selection. Single cell colonies were expanded for testing luciferase regulation.

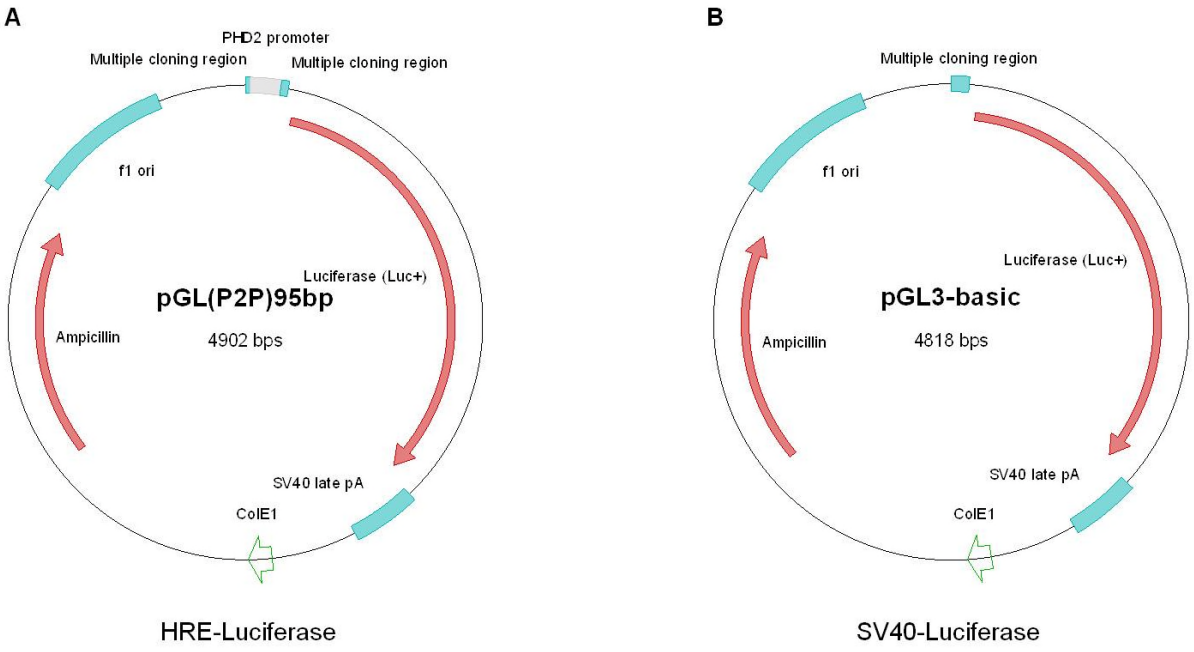

Figure 12. Transfection vectors. Schematic representation of **(A)** the used vectors of the pGL(P2P)95bp (HRE-Luc) vector and **(B)** the control vector pGL3-basic (SV40-Luc) vector.

2.3 Luciferase activity assay

Stably transfected LN229, U87 and GL261 cells were cultured in 6-well plates and incubated for 24h with dimethyloxalylglycine (DMOG, Cayman Chemical) at 1mM in DMSO (Sigma-Aldrich) or only with DMSO for 24 hours in triplicates. Probes were washed and incubated for 15min with 200µl of lysis buffer (Luciferase Assay kit, Promega) before collecting them. Luciferase signal was measured in the supernatant of the probes together with luciferase (Luciferase Assay kit, Promega) in a 1:1 ratio using a luminometer (Berthold technologies). Protein concentration of the collected probes was estimated by mixing 5µl probe supernatant with 995µl Bradford (Bio-Rad) and measuring the absorption at 595nm by spectrophotometer (UV-160A, Shimadzu). The measured luminescence data was calculated over the protein concentration of the measured probes.

2.4 Proliferation assay

Untransfected and stably transfected LN229, U87 and GL261 cells were plated in a 96 well plate at different cell densities (2'500, 5'000, and 10'000 cells per well in 100µl) by using Dulbecco's modified Eagle's medium high-glucose, without phenol red (Sigma-Aldrich) with 2mM of Glutamine (PAA) and 10mM of HEPES buffer (PAA). After two days of cell growing the 10µl CCK-8 solution was added rapidly to the wells. The absorbance at 450nm was measured at different time points during 4h using a Syngery HT multi-mode microplate reader (BIO-TEK).

2.5 Immunoblot assay

Cells were incubated for appropriate time periods with DMOG, (Cayman) at 1mM in DMSO (Sigma-Aldrich) or only with DMSO. After washing the cells twice with cool PBS and adding high salt lysis buffer containing 0.4M NaCl, 0.1% Nonidet P-40, 10mM Tris-HCl pH 8.0, 1mM ethylenediaminetetraacetic acid, 1mM phenylmethylsulfonylfluoride, and protease inhibitor cocktail (Roche), cells were scratched and placed immediately on ice. The concentration of the extracted protein was measured by using a Bradford (Bio-Rad) assay as described before. Probes (10µg/well for the kinetic and 20µg/well for testing of the transfection success) were loaded on a 10% SDS/PAGE (sodium dodecyl sulfate polyacrylamide gel) [192] and let run in a running buffer (25mM Tris, 190mM glycine, and 0.1% SDS in sterile H_2O) at 18mA per gel. The separated proteins on the SDS/PAGE gel were transferred to a nitrocellulose membrane (nitrocellulose membranes, 0.45µm, Bio-Rad) in the middle of filter paper (extra thick blot paper, Bio-Rad) presoaked in Towbin buffer (25mM Tris, 192mM glycine, 20% MeOH in sterile H_2O) for 1h at 65mA followed by 30min at 75mA using a semidry transfer setup (Bio-Rad). Blocking was performed for at least 1h with western blocking reagent (Roche) in TBST (10mM Tris HCl 1M pH 8.0, 150mM NaCl, 0.05% Tween-20 in sterile H_2O). Nitrocellulose membranes were incubated over night at 4°C with the first antibodies: Luciferase (Abcam, ab16366) 1/1'000, α-Actin (Milipore; MAB1501) 1/50'000, HIF-1α (Novus Biological NB100-479) 1/1'000, βIII Tubulin (Promega G712A) 1/2'000). After washing 3 times with TBST the horseradish-peroxidase-labeled antibodies were used as secondary antibody (goat anti-rabbit IgG, #31460, HRP, Thermo Scientific and goat anti-mouse IgG, #AP124P, Millipore) and incubated for 1h at room temperature. After washing 3 times with TBST the immune complexes were detected by SuperSignal West

Chemiluminescent Substrate (Thermo Scientific). Nitrocellulose membranes were shortly incubated in a mixture of the peroxide solution and the luminal/enhancer solution in a ratio 1:1 for 5min and exposed to X-ray films (Thermo Scientific) and were developed at a CAWO film processor (cawomat 2000 IR).

2.6 Mouse model and glioblastoma cell implantation

The study was performed in compliance with the Swiss Law of Animal Protection and approved by the Cantonal Veterinary Office in Zurich (License ZH 168/2010). Immunodeficient Crl:CD1-*Foxn1*^{nu} mice (CD-1® nude mice, from Charles River) were used in this study. For the subcutaneous tumor model 2.5 x 10^6 stably transfected GL261, 5.5 x 10^6 stably transfected LN229, and 1.0 x 10^7 stably transfected U87 cells in PBS/HBSS (both Gibco) solution (1:1) with 30% matrigel (BD) were injected subcutaneously into the left flank of 9 to 11 week old CD-1® nude mice (Charles River). For the intracranial tumor model 9 to 11 week old CD-1® nude mice were anesthetized with isoflurane (Abbott Laboratories), applied analgesic flunixine (Graeub AG) 5µg/g body weight i.p. and fixed into a stereotactic frame (ASI Instruments including additional mouse adaptor and mouse gas anesthesia mask form KOPF). Mouse brain skin was disinfected with braunol (B/Braun) before a skin incision was made along the midline and the scalp was retracted. The hole into the skull was made by hand with a 25 gauge needle 1mm anterior to the bregma and 1.5mm right to the midline. A 26 gauge blunt needle 5µl glass syringe (Hamilton) was inserted 4mm deep into the brain and retracted 1mm backward. 2µl of stably transfected GL261 cells (10^4 cells/µl) were injected over a period of 2min. The syringe needle was left in position for another two minutes and then slowly retracted with a velocity of 1mm/min. The hole in the skull was closed with bone wax (Ethicon) and the skin wound was closed with two stitches using a polypropylene twine (Premilene). Mice recovered in a warmed and ventilated recovery chamber (Harvard apparatus) before placed back to the cage. During one week after the surgery the mice were treated with antibiotic in their drinking water (1ml Borgal (intervet) per 500ml drinking water).

2.7 *In vivo* Bioluminescence Imaging

Mice with GL261, LN229 or U87 tumors were anesthetized with isoflurane (Abott Laboratories) at a concentration 1.5% in an oxygen/air mixture. Ten minutes after intraperitoneal injection of 100µl firefly D-Luciferin (15mg/ml, Caliper Life Sciences) in PBS (DMEM, PAA) bioluminescence signals were detected for different exposure periods between 300 to 10 seconds with small binning by an IVIS 100 (Caliper Life Science) for the subcutaneous tumor bearing mice, respectively an IVIS Spectrum imaging system (Caliper Life Science) for the intracranial tumor bearing mice. Images of 30 seconds exposure time for s.c. GL261 tumors, 3 minutes exposure time for i.c. GL261 tumors and 5 minutes exposure time for s.c. LN229 and s.c. U87 tumors were analyzed with Living Imaging software® 2.6 (Xenogen). A ROI was drawn around the area comprising the bioluminescence intensity (threshold 5% of maximum intensity) and the total number of counts within the ROI as well as its area was determined.

2.8 Magnetic resonance imaging

MRI experiments were performed on a 4.7T (Tesla) animal MR system (Pharmascan 47/16 MRI system, Bruker BioSpin GmbH) using a cryogenic quadrature transmit-receive coil. Anesthetized mice (3% of isoflurane, Abott Laboratories in an air/oxygen mixture 80%/20%), were placed on a cradle specially designed for mouse imaging. In order to maintain the anesthesia for the duration of the experiment, 1.5% of isoflurane in an air/oxygen mixture (80%/20%) was provided to the animal via facemask. Stereotactic fixation was used to avoid head movement during imaging acquisition, and the body temperature was maintained at 37°C using warm water pipes. Spin echo images using the rapid acquisition with relaxation enhancement (RARE) were acquired with following parameters: repetition time/echo time TR/TE = 1000/8ms, field of view FOV = 110µm x 110µm, slice thickness (SLTH) = 600µm in coronal, sagittal and horizontal orientation 1min following the intravenous administration of contrast agent (Dotarem, 0.5mmol Gd/ml, Guerbet S.A.) via the tail vain.

2.9 Tumor volume determination

Volume of the subcutaneous tumors was calculated according to tumor volume formula:

$$tumor\ volume = \frac{length \cdot width^2}{2}$$

(assuming a prolate shape) using caliper measurements. Growth rates were estimated by carrying out a regression analysis assuming exponential tumor growth:

$$y = a \cdot e^{(kx)}$$

The intracranial tumor volume was estimated from the MRI images. The tumor area within individual slices was determinated using the ImageJ software (version 1.47n). The procedure was repeated for the data sets recorded in transverse, sagittal and horizontal orientation and the respective values averaged. As MRI measurements were only carried out at three time points, volume values for intermediate points were estimated using a regression curve assuming exponential tumor growth. For the analysis only data sets from mice measured at all time points was included.

2.10 Immunofluorescence on tissue sections

For histological analysis of hypoxia on the tumors, tumor bearing mice received an i.v. injection of the hypoxia marker pimonidazole (Hypoxy Probe; Natural Pharmacia International; 1.2mg of pimonidazole in 100µl of PBS). After one hour the mice were then i.v. perfused with Hoechst stain (Sigma H33342; 0.5mg in 100µl PBS per animal) for 2min before being euthanized by cervical dislocation. Tumors were excised and suddenly dry ice frozen. The frozen tumor tissue was embedded in Neg-50 Frozen Section Medium (Microm International AG) and sectioned into 12µm thick cryosections using a HYRAX C60 cryostate (Zeiss). Cryosections were stained fixed in 4% PFA (paraformaldehyde, Electron Microscopy Science) for 10 min and washed with PBS (Gibco). Sections were incubated over night at 4°C with the following first antibodies: CD31 (Novus; NB100-1642) 1/1'000, pimonidazole (FITC-MAb1, Hypoxyprobe-1 kit; Natural Pharmacia International) 1/1'000, HIF-1α (Novus; NB100-479) 1/1'000, HIF-2α (Novus; NB100-122) 1/1'000, GLUT1 (Abcam; ab14683) 1/1'000, CA9 (Novus; NB100-417) 1/4'000, Ki67 (Abcam; ab1558) 1/1'000. After 3 times washed with PBS (Gibco) secondary

antibodies Alexa-Fluor 594-coupled IgGs (for goat anti-rat, A-11007 and goat anti-rabbit, A-11012, Life Technologies) at a dilution of 1/1'000 were incubated for 1h at room temperature. Sections were washed 3 times with PBS (Gibco), let to dry and mounted with DAKO mounting medium (DAKO fluorescent mounting medium). Tumor sections were imaged by using the Mirax Midi Slide Scanner (Zeiss) with a 20X objective. For the immunofluorescence analysis only tumors have been included where both pre-terminal injections (pimonidazole and Hoechst stain) could be successfully performed (subcutaneous tumors N=13, intracranial tumors N=10).

2.11 Statistical Analysis

As statistical analysis for the Luciferase assay and the bioluminescence induction, an unpaired 2-tailed student's t-test was performed using GraphPad Prism (version 5.02). A linear mixed model analysis was conducted on the bioluminescence induction in the subcutan and orthotopic GL261 tumor bearing mice using the statistical software R version 2.13.0 (The R Foundation for Statistical Computing, Vienna, Austria) using the lme4 package. A model with time, group and their twofold interactions as fixed effects was designed, and the animal intercepts were set as random effects. A square root transformation was applied on the signal to improve the normality of the residuals. The effect of the group x time interaction as well as the two factors was tested with Likelihood Ratio Tests. A residual analysis of the mixed models was performed with QQ-plots to inspect normal distribution, Tukey-Anscombe plots for the homogeneity of the variance and skewness, and Scale Location plots for homoscedasticity (i.e. the homogeneity of residual variance). The assumption of normally distributed residuals was considered plausible in the subcutan group, and to a lesser extend in the orthotopic group. A statistically significant difference was indicated by a p value of less than $p=0.05$.

3 Results

3.1 Endogenous HIF regulation in the three tested glioblastoma cell lines

To investigate the intrinsic regulation of HIF1α and HIF-2α in hypoxic circumstances of the three glioblastoma cell lines LN229, U87 and GL261, cells were exposed to DMOG during different time periods ranging from 0 to 24 hours. DMOG exposure to cells in culture simulates a hypoxic environment because DMOG inhibits the PHD induced HIF degradation, leading to a stabilization of HIF-α levels and enhancing HIF activity as previously reported [190, 246]. HIF-1α and HIF-2α protein levels were analyzed using western blotting. For the analysis of the HIF-2α protein RCC4 cells which lack of VHL protein were used as positive controls to avoid the proteasomal degradation of HIF-2α thereby inducing HIF signaling even under normoxic conditions [148]. Increased HIF-1α protein expression was observed upon DMOG induced PHD inhibition mimicking hypoxic conditions in all three glioblastoma cell lines (Fig. 13A, 13C, 13D). LN229 glioblastoma cells showed a fast up-regulation of HIF-1α after 8h with a slightly decreased level at later time points (Fig 13A). Also HIF-2α induction was observed in LN229 cells under hypoxic simulation but the intensity of the induction seemed to be rather constant over the period from 8 to 24h (Fig. 13B). HIF-1α protein in GL261 was strongly up-regulated after 8h of PHD inhibition and between 16 and 24 h decreased to a level that was still slightly higher than the baseline levels (Fig. 13D). No HIF-2α induction could be detected in the GL261 cells (Fig. 13E). U87 cells showed a strong HIF-1α increase after 8h of DMOG exposure, with the induction peaking at 16h and afterwards reducing substantially (Fig. 13C). The HIF-2α protein analysis could not be successfully performed in U87 cells as the HIF-2α signal was not detectable by unknown reasons. All three tested cell lines displayed regulation of HIF-1α protein levels by PHD.

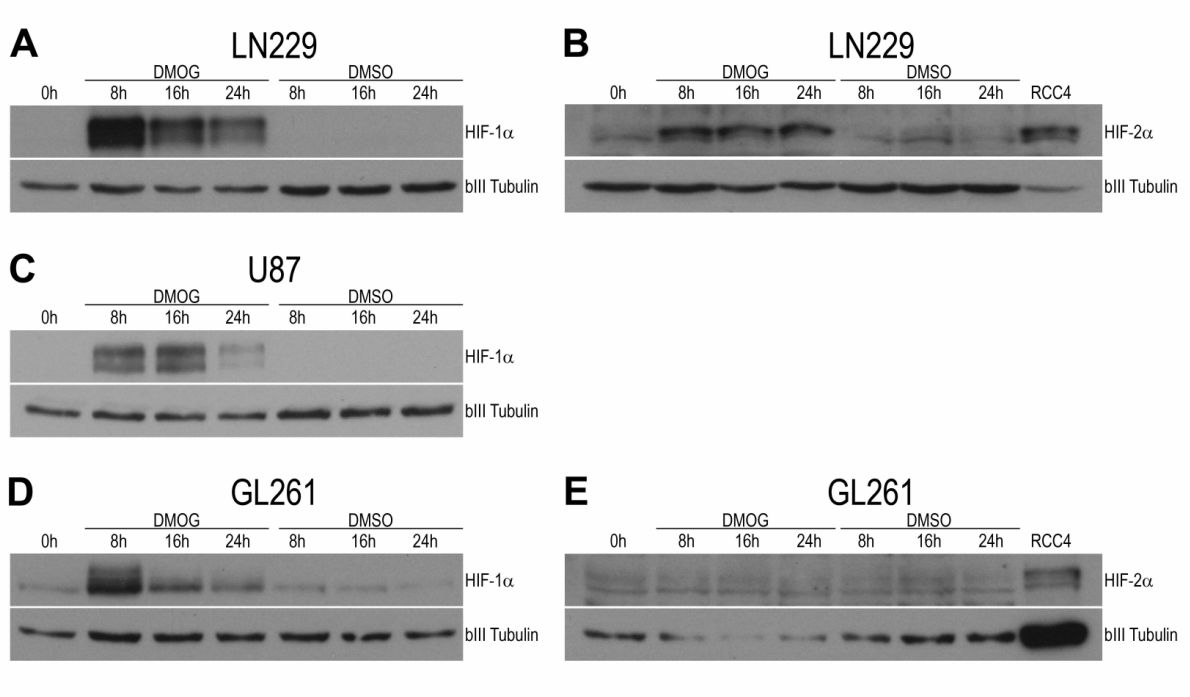

Figure 13. Regulation of endogenous HIF-α. Endogenous HIF-1α protein expression under hypoxic and normoxic conditions was measured by western blot analysis in the glioma cell lines LN229 (**A**), U87 (**C**), and GL261 (**D**). The cells were exposed to DMOG, to simulate hypoxia conditions, or to DMSO, as normoxic control, for different time periods from 0 to 24 hours. The regulation of the endogenous HIF-2α protein comparing hypoxic stimuli with normoxia was measured in LN229 (**B**) and GL261 (**E**) glioma cell lines using western blot analysis. RCC4 cells were used as positive controls for the HIF-2α protein and βIII tubulin detection was used as loading control.

3.2 HIF regulation behavior of transfected glioblastoma cell lines *in vitro*

Glioblastoma cell lines were stable transfected with either a HIF regulated HRE-Luc or a constitutively expressed SV40-Luc construct. The potential of the luciferase expression as reporter gene was investigated using a bioluminescence and western blot assays. Stably transfected cells were exposed to the hypoxia mimicking compound DMOG or to DMSO, as negative control, for 24 hours. LN229 and GL261 cells transfected with the control construct SV40-Luc showed no change in bioluminescence signal and luciferase protein levels upon hypoxia simulation (Fig. 14A, 14B and 14E, 14F). In contrast, the transfection of LN229 cells with the HRE-Luc construct showed a highly significant induction of the bioluminescence signal but only a relatively weak up-regulation of the luciferase protein level upon DMOG stimulation for 24 hours (Fig. 14A and B). LN229/HRE-Luc cells showed significantly lower absolute bioluminescence intensity values compared to the other cell lines measured (Table 4), which might explain the

high induction level despite the low levels of HIF protein under hypoxic conditions (Fig. 14A and B). Even with the relatively low bioluminescence yield, transfected LN229 cells were used further. GL261 cells transfected with the HRE-Luc construct showed a distinct up-regulation in both the bioluminescence (factor 3.4) and the luciferase protein level after the DMOG simulated hypoxic conditions (Fig. 14E and F). Similarly, U87 cells transfected with the HRE-Luc construct showed a significant up-regulation of the bioluminescence signal (factor 3.9) upon PHD inhibition (Fig. 14C). The luciferase protein analysis by western blot illustrates an inconclusive result for the U87/HRE-Luc, whereby the unstimulated cells showed two bands (this was not observed for the other two cell lines LN229 and GL261) while the stimulated cells showed a dominant strong band (Fig. 14D). The U87/SV40-Luc cells showed a decrease in the bioluminescence signal and luciferase protein after 24 hours of DMOG exposure (Fig 14C and D). In another study U87 cells exposed for an extended period of time to DMOG revealed a lower viability (unpublished data). Therefore we conclude the U87/SV40-Luc cells are not recommended to be used for *in vivo* studies.

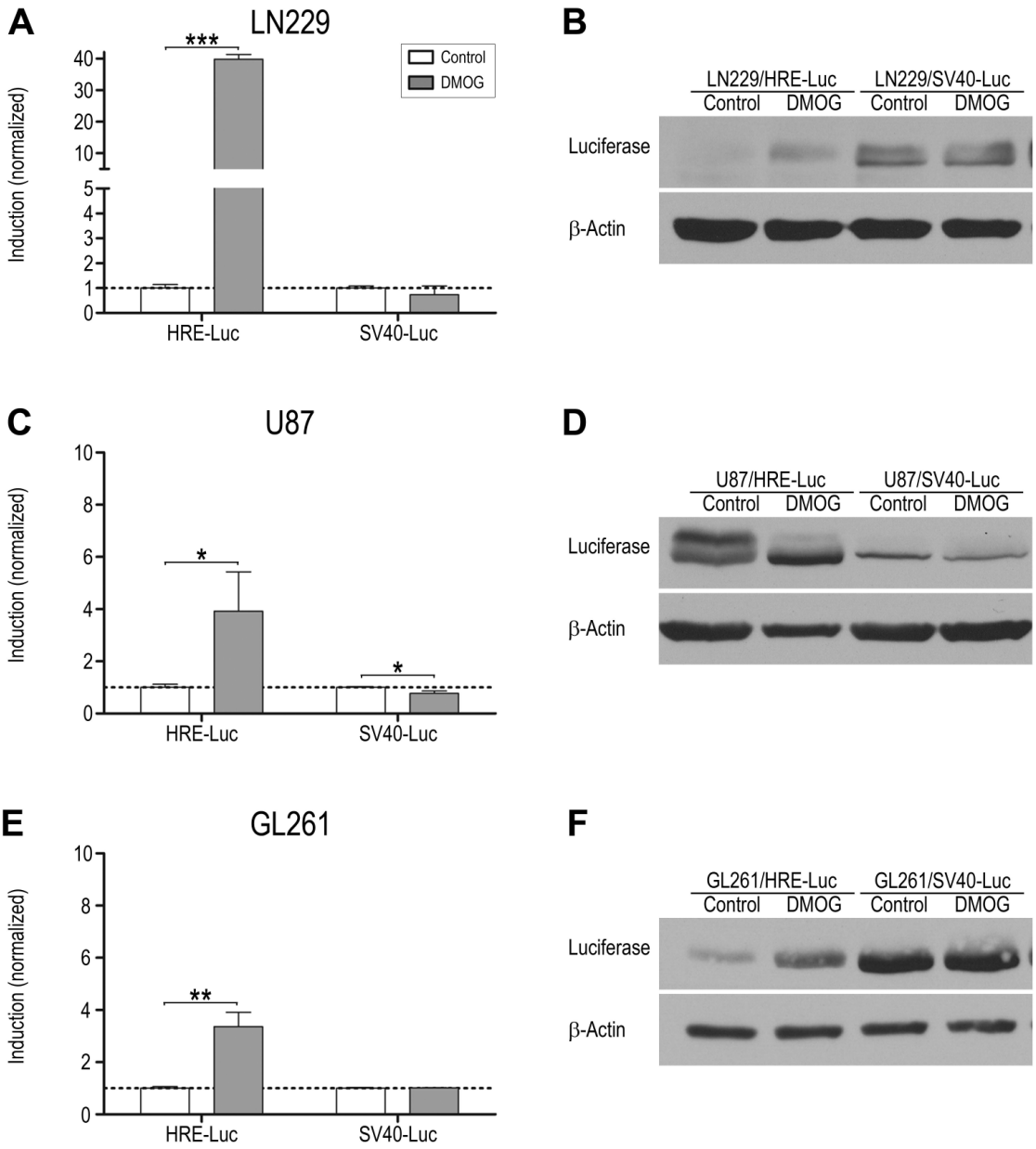

Figure 14. Stably transfected glioma cell lines. Resulting regulation potential was estimated by luciferase measurements for stably transfected LN229 (**A**), U87 (**C**) and GL261 (**E**) glioma cells and analyzing luciferase protein using western blot assay for LN229 (**B**), U87 (**D**), and GL261 (**F**) cells. Cells exposed to the PHD inhibitor DMOG for simulating a hypoxic situation or to DMSO as control for 24 hours in stably transfected LN229, U87 and GL261 cells. A significant luciferase induction in all three DMOG exposed cell lines transfected with HRE-Luc and no luciferase signal change between the DMOG and the control group was observed in LN229/SV40-Luc and GL261/SV40-Luc cells (**A**, **C**, **E**). Luciferase protein analysis is verifying the observed luciferase measurements for LN229 and GL261 (**B**, **C**) cells but not entirely for the U87 cells (**D**) All values are shown as mean ± SD.

Table 4 Absolute and normalized values of the luciferase induction upon PHD inhibition (DMOG) mimicking hypoxic stimuli or under control conditions (DMSO) of stably transfected cell lines LN229, U87 and GL261.

Tumor cell	Construct	Treatment	Counts/total protein concentration		t-test
			Absolute values ± SD	Normalized values ± SD	$p\text{-value}_{(Norm.\ values)}$
LN229	HRE-Luc	DMSO	0.37 ± 0.05	1.00 ± 0.138	<0.001
		DMOG	14.77 ± 0.58	39.73 ± 1.55	
	SV40-Luc	DMSO	234.69 ± 17.99	1.00 ± 0.077	0.2690
		DMOG	172.38 ± 82.32	0.73 ± 0.351	
U87	HRE-Luc	DMSO	467.15 ± 57.96	1.00 ± 0.124	0.0288
		DMOG	1830.76 ± 704.49	3.92 ± 1.508	
	SV40-Luc	DMSO	806.63 ± 21.06	1.00 ± 0.026	0.0156
		DMOG	620.31 ± 76.94	0.77 ± 0.095	
GL261	HRE-Luc	DMSO	88.96 ± 5.53	1.00 ± 0.062	0.0018
		DMOG	298.70 ± 48.92	3.36 ± 0.550	
	SV40-Luc	DMSO	2160.19 ± 63.27	1.00 ± 0.029	0.4768
		DMOG	2191.54 ± 31.67	1.01 ± 0.015	

3.3 Proliferation assay *in vitro*

To examine the effect of the transfection procedure on the cell lines, the proliferation behavior of untransfected and stably transfected cell lines was compared by means of a proliferation assay. Three different numbers of cells were plated and light absorbance was measured upon adding a CCK-8 solution to the cell culture dishes. Comparison of the untransfected LN229 cells, the LN229/HRE-Luc and the LN229/SV40-Luc cells demonstrated no significant difference in proliferation behavior between the cell densities of the plated cells for 2'500 and 5'000 cells/well. Only at the highest density studied (initially 10'000 cells/well) a difference between the LN229/HRE-Luc and LN229/SV40-Luc was observed (Fig. 15A). Comparison between untransfected, transfected with HRE-Luc and SV40-Luc constructs in U87 and GL261 cells showed a significant difference in the proliferation behavior *in vitro* between the different groups at all densities (Fig. 15B and C). For both parent cell lines, transfection with either of the constructs had a negative impact on the growth rate.

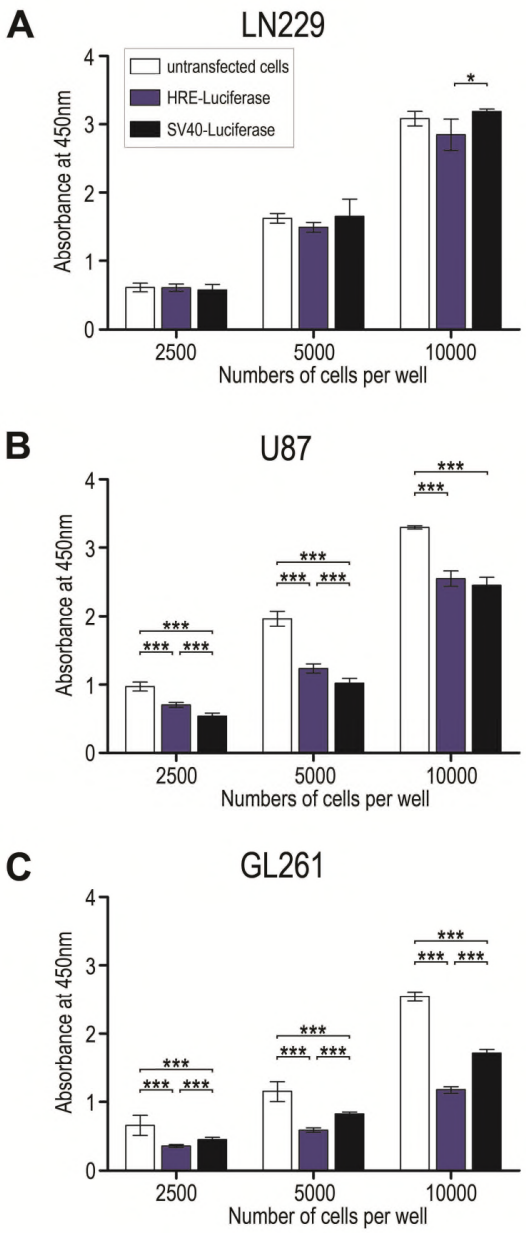

Figure 15. Proliferation behavior after stable transfection. Comparison of proliferation behavior between stably transfected cells with HRE-Luc and SV-40 constructs with untransfected cells of LN229 (**A**), U87 (**B**), GL261 (**C**) cell lines using a proliferation assay. Cells were plated at different confluences of 2'500, 5'000, and 10'000 per well. The proliferation could be measured by color change reaction after adding the substrate CCK-8 to the cell culture medium. LN229 cells in contrary to U87 and GL261 were in general not differing in the proliferation behavior. All values are shown as mean ± SD.

3.4 Evaluation of the HIF pathway regulation *in vivo* for three transfected glioblastoma cell lines

To test how the HIF pathway is regulated in the three glioblastoma cell lines LN229, U87 and GL261, the *in vivo* transfected cells were injected subcutaneously into the left flank of CD-1 nude mice. After cell implantation tumor growth was assessed periodically by caliper measurements. Bioluminescence measurements were initiated from day 11 to 13 following cell implantation. To take account for inter-individual variability the bioluminescence signal was normalized for each time point with regard to the respective tumor volume, and the bioluminescent signal/volume ratios expressed relative to the first measurement point. While this ratio should stay constant for LN229/SV40-Luc transfected cells, for HRE-Luc transfected cells it is expected to change over time as upon modulation of HIF signaling triggered changes in the tumor microenvironment. Both the implanted LN229/HRE-Luc and LN229/SV40-Luc tumors showed minimal or no growth behavior during the experimental period of 39 days after tumor injection (Fig. 16A). While the bioluminescence signal intensity of LN229/SV40-Luc tumors was fluctuating throughout the experimental period at a low emission level, the signal of LN229/HRE-Luc could not be detected (Fig. 16B and D). This is in line with the low absolute *in vitro* bioluminescence photon count measured for the transfected LN229/HRE-Luc cells (Table 4). Due to the absence of a bioluminescent signal in the LN229/HRE-Luc group an induction factor could not be calculated. The normalized bioluminescence intensity in LN229/SV40-Luc tumors showed an increase over time, yet with a large coefficient of variation (Fig. 16C). This increase was attributed to the fact that the tumors did not really develop, which rendered accurate volume determination difficult. For the experiments with U87 only the U87/HRE-Luc cells were tested *in vivo* as the U87/SV40-Luc cells showed to be negatively regulated by *in vitro* experiments. Contrary to the LN229 tumors, HRE-Luc transfected U87 tumors decreased in the apparent tumor volume with a function of time which could be approximated with an exponential decay with a rate of $k=-0.088\ day^{-1}$ (Fig. 17A). Correspondingly the bioluminescence signal intensity decreased over time to reach a plateau after 27 days (Fig. 17B and D). Again estimation of an induction factor is not meaningful and prone to large errors given the small volumes of the tumors toward the end of the experiment (Fig. 17C). In contrast to the previous cell lines the implanted GL261/HRE-Luc and GL261/SV40-Luc transfected cells showed pronounced proliferative activity that could be described by exponential growth behavior. GL261/HRE-Luc tumors

apparently grew slower than the control tumor GL261/SV40 with growth rates of $k_{(HRE-Luc)}$=0.11 day^{-1} and $k_{(SV40-Luc)}$=0.14 day^{-1}, yet this rate difference did not reach statistical significance; also there was no difference when comparing the tumor volumes at any given time point (Fig. 18A). The bioluminescence signal increased as a function of time from day 13 to 27 post-implantation with significant differences in bioluminescent signal intensities comparing GL261/HRE-Luc and Gl261/SV40-Luc at different time points (Fig. 18B and D). A significant transient induction of a factor of 7 (normalized photon counts per tumor volume) was observed in GL261/HRE-Luc tumors peaking at day 22 following inoculation and followed by a steady decrease until the end of the experiment (day 27). In contrast, the control group GL261/SV40-Luc yield constant normalized intensity values with fluctuating signals toward the end of the experiment (Fig. 18C). A significant difference between the normalized signal intensities of GL261/HRE-Luc and GL261/SV40-Luc groups was found around the peak of induction (days 18-22) by t-test analysis. By comparing both groups over time a highly significant difference was observed by a mixed model analysis indicated by a p value of the group to time effect (g:t) of 0.0004 (Fig. 18C).

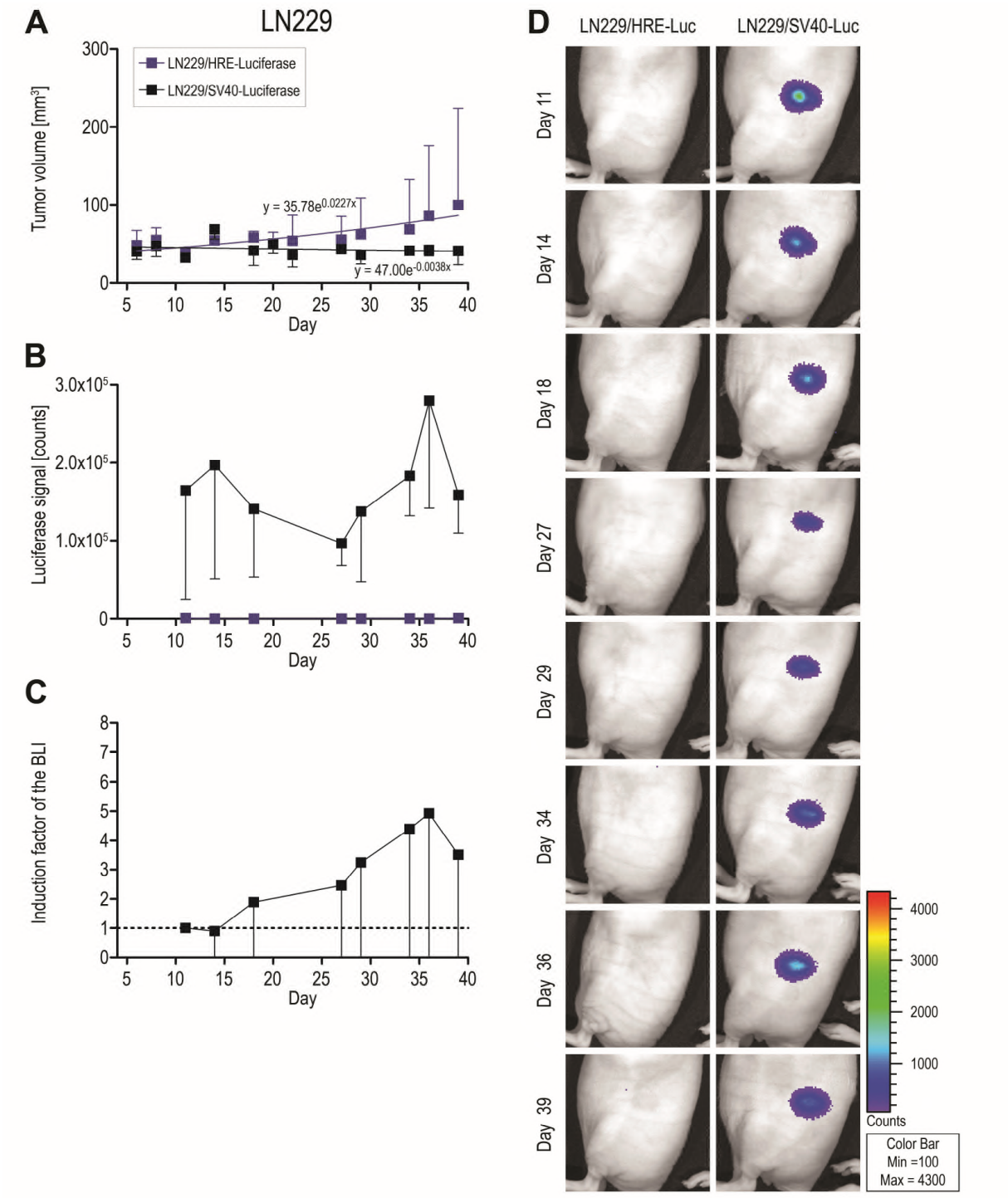

Figure 16. ***In vivo*** **bioluminescence signal in subcutaneous LN229 tumors. A.** Regularly measured tumors growth showed no clear change within the experimental period until day 39 after tumor cell injection. **B, D.** The measured bioluminescence signal showed a fluctuating signal for LN229/SV40-Luc and a not detectable signal for LN229/HRE-Luc tumors. **C.** Normalization of the bioluminescence signal over the tumor volume showed a slightly increasing signal for LN229/SV40-Luc tumors with a large standard deviation. All values are shown as mean ± SD.

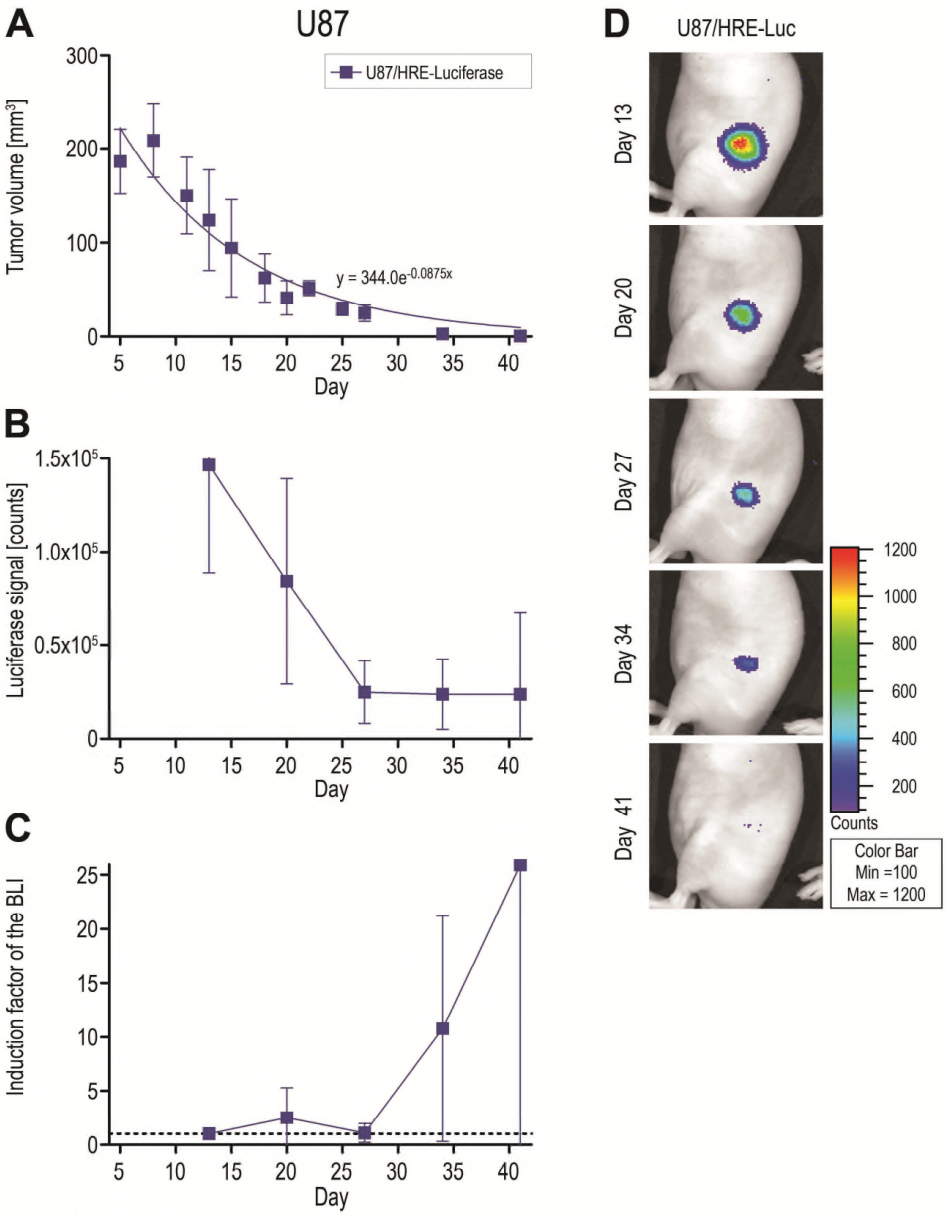

Figure 17. ***In vivo*** **bioluminescence signal in subcutaneous U87 tumors. A.** The implanted GL261/HRE-Luc tumors showed a decrease over the time of the experiment until day 41 after tumor implantation that fits well with a negative exponential regression line. **B, D.** The measured bioluminescence signal was decreasing until day 27 after tumor implantation and stayed at this level until the terminal measurement at day 41. **C.** Normalized signal over volume data showed a stable signal until day 27 p.i. and thereafter a signal induction with a large standard deviation until the terminal experimental day 41 after implantation. All values are shown as mean ± SD.

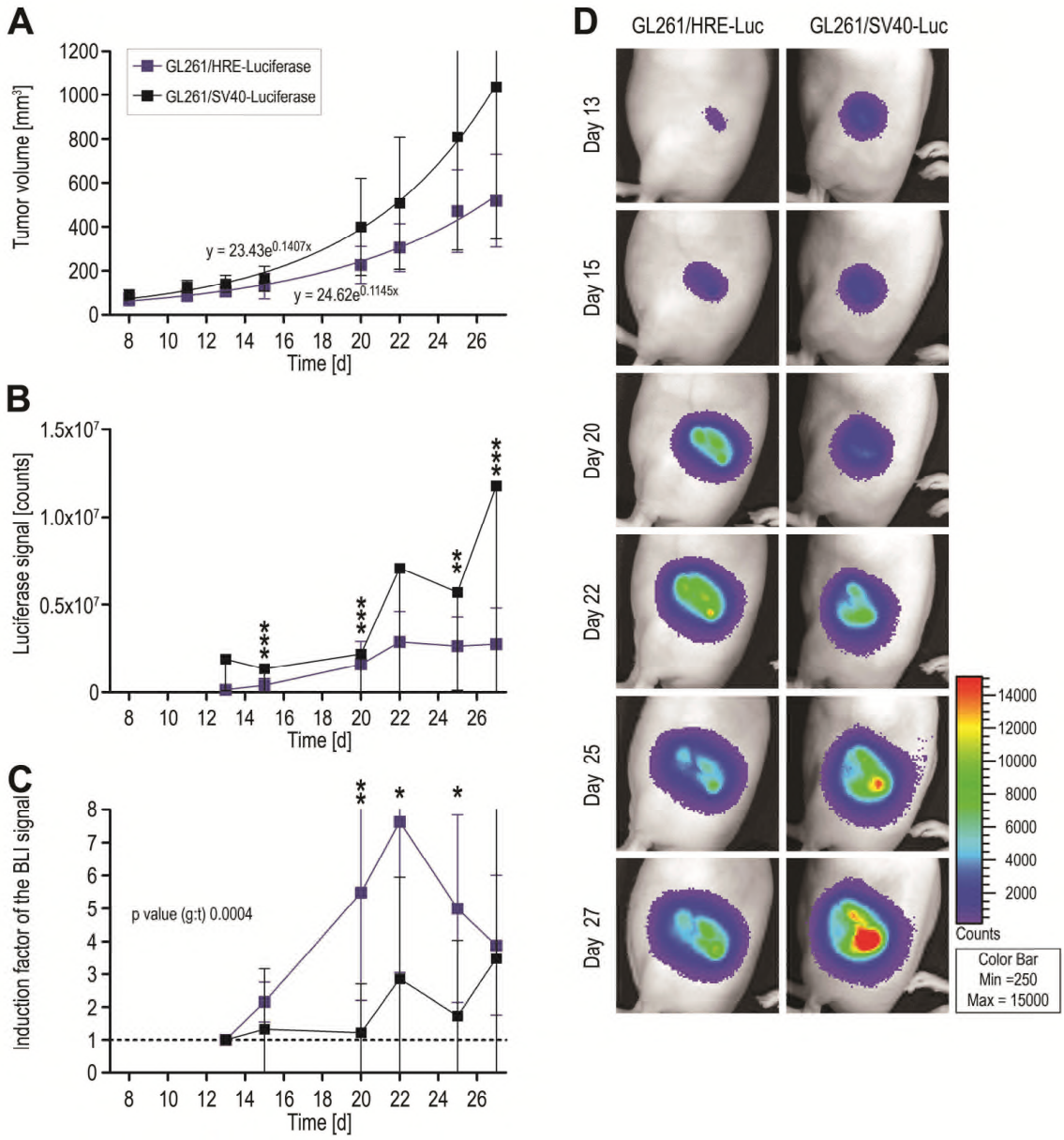

Figure 18. ***In vivo*** **bioluminescence signal in subcutaneous GL261 tumors. A.** Tumor growth was observed in the experimental period within 27 days after tumor cell implantation in both tumor groups GL261/HRE-Luc and GL261/SV40-Luc. **B**, **D.** Bioluminescence signal increases over time (from day 13 to 27 p.i.) whereby the GL261/HRE-Luc bioluminescence signal was in average at several time points significantly smaller than the signal measured in GL261/SV40-Luc tumors. **C.** A significant transient signal induction by a factor of 7.6 of normalized bioluminescent signal over tumor volume of GL261/HRE-Luc tumors was observed peaking at day 20 post implantation. The normalized signal of GL261/SV40-Luc stays at basal level until day 20 p.i. and thereafter the signal induction fluctuates until the end of the experiment. Group-time (g:t) interaction effect indicated a significant difference in normalized luciferase signal between GL261/HRE-Luc and GL261/SV40-Luc represented with p-values (**C**). All values are shown as mean ± SD.

Based on the experiments carried out with subcutaneously implanted tumors it was decided to carry out studies with orthotopic implantation using only the transfected GL261 cell lines. Hence, 2 x 10^4 transfected GL261 cells were injected intracranially into the right striatum of CD-1 nude mice. The intracranial tumor volume was determined by three MRI measurements. To improve the detectability of tumors, a gadolinium(III)-based contrast agent (GdDOTA), that does not cross the intact blood-brain-barrier but readily extravasates in the tumor extracellular space was administered (Fig. 19). This enables an accurate determination of the tumor boundaries in three orthogonal orientations. Volume determination was carried out at days 10, 17 and 24 following implantation (Fig. 19A, 19B and 20A). Volumes measures at days in between, which are required for the normalization of the bioluminescence signal, were calculated by interpolation assuming an exponential growth behavior. Similar to the subcutaneous GL261 tumors, the growth rate of the GL261/SV40-Luc group appeared faster than that of the GL261/HRE-Luc tumors though again the difference did not reach statistical significance. Growth rates corresponded to a volume doubling time of 3.6 days for the GL261/SV40 group (as compared to 4.9 days for the subcutaneous tumors), and 4.2 days (as compared to 6.1 days) for the GL261/HRE-Luc tumors (Fig. 18A and 20A). The measured bioluminescence signal was steadily increasing as a function of time (Fig. 20B and D). The normalized photon counts per volume of GL261/HRE-Luc tumors showed an induction factor of 3.2 between day 11 and 18. The GL261/SV40-Luc group stayed at basal level and after day 18 both groups showed an increased fluctuation until the end of the experiment (Fig. 20C). Analysis of the intracranial GL261/HRE-Luc group compared to the GL261/SV40-Luc group over time showed a significant difference indicated by the p value of the group – time interaction effect (g:t) of 0.0411 (Fig. 20C).

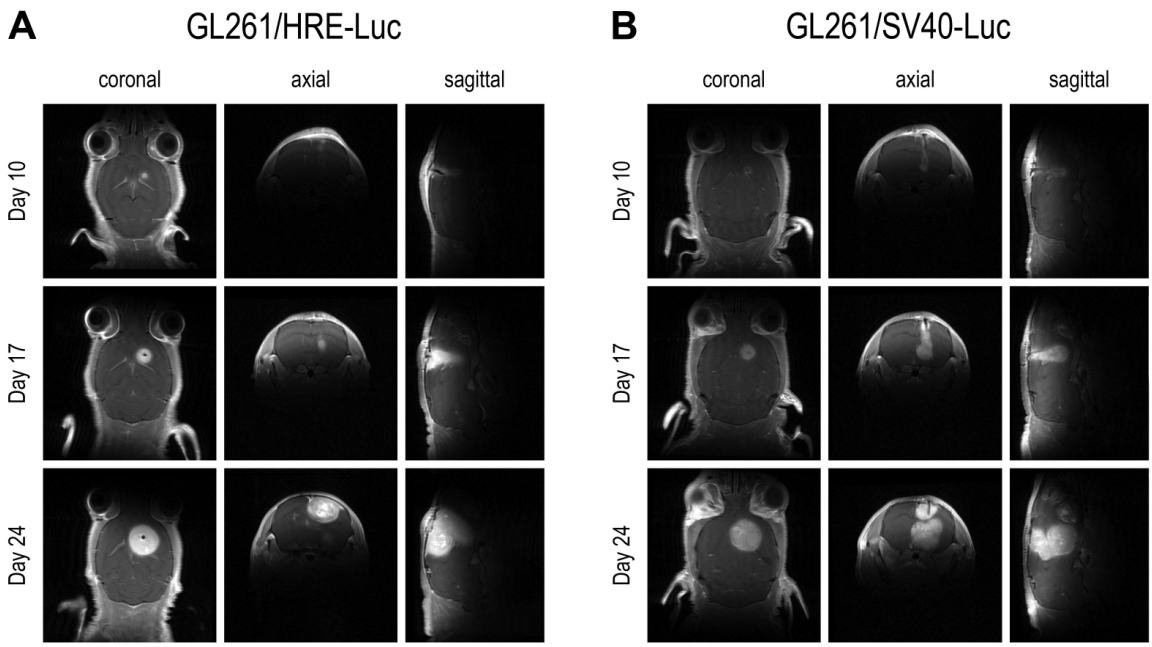

Figure 19. Intracranial tumor volume detection. Brain tumor volume was estimated by analyzing contrast enhanced MR images of nude mice with intracranial implanted GL261/HRE-Luc (**A**) and GL261/SV40-Luc (**B**) tumors. The images were recorded after the administration of the contrast agent Dotarem, which improves the contrast-to-noise ratio between tumor and brain tissue.

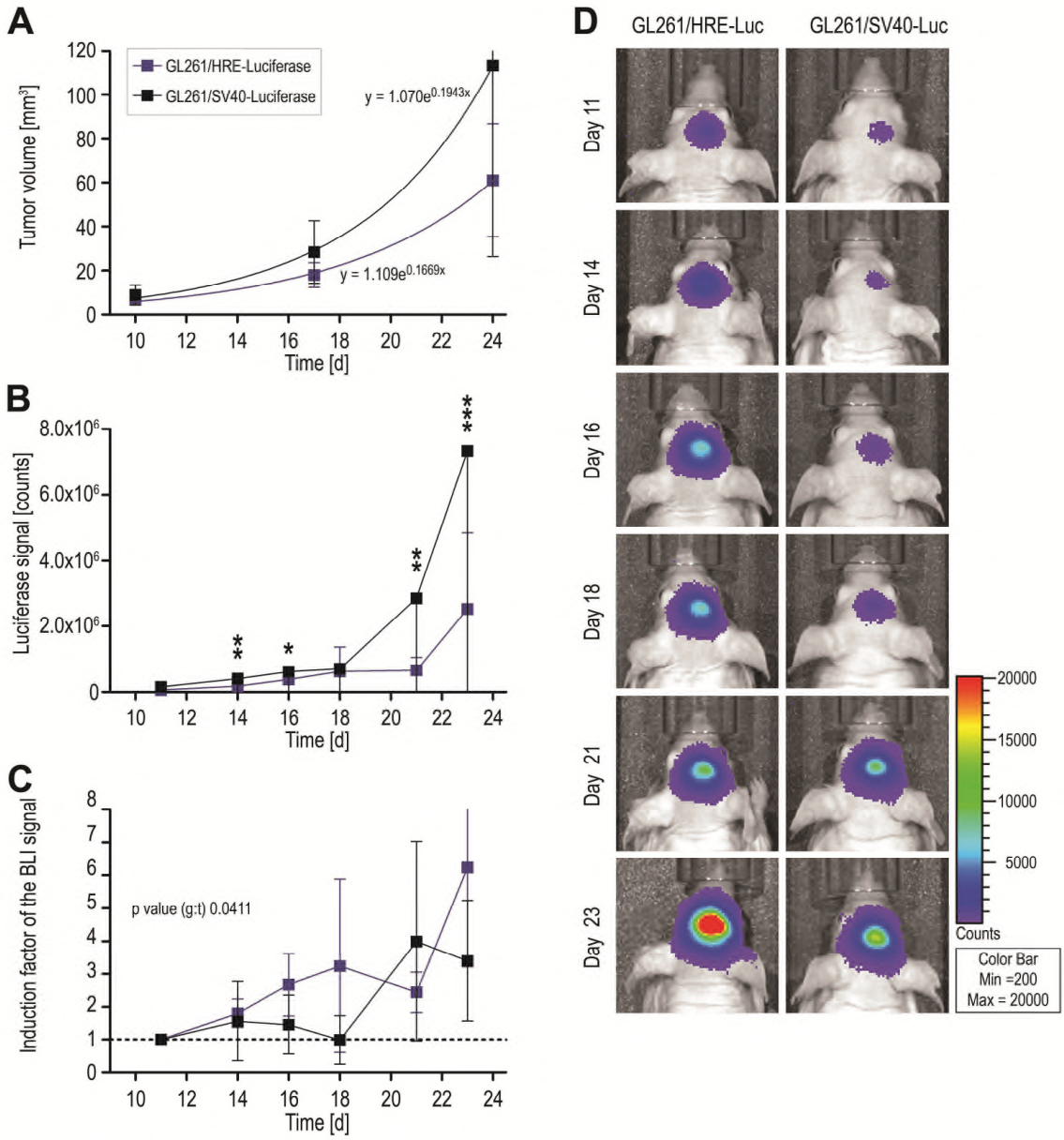

Figure 20. ***In vivo*** **bioluminescence signal in intracranial GL261 tumors. A.** Tumor growth was estimated by analyzing contrast enhanced MR images of GL261/HRE-Luc and GL261/SV40-Luc tumors. **B, D.** Bioluminescence signal only changed slightly until day 20 p.i. for GL261/HRE-Luc respectively day 18 p.i. for GL261/SV40-Luc tumors. **C.** The normalized bioluminescence signal over tumor volume indicates a weak induction by the factor 3.2 in GL261/HRE-Luc tumors at day 18 p.i. whereby the control tumors GL261/SV40-Luc stayed at basal level. Both tumor groups showed a fluctuating signal thereafter. Group-time (g:t) interaction effect indicated a significant difference in normalized luciferase signal between GL261/HRE-Luc and GL261/SV40-Luc represented with p-values (**C**). All values are shown as mean ± SD.

3.5 Comparison of intratumoral protein expression by immunofluorescence analysis

Following termination of the imaging studies tumor tissue from subcutaneous and intracranial GL261 tumors was harvested and tumor sections were analyzed using the immunofluorescence method. 60min prior to sacrifice mice were injected first with pimonidazole, a chemical agent that is reduced in hypoxic conditions and binds covalently to thiol-domains of proteins in hypoxic cells [193] thus highlighting hypoxic tumor areas and secondly (2min prior to sacrifice) with a perfusion marker (Hoechst stain) [36]. One section from a GL261/HRE-Luc tumor is shown as representative of all tumor sections for each anatomical location (Fig. 21 and 22). The top panels serve as overview of the tumor section analyzed from both injection sites, subcutaneous and intracranial. The presence of hypoxic domains within the tumor was detected in all subcutaneous and half of the intracranial tumors. Unlike in the subcutaneous tumors, and in line with the lower bioluminescent intensity observed *in vivo*, the pimonidazole staining was significantly less observed for intracranial tumors and mostly restricted to small irregular patchy areas. In the subcutaneous tumor a clear distance could be observed between hypoxic areas and the blood vessels highlighted by the presence of CD31 positive endothelial cells (Fig. 21B). Such a clear distinction between hypoxic domain and perfused areas was not observed in orthotopic GL261 tumors, for which many small blood vessels were observed mainly in normoxic tissue (Fig. 22B). It appears that the vasculature system of orthotopic tumor consists of many small blood vessels (capillaries) while in subcutaneous tumor it comprises larger vessels.

It is well established that hypoxia triggers HIF-α stabilization [82]. Therefore the tissue sections from GL261/HRE-Luc were stained for HIF-1α and HIF-2α to investigate the correlation of these proteins with hypoxia. Regions stained positively for pimonidazole did only colocalized in part with regions stained positively for HIF-1α and HIF-2α, respectively, in both subcutaneous and orthotopically tumors (Fig. 21C, 21D, 22C and 22D). These finding are in line with earlier findings that reported a substantial disconnection between the hypoxia and HIF activity both in space and time [190, 194, 195].

HIF activity regulates the expression of HIF target genes such as glucose transporter 1 (GLUT1) and carbonic anhydrase 9 (CA9) [73, 196, 197]. A colocalization of these two target genes with hypoxic areas has been observed in previous studies [196, 197]. To investigate the downstream regulation of the HIF pathway the tumor sections were

stained for GLUT1 and CA9. The expected coexpression of pimonidazole with GLUT1 respectively CA9 could be shown in both, subcutaneous and intracranial GL261/HRE-Luc tumor sections (Fig. 21E, 21F, 22E and 22F). The GLUT1 and CA9 expression in subcutaneous GL261/HRE-Luc tumor sections was detected primarily at perinecrotic tumor regions (Fig. 21E and 21F) in agreement with earlier reports [198-200]. In subcutaneous GL261/HRE-Luc tumor sections the GLUT1 showed a weaker protein expression and colocalization with pimonidazole positive areas than the CA9 (Fig. 21E and 21F). In intracranial tumors GLUT1 and CA9 seemed to be expressed in similar regions but to a large percentage the expression was detected in non-hypoxic tumor tissue (Fig. 22E and 22F). In these tumors GLUT1 and CA9 displayed a similar spatial pattern as the HIF-2α expression (Fig. 22D-F).

As a large fraction of the subcutaneous tumor tissue showed necrotic areas, Ki67 staining [247] was performed to investigate the proliferation of the intact cells of the GL261/HRE-Luc tumor tissue sections. From the immunohistological analysis of subcutaneous and intracranial GL261 tumor sections it can be observed that the Ki67 positive stained cells are distributed and expressed within the tumor area whereas a clear preference in expression between hypoxic and non-hypoxic regions cannot be distinguished (Fig. 21G and 22G).

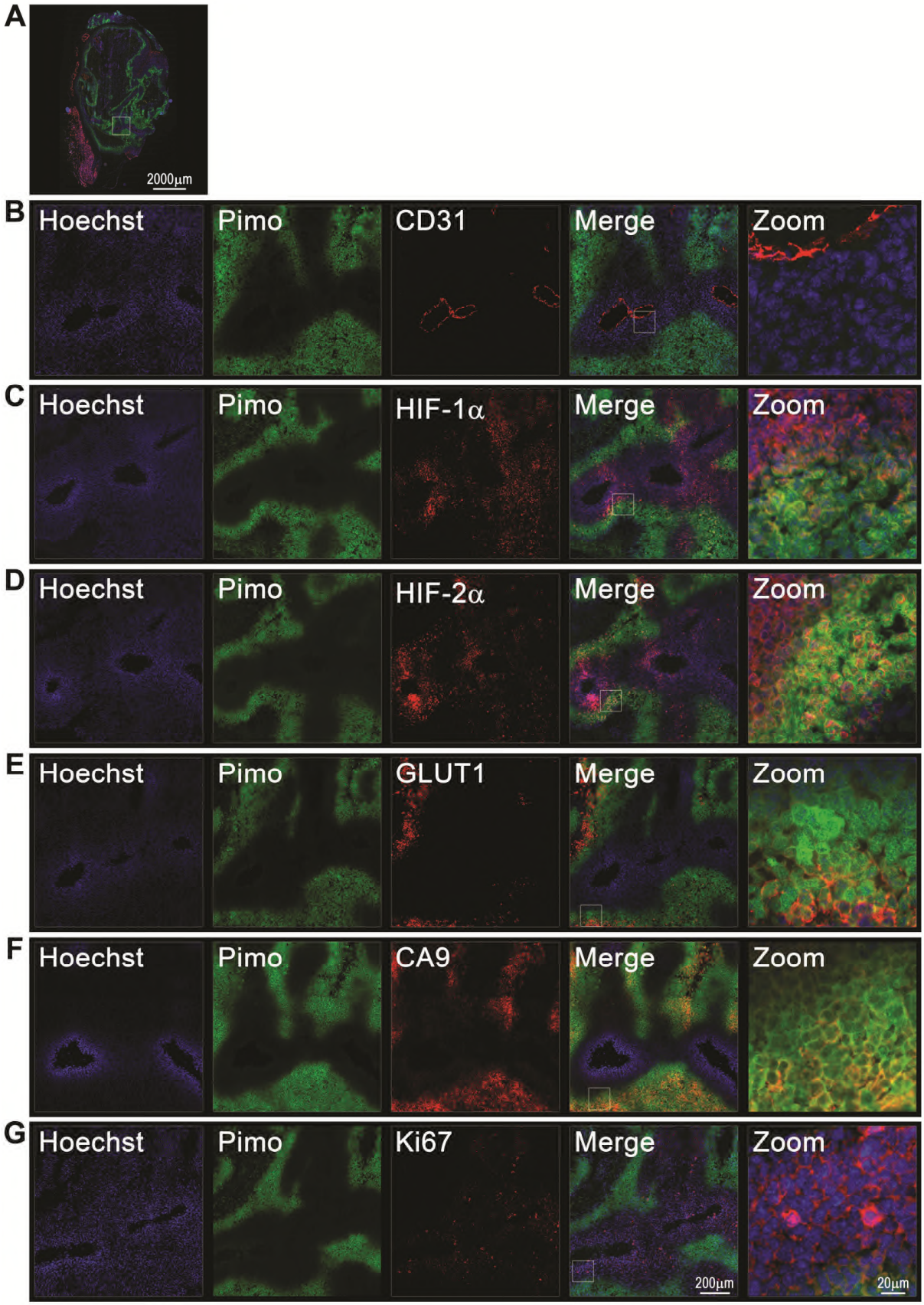

Figure 21. Immunofluorescence analysis of subcutaneous GL261 tumor. See page 67.

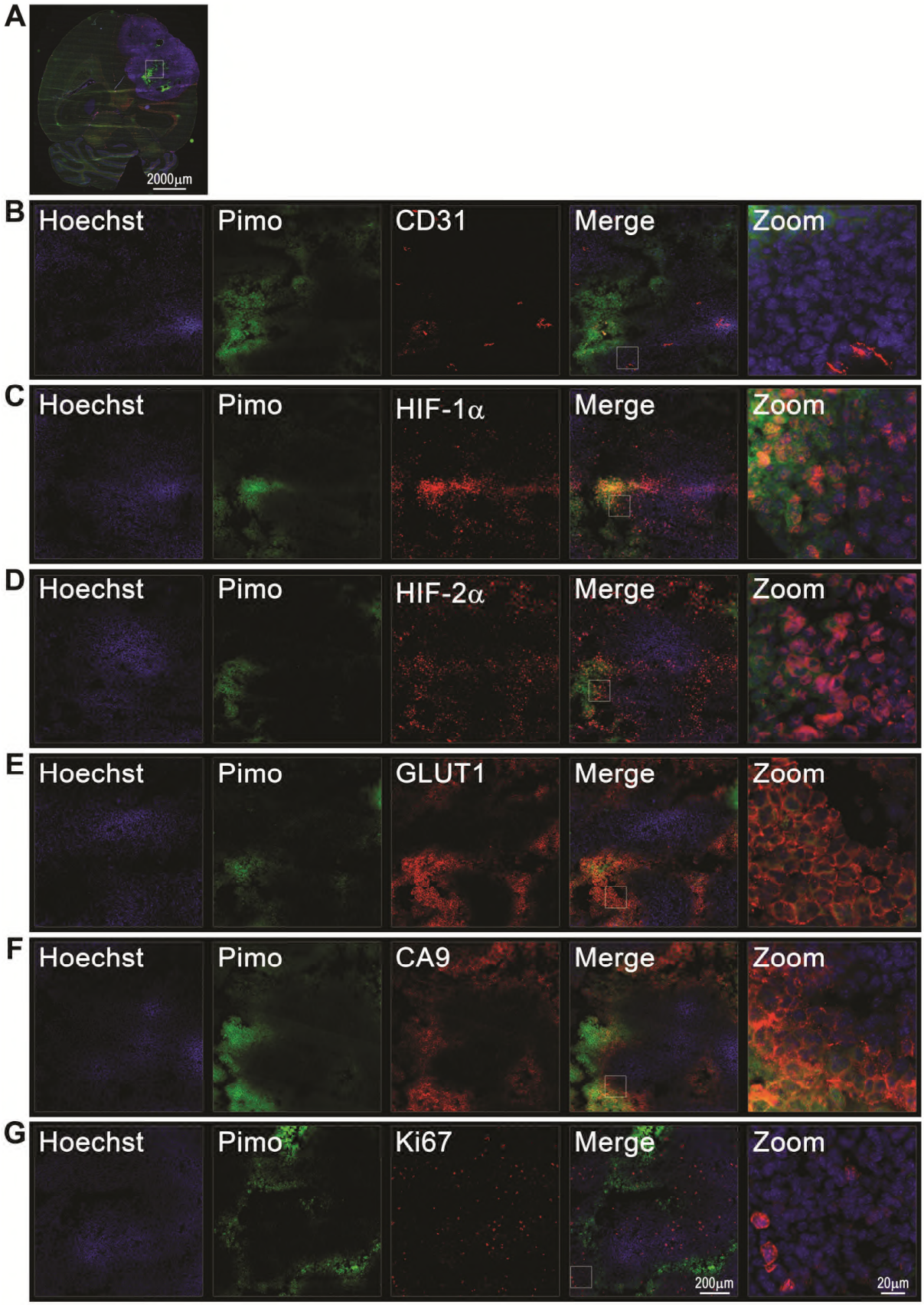

Figure 22. Immunofluorescence analysis of intracranial GL261 tumor. See page 67.

Legend to figure 21. Immunofluorescence analysis of subcutaneous GL261 tumor. A. An overview about a representative GL261/HRE-Luc tumor for all 13 isolated subcutaneous GL261 tumors as demonstration where the field of interest is indicated with the white frame. As standard reference all tumors were stained with the perfusion marker Hoechst stain (blue) and the hypoxia marker pimonidazole labeled as pimo (green). The third staining (red) was performed by staining the cryosections with the endothelial cell marker CD31 (**B**), with the HIF proteins HIF-1α (**C**) and HIF-2α (**D**), the HIF targets GLUT1 (**E**) and CA9 (**F**) and with the proliferation marker Ki76 (**G**).

Legend to figure 22. Immunofluorescence analysis of intracranial GL261 tumor. A. An overview about a representative GL261/HRE-Luc tumor for all 10 isolated intracranial GL261 tumors as demonstration where the field of interest is indicated with the white frame. As standard reference all tumors were stained with the perfusion marker Hoechst stain (blue) and the hypoxia marker pimonidazole labeled as pimo (green). The third staining (red) was performed by staining the cryosections with the endothelial cell marker CD31 (**B**), with the HIF proteins HIF-1α (**C**) and HIF-2α (**D**), the HIF targets GLUT1 (**E**) and CA9 (**F**) and with the proliferation marker Ki67 (**G**).

4 Discussion

Despite the vast amount of research that has been carried out in the cancer field of cancer and despite the significant progress that has been achieved in the last decades regarding the understanding of the basic mechanisms underlying the malignant transformation of cells and their progression into tumor masses, many questions remain open. Notwithstanding the significant improvement in survival chances and life expectancy that treatment has reached for many types of cancer, malignant tumors are still considered a difficult to cure, devastating disease. This is certainly true for brain tumors and among those, in particular, for glioblastomas [33, 201]. For these patients the standard of care includes surgical resection of the tumor, radiotherapy and chemotherapy using e.g. temozolomide, and alkylating cytostatic agent that penetrates the blood-brain barrier [10, 30, 33]. Novel strategies include antiangiogenic therapies using the VEGF antibody bevacizumab [33, 44]. Yet, after many years of research no significant improved in the treatment approach of brain tumors could be found and at best a prolongation in the life span of the patient has been achieved [10, 33].

The intention of this study was not to seek for novel therapies, but rather to contribute in enhancing the understanding of the mechanisms that play a key role in tumorigenesis or that may interfere with therapeutic interventions. Tissue hypoxia and HIF signaling are of central interest to this purpose. On the one hand they trigger important molecular and cellular events that affect the proliferative potential of tumor cells, allowing them to survive in a harsh microenvironment and facilitating the invasion of host tissue and the formation of distant metastases [73]. Interestingly, these processes are also of importance for gliomas/glioblastomas despite the fact that they grow in the heavily vascularized brain environment [19, 20, 36, 38, 202]. Hence this thesis is aimed at the development of tools that allow monitoring the activation of HIF signaling in a non-invasive and longitudinal manner. The availability of such tools may be of value for future studies aimed at the development of novel therapies that potentially circumvent this central molecular mechanism key to tumor genesis and malignancy.

4.1 Luciferase reporter gene assay as a good method to investigate the HIF pathway during tumor growth

Activation of hypoxia signaling is a triggering event in the development of tumors but also plays an important role in the efficiency resulting of tumor therapy [164, 203]. This explains why so many imaging studies analyzing the role of the HIF signaling pathway in tumor development have been published. Imaging studies are typically based on reporter gene assays. Three strategies can be pursued: direct targeting of the regulated subunit HIF-1α [190], of its oxygen dependent degradation domain (ODDD) [204, 205], or by evaluating HIF activity through its DNA binding sequence HRE [190, 206]. These imaging approaches are often used in combination with a bioluminescence reporter gene assay in subcutaneous tumor models. Expression of the reporter protein indicates either (hypoxia) induced HIF-1α stability or its signaling activity through a non-invasive *in vivo* imaging method [190, 204-206].

Bioluminescence imaging using a luciferase reporter gene is a widely used method for preclinical studies to investigate the regulation of a specific gene and the effect of therapies at the molecular level in a non-invasive, longitudinal way [174, 176]. Compared to fluorescence imaging, bioluminescence has the important advantage that its mechanism is based on a catalytic reaction with essentially no intrinsic background signal as mammalian tissue does not express the reporter gene [178]. Many studies have successfully investigated the HIF signaling pathway by means of a luciferase reporter gene assay in combination with bioluminescence imaging in different tumor types [190, 204, 207], including glioblastomas [191, 205]. Compared to these earlier studies our work was designed to investigate the regulation of HIF activity in standardized time intervals (6 to 8 times) over a period of two weeks at two different anatomical locations (subcutaneous and orthotopic) to compare its activity regulation. The luciferase reaction is dependent on the availability of oxygen as co-substrate, i.e. requires one oxygen molecule for each generated photon, which may constitute an issue when combined with a hypoxia readout [208]. Yet it has been demonstrated that bioluminescence imaging yields correct results even in an oxygen deprived environment. Even at severe hypoxia (oxygen levels of 0.2%) 50% of the photon counts measured at normoxia could still be detected [184]. Only at these extreme conditions an underestimation of the luciferase activity becomes evident. As alternative, the luciferase reporter might be exchanged with a fluorescence protein, which is virtually independent of the oxygen tension and where oxygen is required only to form the

active fluorophore [185, 208]. Fluorescence imaging though has the disadvantage of intrinsic tissue fluorescence background which may reduce the sensitivity of the readout. By developing red-shifted and even near infrared fluorescent proteins this problem can be addressed in part [174, 185].

An important aspect when studying enzymatic reactions is to avoid the situation in which the reaction is saturated to excessive substrate availability. Previous studies have shown that luciferase expression is not saturated by intraperitoneal (i.p.) substrate administration [176, 209]. Hence the signal intensity can be enhanced by increasing the local dose of the substrates, i.e. by increasing either the amount injected or by increasing the bioavailability. For instance, it has been shown that an optimization of the signal might be reached by intravenous (i.v.) substrate application [176, 183]. In this case the i.v. substrate application increased the brightness of the luciferase signal approximately five to ten times [176]. However, the application of the substrate i.v. is technically more difficult, in particular in parallel, resulting in a less reliable procedure and an increased number of needed experimental animals [183, 176].

Our experiments have corroborated the notion that bioluminescence imaging yields reliable signaling even under low oxygen conditions. In fact, the measured luciferase expression demonstrated a stable and constant volume-normalized photon output throughout the duration of the entire experimental period in both subcutaneous and orthotopic tumors grown for GL261/SV40-Luc cells that express the reporter construct at a constant level and despite the fact that tumors experience a comparable degree of hypoxia as demonstrated by induction of HIF signaling *in vivo* and by the *ex vivo* analysis.

4.2 Differences in the establishment of the reporter gene assay between the glioma cell lines *in vitro*

All three glioblastoma cell lines LN229, U87 and GL261 showed an endogenous HIF-1α regulation upon DMOG administration, which inhibits PHD and correspondingly proteasomal HIF-1α degradation [190, 246]. To investigate the HIF signaling pathway during growth these three cell lines were stably transfected with a HRE-Luc construct, for which the luciferase expression is driven under the control of a promoter sequence comprising the HRE motif, which is a core element of all promoters of HIF target genes,

to which HIF is binding to regulate their expression [84, 85]. As a consequence, luciferase is only expressed upon HIF mediated signaling. In contrast, the control cells were stably transfected with a construct that constitutively expresses luciferase under the control of a simian virus 40 promoter (SV40-Luc). To stably transfer a DNA sequence into the genome of a cell there are different transfection methods available. Viral transfection is a widely used method with a high efficiency for a limited length DNA sequence and it contains the risk of the insertion of mutagenesis [210]. On the other side non-viral transfection methods offer a simple procedure to insert a flexible DNA sequence of a larger size into the genome but with a lower efficiency. These methods include two different strategies for penetrating the cellular/nuclear membrane: using chemically enhanced membrane passage agents such as calcium phosphate or transfection agents such as cationic polymers, or physically based methods such as electroporation or direct microinjection [210, 211]. Stable transfection has been successfully accomplished for cell lines in this study using the chemical approach with PEI (polyethylenimine) as transfection agent, except for the GL261/HRE-Luc cells. This cell line was therefore transfected using electroporation. This could eventually explain the difference in the proliferation behavior between GL261/HRE-Luc and GL261/SV40-Luc [176]. Interestingly, the growth rate difference between the two transfected cell lines is less obvious than the corresponding difference between the transfected and the untransfected GL261 cells. Thus, we assume that the transfection method might affect the growth behavior of the transfected GL261 cells. Similar result have been obtained for the U87 cell line, through for this patent cell line both groups U87/HRE-Luc and U87/SV40-Luc were transfected using chemical transfection with PEI. U87 cells are widely used in preclinical studies; yet, during the transfection procedure they appeared to be the most sensitive cells by needing a longer time period to recover as compared to GL261 and LN229 cells. Difference in the tumor cell proliferation rates between transfected and untransfected cells has been reported and may be caused by the transfection method, by the nature of the construct, or by the insertion location loci on the host DNA [176]. However, these effects obviously depend on the cell line used. For example, the results of the proliferation assay of the LN229 cells indicated a minor influence of the introduction of a foreign gene as essentially no difference was detected between LN229/HRE-Luc, LN229/SV40-Luc and native LN229 cells.

In all three glioblastoma cell lines the successful function regulation of the transfected constructs could be demonstrated *in vitro* by measuring luminescence activity. A significant increase in the luciferase signal could be demonstrated in cells stably transfected with a HRE-Luc construct upon simulated hypoxia by DMOG exposure, whereas no change was detected in cells transfected with the control construct SV40-Luc. Only U87/SV40-Luc control cells showed a significant reduction upon DMOG exposure what could as well be observed on the protein level. A possible explanation might be the increased gene susceptibility of U87 cells which have undergone the transfection procedure. Despite the high induction factors measured for LN229/HRE-Luc cells upon administration of DMOG, this cell line was not considered for *in vivo* studies as the absolute protein level was low, which compromises the sensitivity of the assay (much lower counts per total protein level compared to those in U87 and GL261 cell lines). Although the results of the *in vitro* characterization may not be translated one-to-one to the *in vivo* conditions as it is another environment, these experiments constitute an important step to estimate the possible outcome of the different cell lines in the living mouse.

4.3 Evaluation of HIF signaling in tumor growth progression in vivo

The subcutaneous tumor model is widely used in oncological research because of its experimental simplicity, yet its suffers from the substantial limitation that tumors grow in an artificial environment, which might have significant impact on study results [212]. As the interaction between tumor and its microenvironment is more and more recognized as a critical factor determining outcome [79, 248], results obtained with the subcutaneous model are to be interpreted with care. For example it has been shown that the tumor vascular architecture critically depends on the implantation site [189]. Therefore, it is important to validate data obtained from this model and to judge the influence of the native microenvironment by comparison with results obtained from experiments using orthotopic implantation. Therefore, we investigated HIF signaling activity both in subcutaneous and intracranial implanted glioblastomas as a function of time using *in vivo* bioluminescence imaging. Of the three cell lines evaluated *in vitro* only transfected GL261 cells developed solid proliferating tumors under *in vivo* conditions, while LN229 and U87 failed to do so. We may speculate, why this was the case. Transfected U87 cells tended to become very susceptible to stressors, which may

have led to their loss probably because of apoptosis. Already under *in vitro* conditions, the cells behaved differently from the other two cell lines (e.g. two 'HIF-1α' lines). LN229 apparently showed very low HIF-1α levels under non-stimulated conditions. Even after strong induction the absolute levels were still comparatively low. This may limit the adaptive capability of these cells, i.e. by limiting their potential to develop a vascular network in the inherently avascular subcutaneous compartment and thereby preventing proliferation. The low absolute levels of HIF are also reflected by the absence of a detectable bioluminescence signal of tumors from LN229/HRE-Luc cells despite the fact there was a palpable tumor mass and in view of the fact that the bioluminescence imaging assay is a robust and sensitive imaging method, which has been shown to only need a few thousand cells to detect a signal (depending on the bioluminescence expression level within the cells) [176, 181, 183]. This clearly indicates that luciferase activity within these cells must have been very low.

We speculate that the stagnancy in tumor volume of s.c. LN229 tumors can be based on the premature start of the experiment. The LN229 cells may need more time to settle down before they can start to proliferate. Our results with the transfected LN229 cells do not correspond with findings reported in the literature, describing positive growth of LN229 tumors implanted in different athymic nude mice, albeit in these studies different amounts of cells were injected [213-215]. We speculate that both, the chosen mouse strain as well as the used amount of implanted tumor cells can influence the growing behavior of the tumor. In contrast to the subcutaneous LN229/HRE-Luc tumors, luciferase signaling could be measured in tumors grown from LN229/SV40-Luc throughout the experimental period despite the fact that they were similar in size to the tumors from LN229/HRE-Luc cells. To continue work with this cell line (e.g. in orthotopic locations), in future experiments the sensitivity of the assay could be increased by injection of the substrate i.v. as this has been shown to strongly increase the single intensity [209]. A remaining question is if our transfected LN229 cells would grow better under orthotopic conditions as the brain is more vascularized. For the establishment of our glioblastoma bioluminescent mouse model we decided to first continue orthotopic experiments only with cells lines giving promising results in subcutaneous experiments.

The subcutaneous U87 tumor model is a widely used tumor model and typically is reported to show a normal growing behavior [159, 205]. In contrast, the U87/HRE-Luc tumors in our experiments showed decreasing volumes over time. Similarly the intensity of the luciferase induced bioluminescence signal decreased from the beginning of the experiments. As infections by mycoplasma often negatively influence the growth of tumors [216, 217], we tested our cell culture preparations regularly for mycoplasms; we therefore can exclude mycoplasmal infections to be the cause of the tumor regression. The most likely explanation is that the inserted cassette has led to a negative tumor growth *in vivo*.

Comparing the growth rate of the subcutaneous and the intracranial implanted GL261 tumors both tumor groups GL261/HRE-Luc and GL261/SV40-Luc showed an approximately tenfold increase in volume within the experimental period of two weeks. Interestingly in both subcutaneous and intracranial implanted tumors the GL261/HRE-Luc showed a slightly slower growing rate compared to the GL261/SV40-Luc tumors, which was not statistically significantly different. A related observation has been done in U251 cells transfected with HRE-Luc, which showed slower growth kinetics than the control cells [191].

A significant transient induction of the luciferase signal was observed for the subcutaneous GL261/HRE-Luc tumors suggesting transiently increased HIF signaling activity during tumor growth, whereas the measured luciferase signal of the control group (GL261/SV40-Luc) stayed at baseline levels during the whole experimental period. This is most likely related to the much smaller volume of the intracranial tumors, which are typically an order of magnitude smaller than the subcutaneous ones. Hence, orthotopic tumors are expected to be less hypoxic leading to less HIF pathway activation. This is also supported by the histological analysis (see next section). While HIF induction in subcutaneous tumors significantly declined for large tumors (toward the end of the experiment), this was not obvious for the intracranial ones. For the latter the highest induction values were measured at the last time point; these values were similar to the maximal induction factors obtained for the subcutaneous tumors, though the variability was rather high. Nevertheless, the different levels of hypoxia determined for the two implantation sites are most likely not just a consequence of the difference in size but may reflect the local microenvironment of the skinfold as compared to cerebral tissue.

The observed differences between the two groups GL261/HRE-Luc and GL261/SV40-Luc was supported by statistical analysis of the signal as function of time after implantation revealing a significant effect (subcutaneous: p=0.0004, orthotopic: p=0.0411). The higher significance level obtained for the subcutaneous tumors was corroborated by further t-test analysis that yielded a significant difference between GL261/HRE-Luc and GL261/SV40-Luc signals at days 20, 22 and 25 post implantation.

The peak of luciferase induction in subcutaneous GL261/HRE-Luc tumors was detected around day 22 after tumor cell injection followed by a steady decrease until the end of the experiment. This is in line with a transient induction of the HIF signaling observed in a subcutaneous colon cancer model, for which the phenomena of the transient HIF signaling induction was explained by a possible HIF induced negative feedback mechanism, which becomes relevant under chronic hypoxic conditions, i.e. chronic HIF stimulation [190]. While this appears a plausible explanation for the transient induction of the activity marker luciferase in subcutaneous GL261/HRE-Luc tumors, the occurrence of necrotic tumor areas might also contribute to the effect. In fact these GL261 tumors started to develop necrotic areas at late stage. Necrosis is an often observed phenomenon in glioblastoma and it was shown to be negatively correlated with clinical outcome [17]. As we observed an increased degree of necrosis accompanied by severe hypoxia in the peri-necrotic area within the tumor section collected at the terminal experimental day, this decrease of living cells might also account for or at least contribute to the reduced luciferase signal.

4.4 *In vivo* HIF signaling in relation to its *ex vivo* analysis

Histological analysis of the isolated tumor demonstrated the presence of hypoxic areas stained by hypoxia marker pimonidazole in all subcutaneous and in 50% of the orthotopic tumor tissue sections studied. The distribution of hypoxia was similar for GL261/HRE-Luc and GL261/SV40-Luc tumors. In accordance with the detected induction of luciferase in GL261/HRE-Luc cells representing HIF activity, upregulation of the HIF downstream products GLUT1 and CA9 was detected distributed over the tumor tissue. A widespread distribution cells stained positively for Ki67 demonstrated the viability of these tumor sections. These *ex vivo* results confirmed those *in vivo* which showed pronounced HIF activity in these tumors.

Histology revealed the development of necrotic areas in subcutaneous tumors at late stages. These may have contributed to the decline in the bioluminescence signal intensity of the volume normalized tumors, as the necrotic areas would start to appear at day 22 and beyond. The difference in the size and location of these necrotic areas within the tumor that did not show positive stains for HIF-1α and HIF downstream products, will contribute to the variability in the bioluminescence signal intensity. Similarly, changes in tumor volume (different length of photon path in the tissue) and location of the bioluminescent sources with regard to the camera will have an impact on the reproducibility of the measurement and may explain in part the considerable variability in the results [176, 180]. In the peri-necrotic area we found an increased degree of pimonidazole staining indicating tissue hypoxia as well as high levels of the HIF target GLUT1 indicating high glycolytic activity [200, 218].

In intracranial tumors derived from GL261/HRE-Luc cells only a weak induction of the luciferase signal was detectable indicating that the HIF signaling pathway was active to a lesser degree than in the subcutaneous GL261/HRE-Luc. However, there was still a significant difference in normalized signal induction over time between the orthotopic GL261/HRE-Luc and GL261/SV40 tumor models. This induction of bioluminescence signal *in vivo* is in line with the originally measured weak induction factor of GL261/HRE-Luc cells measured by *in vitro* luciferase assay. Histological analysis demonstrated relatively small hypoxic areas located typically in the center of the tumors in half of the analyzed intracranial tumor tissues (Fig. 22A), what could be a reason for the weaker luciferase signal in orthotopic compared to subcutaneous GL261/HRE-Luc tumors. This low degree of hypoxia in intracranial GL261 tumors might be due to the highly vascularized environment in which the tumor develops. Positively stained endothelial cells by the CD31 indicate numerous small blood vessels all over the intracranial tumors, an observation that has been reported previously [36, 219]. A second factor to consider is the much smaller size of the intracranial with respect to the subcutaneous tumors. As discussed above, when comparing tumors for the two implantation sites of similar size, comparable induction factors are found.

Although hypoxia triggers the stabilization of HIF-α, which triggers HIF signaling and the expression of HIF downstream readouts, we cannot expect these effects to be completely synchronized in space and time. In fact, previous studies have shown a temporal disconnection between tissue hypoxia and HIF signaling when comparing

hypoxia using [^{18}F]-fluoromisonidazole PET with both tissue the HIF-1α levels and HIF activity using HRE-Luc reporter gene assay in colon cancer. This lack of correspondence was revealed as well by histological analysis, which showed a poor spatial correlation between readouts of hypoxia and HIF signaling [190]. The subcutaneous GL261 tumors analyzed in the actual study showed a strong induction of the HIF signaling measured by *in vivo* luciferase activity as well as large areas of hypoxia as revealed by histology. However, similar to the colon cancer examples there was only a weak spatial correlation between the pimonidazole stained hypoxic areas and areas stained positively for HIF-α staining. This may among other reasons reflect a timing issue: hypoxia, HIF-1α stabilization and the expression of HIF downstream products are sequential events [196, 197]. In addition, due to the chaotic nature of the tumor vasculature blood flow and correspondingly oxygen supply are fluctuating [21, 73]. Thus one can assume that previously hypoxic areas might be re-oxygenated, while HIF signaling, once triggered has led to the expression of HIF targets. Alternatively, non-hypoxia related HIF activation might account for this discrepancy. Several hypoxia independent mechanisms have been shown to induce HIF signaling [220, 221]. A mutation of the PTEN is a frequently occurring alteration in glioblastomas, which typically leads to an enhanced level of HIF-α and activation of HIF signaling via the PI3K/AKT pathway [151]. Many glioma cell lines contain a loss of function mutation of the glycolytic enzyme isocitrate dehydrogenase 1 (IDH1), which results in a diminished level of α-ketoglutarate, a cosubstrate of PHD [149]. The reduced PHD activity would then result in HIF-1α stabilization and activation of the HIF signaling pathway [149]. Facing the fact that in orthotopic GL261/HRE-Luc tumors the histological analysis revealed significant GLUT1 and CA9 expression also in areas that did not stain positively for pimonidazole staining, might suggest the impact of such non-hypoxia triggered signaling. On the other side, the absence of GLUT1 and CA9 in pimonidazole positive tumor regions might be attributable to the negative HIF induced feedback mechanism discussed earlier [190].

The histological analysis suggests that in general a better colocalization has been detected between hypoxic areas stained by pimonidazole, HIF-α and HIF downstream products in orthotopic compared to subcutaneous GL261/HRE-Luc tumors. A reason for this might be found in lower degree of hypoxia, i.e. the reduced hypoxic stress in tumors grown intracranially. This is reflected by the small hypoxic areas in intracranial

tumors revealed by histological analysis and by the weaker induction of the luciferase signal measured by *in vivo* bioluminescence measurements. Therefore we speculate that the downregulation of the HIF signaling had not yet happened so that an enhanced spatial correlation could be observed in the orthotopic GL261/HRE-Luc tumors. Another possibility is that the non-hypoxic HIF activation is differently regulated in subcutaneous and orthotopic GL261 tumors.

Interestingly, for intracranial tumors we found again a relatively weak correlation between areas displaying hypoxia and areas showing high HIF-1α expression; yet a better colocalization was observed when comparing hypoxic regions with regions displaying the HIF downstream products CA9, which to a lesser extent also holds for GLUT1. This might reflect a timing issue: It has been shown that the stability of HIF downstream products is higher than that of HIF-1α, which is rapidly degradated [196]. Therefore the HIF-α levels are low and more difficult to detect. Nevertheless, the correspondence was not perfect: expression of GLUT1 and CA9 was detected as well distant from hypoxic areas. This may again be traced back to mechanisms that activate HIF in the presence of oxygen (see above).

Metabolic reprogramming is characteristic for tumor tissue. Energy production in the cells is switched from oxidative phosphorylation to glycolysis [100-102]. The lower efficiency of glycolysis in producing ATP requires an increased uptake of glucose by the cells [26, 73]. This is achieved by increased expression of GLUT1 and GLUT3, two downstream targets of HIF [73, 105]. Glucose is a major energy substrate for the brain, which implies high levels of GLUT1 expression in the brain and the blood-brain barrier to ensure its glucose supply [105]. GLUT1 levels constitute an important indicator of HIF activity that can readily be assessed using histology. In fact elevated GLUT1 levels could be detected in GL261/HRE-Luc tumors, which were well colocalized with hypoxic tumor regions in orthotopic and to a lesser degree in subcutaneous tumors (see above). This link between GLUT1 expression and HIF signaling was confirmed by colocalization with a second HIF downstream protein CA9 [196, 198]. It was shown that malignant gliomas have an increased glucose preference, poor functional perfusion and areas of hypoxia. In addition to the histological analysis, all these issues can be analyzed by non invasive *in vivo* imaging methods like: [^{18}F]-2-fluoro-2-deoxyglucose positron emission tomography ([^{18}F]FDG-PET) for measuring the glucose utilization [27], DCE MRI for

measuring the perfusion [166, 170], and [^{18}F]-fluoromisonidazole ([^{18}F]-FMISO) for the detection of hypoxic areas [27, 222].

4.5 Comparison between different anatomical tumor locations

Subcutaneous tumors have many advantages especially by the more simple implanting procedure and higher accessibility for manipulations. However their clinical relevance is debated because they grow in an unnatural environment, which is not a proper emulation of real life conditions [212]. To investigate the influence of the native microenvironment it is inevitable to conduct experiments with tumor cells implanted in the orthotopic anatomical location [212]. For example it has been shown that freshly harvested glioma cells from a patient readily developed a tumor when implanted orthotopically in mice but did not proliferate at all when implanted subcutaneously, indicating the influence of the native environment by providing e.g. improved oxygen supply due to the better vascularization or growth factor required for proliferation [18]. The influence of the different implantation sites became also evident from cancer treatment experiments, in which a different sensitivity to the chemotherapeutic agent has been observed for subcutaneous and intracranial grown tumors [223]. Factors contributing to this difference are the different tumor morphology at the two sites (e.g. occurrence of necrotic areas) as well as differences in vascular architecture in the two sites, which would influence the biodistribution of the agent within the tumor. The second factor was explicitly addressed. The vascular system in subcutaneous tumors was characterized by higher vascular permeability and a lower blood flow as compared to the intracranial tumor. In particular low blood flow will have a negative impact on the drug delivery [224, 225]. The results from our histological analysis of subcutaneous GL261 tumors demonstrated a less intratumoral vascularization in accordance with an increased level of hypoxia, the presence of necrosis and a higher presence of HIF downstream products GLUT1 and CA9, compared to the intracranial tumors. It has been observed that HIF induced angiogenesis results in a chaotic vessel architecture with poorly functional vessels, which furthermore display high permeability indicative of an immature vascular wall [21, 107, 226]. The influence of the implantation site on angiogenesis seems to be of general importance. Recently it has been shown for mammary tumors that their vascular system architecture depended on whether they were implanted subcutaneously, orthotopically or in the brain (brain metastasis) [227].

4.6 Outlook

It would definitely be of interest to compare the HIF signaling with regard to various downstream readouts such as proliferation rate, angiogenesis, metabolic reprogramming, proinflammatory response and infiltrative behavior in various glioma/glioblastoma cell lines. Such a comparison might reveal a link between HIF activity and tumor malignancy/aggressiveness. Such studies will require additional readouts that complement the established ones on angiogenesis (DCE MRI) [166, 170], glucose utilization (FDG PET) [27, 172], or proliferation measurements by [^{18}F]-fluorothymidine (FLT-PET), which measures the uptake and phosphorylation of a thymidine analogue [228]. Inflammatory processes might be targeted by labeling of inflammatory cells [229, 230] or the expression of chemokine or cytokine receptors [229, 231, 232]. Infiltration of host tissue might be estimated by measuring protease activity as these enzymes play an essential role in the degradation of the extracellular matrix, a prerequisite for tumor cells to migrate within host tissue [233, 234]. Comparison of such studies with clinical data obtained from glioma patients – some of the assays can be readily translated into the clinics – might help to validate the preclinical models.

A characteristic feature of tumor cells is genetic instability leading to a heterogeneous phenotype and to changing properties, which renders tumor therapy increasingly difficult [235, 236]. For example, it has been shown that several targets in glioblastoma cells show a transient expression, e.g. the transient induction of HIF signaling seen in this study or transient up-regulation of EGFR as shown in some cancer cell lines [237]. The availability of multimodal *in vivo* imaging tools would allow to monitor these events in a time-resolved manner, which should enhance our basic understanding of the processes but also yield valuable information on the proper timing for a therapeutic intervention.

Tumors are intrinsically heterogeneous which has important implications with regard to diagnosis and therapy [10]. Histological determination of the tumor type will depend on the tumor region sampled. Assessment of therapy response is hampered by the fact that different tumor regions will respond differently [41, 42], which raises the question how to assess efficacy: by evaluating the tumor response as a whole or by analyzing specific subregions? Temporo-spatially resolved information characterizing heterogeneity is certainly of importance in this context. Another consequence of the heterogeneous nature becomes also apparent in tumor models grown under rather

controlled conditions with regard to the number of injected cells, implantation site and timing. Huge differences in volume (and morphology) are frequently observed, which renders comparative studies difficult. It would be attractive to stratify the animal groups at baseline on the basis of the tumor volume. In the case of orthotopic models this requires a non-invasive imaging method. Bioluminescence or fluorescence imaging are not optimal in this regard due to the non-linear nature of the signal, in general the correlation between tumor volume and light output is rather weak [183, 190]. MRI would be the method of choice, as volumes could be assessed accurately and the method would in addition provide information on the morphology. It would be of advantage to use a dual imaging system for analyzing tumor volume (MRI) and the HIF regulation (optical imaging) simultaneously as previously shown for other systems [179, 188, 238]. In fact dual and triple bioluminescence imaging system had been presented that allow to focus at the same time on other genes of interest [239, 240]. It should be a goal of each study to reduce the number of mice required, i.e. to maximize the information content obtained from a single animal.

The combination of optical studies with MRI would be attractive as MRI is multimodal itself: in addition to structural data MRI might provide information on the vascularization and blood flow regulation [164, 170]. A multimodal imaging approach including hypoxia detection during the tumor growth would further extend the scope of potential studies. E.g. PET would allow studying tissue hypoxia, glucose utilization and/or proliferative activity [27, 172, 228]. Alternative methods are on the verge, e.g. multispectral optical tomography (MSOT) [27, 241]. Given the complementarity of all these techniques and the need for multiparametric characterization of complex characterizing pathological features such as malignant tumors, it is not surprising that considerable efforts are invested into the development of hybrid technologies.

Glioblastomas characteristically show a diffuse infiltrative growing behavior [10]. Like intratumoral hypoxia, the huge interface between tumor tissue and host tissue renders the treatment of glioblastomas difficult. It would be of interest to develop imaging tools that specifically target the tumor-microenvironment interaction and to combine these readouts with HIF activity imaging methods as HIF is known to influence cell migratory behavior. Migrating cells in glioblastomas have been shown to migrate along the blood vessels and nerve tracts of the white matter [242]. These cells were rarely proliferating during their migration but metabolically they are as active as cells located

within the tumor mass [243, 244]. In combination to the HIF reporter gene assay it would be interesting to analyze the change in white matter by MRI DTI and the metabolic activity by MRS to investigate if glioblastomas with an increased HIF signaling pathway show a particular level of migration.

Bioluminescence assays have the limitation that they possess a poor special resolution, give no 3D information and, probably the most important limitation, they are not directly translational to clinical studies [174, 176]. Therefore in the future the focus should be laid more on research of the HIF pathway in cancer and glioblastomas on imaging approaches that are/or have the potential to be translational to clinics. For examples the targeting of tumor hypoxia by [^{18}F]-FMISO PET [27], inflammatory cells using GdL1-3 MRI contrast agents [230], or HIF downstream products such as CA9 by using the fluorescence hypoxysense probe [245].

4.7 Conclusion

In conclusion only the GL261 out of three tested glioblastoma tumor cell lines could successfully be established up to *in vivo* bioluminescence imaging experiments. The *in vivo* bioluminescence reporter gene assay revealed a significant transient induction of HIF activity in subcutaneous and to a lesser extent in intracranial implanted tumors. The ensuing decrease in luciferase activity toward the end of the experiment may be related to a negative HIF induced feedback loop and/or to an increasing level of intratumoral necrosis. The *in vivo* results were confirmed by histological analysis. Large amount of hypoxic areas and corresponding high levels of HIF downstream products supporting the *in vivo* results were detected in subcutaneous GL261 tumors. The hypoxic areas within intracranial GL261 tumors were small and patchy. Contrary to the subcutaneous tumors high GLUT1 and, to a lesser extent, CA9 expression could also be detected in non-hypoxic regions which did not display pimonidazole staining. This suggests that in orthotopic tumors HIF downstream products were driven in addition to the hypoxic also by non-hypoxic HIF activation unless this finding is not caused by a temporo-spatial disconnection. Our luciferase reporter gene assay allowed a longitudinal and non-invasive following of the intratumoral HIF activity. The results bring light in the field of HIF regulating factors, which may contribute to the development and improvement of treatment protocols for hypoxic glioblastomas in patients.

5 References

1. Globocan, *Estimated Incidence, Mortality and Prevalence Worldwide in 2012*. IARC, 2012.
2. Bray, F., et al., *Global cancer transitions according to the Human Development Index (2008-2030): a population-based study*. Lancet Oncol, 2012. **13**(8): p. 790-801.
3. Lobo, N.A., et al., *The biology of cancer stem cells*. Annu Rev Cell Dev Biol, 2007. **23**: p. 675-99.
4. Bernstein, C., et al., *DNA Damage, DNA Repair and Cancer*. New Research Directions in DNA Repair, Prof. Clark Chen (Ed.), 2013.
5. Hanahan, D. and R.A. Weinberg, *Hallmarks of cancer: the next generation*. Cell, 2011. **144**(5): p. 646-74.
6. Sanai, N., A. Alvarez-Buylla, and M.S. Berger, *Neural stem cells and the origin of gliomas*. N Engl J Med, 2005. **353**(8): p. 811-22.
7. Holland, E.C., *Gliomagenesis: genetic alterations and mouse models*. Nat Rev Genet, 2001. **2**(2): p. 120-9.
8. Singh, S.K., et al., *Identification of human brain tumour initiating cells*. Nature, 2004. **432**(7015): p. 396-401.
9. Louis, D.N., et al., *The 2007 WHO classification of tumours of the central nervous system*. Acta Neuropathol, 2007. **114**(2): p. 97-109.
10. Wen, P.Y. and S. Kesari, *Malignant gliomas in adults*. N Engl J Med, 2008. **359**(5): p. 492-507.
11. Larjavaara, S., et al., *Incidence of gliomas by anatomic location*. Neuro Oncol, 2007. **9**(3): p. 319-25.
12. Simpson, J.R., et al., *Influence of location and extent of surgical resection on survival of patients with glioblastoma multiforme: results of three consecutive Radiation Therapy Oncology Group (RTOG) clinical trials*. Int J Radiat Oncol Biol Phys, 1993. **26**(2): p. 239-44.

13. Rousseau, A., K. Mokhtari, and C. Duyckaerts, *The 2007 WHO classification of tumors of the central nervous system - what has changed?* Curr Opin Neurol, 2008. **21**(6): p. 720-7.

14. Ohgaki, H. and P. Kleihues, *Population-based studies on incidence, survival rates, and genetic alterations in astrocytic and oligodendroglial gliomas.* J Neuropathol Exp Neurol, 2005. **64**(6): p. 479-89.

15. Neglia, J.P., et al., *Second neoplasms after acute lymphoblastic leukemia in childhood.* N Engl J Med, 1991. **325**(19): p. 1330-6.

16. Ohgaki, H., *Epidemiology of brain tumors.* Methods Mol Biol, 2009. **472**: p. 323-42.

17. Homma, T., et al., *Correlation among pathology, genotype, and patient outcomes in glioblastoma.* J Neuropathol Exp Neurol, 2006. **65**(9): p. 846-54.

18. Claes, A., et al., *Phenotypic and genotypic characterization of orthotopic human glioma models and its relevance for the study of anti-glioma therapy.* Brain Pathol, 2008. **18**(3): p. 423-33.

19. Wesseling, P., D.J. Ruiter, and P.C. Burger, *Angiogenesis in brain tumors; pathobiological and clinical aspects.* J Neurooncol, 1997. **32**(3): p. 253-65.

20. Brem, S., R. Cotran, and J. Folkman, *Tumor angiogenesis: a quantitative method for histologic grading.* J Natl Cancer Inst, 1972. **48**(2): p. 347-56.

21. Jain, R.K., et al., *Angiogenesis in brain tumours.* Nat Rev Neurosci, 2007. **8**(8): p. 610-22.

22. Leenders, W.P., B. Kusters, and R.M. de Waal, *Vessel co-option: how tumors obtain blood supply in the absence of sprouting angiogenesis.* Endothelium, 2002. **9**(2): p. 83-7.

23. Smith, J.S. and R.B. Jenkins, *Genetic alterations in adult diffuse glioma: occurrence, significance, and prognostic implications.* Front Biosci, 2000. **5**: p. D213-31.

24. DeAngelis, L.M., *Brain tumors.* N Engl J Med, 2001. **344**(2): p. 114-23.

25. Young, G.S., *Advanced MRI of adult brain tumors.* Neurol Clin, 2007. **25**(4): p. 947-73, viii.

26. Vander Heiden, M.G., L.C. Cantley, and C.B. Thompson, *Understanding the Warburg effect: the metabolic requirements of cell proliferation*. Science, 2009. **324**(5930): p. 1029-33.

27. Chen, W., *Clinical applications of PET in brain tumors*. J Nucl Med, 2007. **48**(9): p. 1468-81.

28. Chen, W., et al., *18F-FDOPA PET imaging of brain tumors: comparison study with 18F-FDG PET and evaluation of diagnostic accuracy*. J Nucl Med, 2006. **47**(6): p. 904-11.

29. D'Angelo, G., et al., *Hypoxia up-regulates prolyl hydroxylase activity: a feedback mechanism that limits HIF-1 responses during reoxygenation*. J Biol Chem, 2003. **278**(40): p. 38183-7.

30. de Vries, N.A., J.H. Beijnen, and O. van Tellingen, *High-grade glioma mouse models and their applicability for preclinical testing*. Cancer Treat Rev, 2009. **35**(8): p. 714-23.

31. Lacroix, M., et al., *A multivariate analysis of 416 patients with glioblastoma multiforme: prognosis, extent of resection, and survival*. J Neurosurg, 2001. **95**(2): p. 190-8.

32. Buatti, J., et al., *Radiation therapy of pathologically confirmed newly diagnosed glioblastoma in adults*. J Neurooncol, 2008. **89**(3): p. 313-37.

33. Anton, K., J.M. Baehring, and T. Mayer, *Glioblastoma multiforme: overview of current treatment and future perspectives*. Hematol Oncol Clin North Am, 2012. **26**(4): p. 825-53.

34. Hegi, M.E., et al., *MGMT gene silencing and benefit from temozolomide in glioblastoma*. N Engl J Med, 2005. **352**(10): p. 997-1003.

35. Shiraishi, A., K. Sakumi, and M. Sekiguchi, *Increased susceptibility to chemotherapeutic alkylating agents of mice deficient in DNA repair methyltransferase*. Carcinogenesis, 2000. **21**(10): p. 1879-83.

36. Bernsen, H.J., et al., *Hypoxia in a human intracerebral glioma model*. J Neurosurg, 2000. **93**(3): p. 449-54.

37. Evans, S.M., et al., *Hypoxia is important in the biology and aggression of human glial brain tumors*. Clin Cancer Res, 2004. **10**(24): p. 8177-84.

38. Søndergaard, K.L., et al., *Expression of hypoxia-inducible factor 1alpha in tumours of patients with glioblastoma.* Neuropathol Appl Neurobiol, 2002. **28**(3): p. 210-7.

39. Eramo, A., et al., *Chemotherapy resistance of glioblastoma stem cells.* Cell Death Differ, 2006. **13**(7): p. 1238-41.

40. Bao, S., et al., *Glioma stem cells promote radioresistance by preferential activation of the DNA damage response.* Nature, 2006. **444**(7120): p. 756-60.

41. Moeller, B.J., R.A. Richardson, and M.W. Dewhirst, *Hypoxia and radiotherapy: opportunities for improved outcomes in cancer treatment.* Cancer Metastasis Rev, 2007. **26**(2): p. 241-8.

42. Liang, B.C., *Effects of hypoxia on drug resistance phenotype and genotype in human glioma cell lines.* J Neurooncol, 1996. **29**(2): p. 149-55.

43. Charalambous, C., T.C. Chen, and F.M. Hofman, *Characteristics of tumor-associated endothelial cells derived from glioblastoma multiforme.* Neurosurg Focus, 2006. **20**(4): p. E22.

44. Chamberlain, M.C., *Bevacizumab for the treatment of recurrent glioblastoma.* Clin Med Insights Oncol, 2011. **5**: p. 117-29.

45. Huszthy, P.C., et al., *In vivo models of primary brain tumors: pitfalls and perspectives.* Neuro Oncol, 2012. **14**(8): p. 979-93.

46. Newcomb, E.W. and D. Zagzag, *The Murine GL261 Glioma Experimental Model to Assess Novel Brain Tumor Treatments.* In CNS Cancer: Models, Markers, Prognostic Factors, Targets and Therapeutic Approaches (Meir EG, ed), 2009: p. 227-241.

47. Ishii, N., et al., *Frequent co-alterations of TP53, p16/CDKN2A, p14ARF, PTEN tumor suppressor genes in human glioma cell lines.* Brain Pathol, 1999. **9**(3): p. 469-79.

48. Weller, M., et al., *Predicting chemoresistance in human malignant glioma cells: the role of molecular genetic analyses.* Int J Cancer, 1998. **79**(6): p. 640-4.

49. Koul, D., et al., *Inhibition of Akt survival pathway by a small-molecule inhibitor in human glioblastoma.* Mol Cancer Ther, 2006. **5**(3): p. 637-44.

50. Schlapbach, R. and A. Fontana, *Differential activity of bcl-2 and ICE enzyme family protease inhibitors on Fas and puromycin-induced apoptosis of glioma cells.* Biochim Biophys Acta, 1997. **1359**(2): p. 174-80.

51. Pontén, J., *Neoplastic human glial cells in culture*. In Human Tumor Cells in Vitro (Fogh J, ed), 1975: p. 175-185.

52. Radaelli, E., et al., *Immunohistopathological and neuroimaging characterization of murine orthotopic xenograft models of glioblastoma multiforme recapitulating the most salient features of human disease*. Histol Histopathol, 2009. **24**(7): p. 879-91.

53. Jacobs, V.L., et al., *Current review of in vivo GBM rodent models: emphasis on the CNS-1 tumour model*. ASN Neuro, 2011. **3**(3): p. e00063.

54. Fussenegger, M. and J.E. Bailey, *Molecular regulation of cell-cycle progression and apoptosis in mammalian cells: implications for biotechnology*. Biotechnol Prog, 1998. **14**(6): p. 807-33.

55. Seligman, A. and M. Shear, *Experimental Production of Brain Tumors in Mice with Methylcholanthrene*. Am J Cancer, 1939. **37**: p. 364-395.

56. Zagzag, D., et al., *Green fluorescent protein immunohistochemistry as a novel experimental tool for the detection of glioma cell invasion in vivo*. Brain Pathol, 2003. **13**(1): p. 34-7.

57. Oh, T., et al., *Immunocompetent murine models for the study of glioblastoma immunotherapy*. J Transl Med, 2014. **12**(1): p. 107.

58. Szatmári, T., et al., *Detailed characterization of the mouse glioma 261 tumor model for experimental glioblastoma therapy*. Cancer Sci, 2006. **97**(6): p. 546-53.

59. Weiner, N.E., et al., *A syngeneic mouse glioma model for study of glioblastoma therapy*. J Neuropathol Exp Neurol, 1999. **58**(1): p. 54-60.

60. Chen, E.Y., M. Fujinaga, and A.J. Giaccia, *Hypoxic microenvironment within an embryo induces apoptosis and is essential for proper morphological development*. Teratology, 1999. **60**(4): p. 215-25.

61. Simon, M.C. and B. Keith, *The role of oxygen availability in embryonic development and stem cell function*. Nat Rev Mol Cell Biol, 2008. **9**(4): p. 285-96.

62. Hultén, L.M. and M. Levin, *The role of hypoxia in atherosclerosis*. Curr Opin Lipidol, 2009. **20**(5): p. 409-14.

63. Zhang, X. and W. Le, *Pathological role of hypoxia in Alzheimer's disease*. Exp Neurol, 2010. **223**(2): p. 299-303.

64. Brahimi-Horn, M.C., J. Chiche, and J. Pouyssegur, *Hypoxia and cancer*. J Mol Med (Berl), 2007. **85**(12): p. 1301-7.

65. Wang, G.L., et al., *Hypoxia-inducible factor 1 is a basic-helix-loop-helix-PAS heterodimer regulated by cellular O2 tension*. Proc Natl Acad Sci U S A, 1995. **92**(12): p. 5510-4.

66. Cowden, K.D. and M.C. Simon, *The bHLH/PAS factor MOP3 does not participate in hypoxia responses*. Biochem Biophys Res Commun, 2002. **290**(4): p. 1228-36.

67. Gu, Y.Z., et al., *Molecular characterization and chromosomal localization of a third alpha-class hypoxia inducible factor subunit, HIF3alpha*. Gene Expr, 1998. **7**(3): p. 205-13.

68. Kallio, P.J., et al., *Signal transduction in hypoxic cells: inducible nuclear translocation and recruitment of the CBP/p300 coactivator by the hypoxia-inducible factor-1alpha*. Embo J, 1998. **17**(22): p. 6573-86.

69. Pugh, C.W., et al., *Activation of hypoxia-inducible factor-1; definition of regulatory domains within the alpha subunit*. J Biol Chem, 1997. **272**(17): p. 11205-14.

70. Jaakkola, P., et al., *Targeting of HIF-alpha to the von Hippel-Lindau ubiquitylation complex by O2-regulated prolyl hydroxylation*. Science, 2001. **292**(5516): p. 468-72.

71. Ruas, J.L., L. Poellinger, and T. Pereira, *Functional analysis of hypoxia-inducible factor-1 alpha-mediated transactivation. Identification of amino acid residues critical for transcriptional activation and/or interaction with CREB-binding protein*. J Biol Chem, 2002. **277**(41): p. 38723-30.

72. Koh, M.Y. and G. Powis, *Passing the baton: the HIF switch*. Trends Biochem Sci, 2012. **37**(9): p. 364-72.

73. Dayan, F., et al., *A dialogue between the hypoxia-inducible factor and the tumor microenvironment*. Cancer Microenviron, 2008. **1**(1): p. 53-68.

74. Masson, N. and P.J. Ratcliffe, *HIF prolyl and asparaginyl hydroxylases in the biological response to intracellular O(2) levels*. J Cell Sci, 2003. **116**(Pt 15): p. 3041-9.

75. Bruick, R.K. and S.L. McKnight, *A conserved family of prolyl-4-hydroxylases that modify HIF*. Science, 2001. **294**(5545): p. 1337-40.

76. Masson, N., et al., *Independent function of two destruction domains in hypoxia-inducible factor-alpha chains activated by prolyl hydroxylation.* Embo J, 2001. **20**(18): p. 5197-206.

77. Lando, D., et al., *FIH-1 is an asparaginyl hydroxylase enzyme that regulates the transcriptional activity of hypoxia-inducible factor.* Genes Dev, 2002. **16**(12): p. 1466-71.

78. Lando, D., et al., *Asparagine hydroxylation of the HIF transactivation domain a hypoxic switch.* Science, 2002. **295**(5556): p. 858-61.

79. Oliver, L., et al., *Hypoxia and the malignant glioma microenvironment: regulation and implications for therapy.* Curr Mol Pharmacol, 2009. **2**(3): p. 263-84.

80. Richard, D.E., et al., *p42/p44 mitogen-activated protein kinases phosphorylate hypoxia-inducible factor 1alpha (HIF-1alpha) and enhance the transcriptional activity of HIF-1.* J Biol Chem, 1999. **274**(46): p. 32631-7.

81. Koivunen, P., et al., *Catalytic properties of the asparaginyl hydroxylase (FIH) in the oxygen sensing pathway are distinct from those of its prolyl 4-hydroxylases.* J Biol Chem, 2004. **279**(11): p. 9899-904.

82. Dayan, F., et al., *The oxygen sensor factor-inhibiting hypoxia-inducible factor-1 controls expression of distinct genes through the bifunctional transcriptional character of hypoxia-inducible factor-1alpha.* Cancer Res, 2006. **66**(7): p. 3688-98.

83. Wood, S.M., et al., *The role of the aryl hydrocarbon receptor nuclear translocator (ARNT) in hypoxic induction of gene expression. Studies in ARNT-deficient cells.* J Biol Chem, 1996. **271**(25): p. 15117-23.

84. Wenger, R.H., D.P. Stiehl, and G. Camenisch, *Integration of oxygen signaling at the consensus HRE.* Sci STKE, 2005. **2005**(306): p. re12.

85. Semenza, G.L., et al., *Hypoxia-inducible nuclear factors bind to an enhancer element located 3' to the human erythropoietin gene.* Proc Natl Acad Sci U S A, 1991. **88**(13): p. 5680-4.

86. Seidel, S., et al., *A hypoxic niche regulates glioblastoma stem cells through hypoxia inducible factor 2 alpha.* Brain, 2010. **133**(Pt 4): p. 983-95.

87. Ema, M., et al., *A novel bHLH-PAS factor with close sequence similarity to hypoxia-inducible factor 1alpha regulates the VEGF expression and is potentially involved in lung and vascular development*. Proc Natl Acad Sci U S A, 1997. **94**(9): p. 4273-8.

88. Makino, Y., et al., *Inhibitory PAS domain protein is a negative regulator of hypoxia-inducible gene expression*. Nature, 2001. **414**(6863): p. 550-4.

89. Carroll, V.A. and M. Ashcroft, *Role of hypoxia-inducible factor (HIF)-1alpha versus HIF-2alpha in the regulation of HIF target genes in response to hypoxia, insulin-like growth factor-I, or loss of von Hippel-Lindau function: implications for targeting the HIF pathway*. Cancer Res, 2006. **66**(12): p. 6264-70.

90. Zarember, K.A. and H.L. Malech, *HIF-1alpha: a master regulator of innate host defenses?* J Clin Invest, 2005. **115**(7): p. 1702-4.

91. Gatenby, R.A. and R.J. Gillies, *Why do cancers have high aerobic glycolysis?* Nat Rev Cancer, 2004. **4**(11): p. 891-9.

92. Helmlinger, G., et al., *Interstitial pH and pO2 gradients in solid tumors in vivo: high-resolution measurements reveal a lack of correlation*. Nat Med, 1997. **3**(2): p. 177-82.

93. Shweiki, D., et al., *Vascular endothelial growth factor induced by hypoxia may mediate hypoxia-initiated angiogenesis*. Nature, 1992. **359**(6398): p. 843-5.

94. Gerhardt, H., et al., *VEGF guides angiogenic sprouting utilizing endothelial tip cell filopodia*. J Cell Biol, 2003. **161**(6): p. 1163-77.

95. Plate, K.H., et al., *Vascular endothelial growth factor is a potential tumour angiogenesis factor in human gliomas in vivo*. Nature, 1992. **359**(6398): p. 845-8.

96. Maisonpierre, P.C., et al., *Angiopoietin-2, a natural antagonist for Tie2 that disrupts in vivo angiogenesis*. Science, 1997. **277**(5322): p. 55-60.

97. Tait, C.R. and P.F. Jones, *Angiopoietins in tumours: the angiogenic switch*. J Pathol, 2004. **204**(1): p. 1-10.

98. Holash, J., S.J. Wiegand, and G.D. Yancopoulos, *New model of tumor angiogenesis: dynamic balance between vessel regression and growth mediated by angiopoietins and VEGF*. Oncogene, 1999. **18**(38): p. 5356-62.

99. Holash, J., et al., *Vessel cooption, regression, and growth in tumors mediated by angiopoietins and VEGF*. Science, 1999. **284**(5422): p. 1994-8.

100. Warburg, O., K. Posener, and E. Negelein, *Über den Stoffwechsel der Carcinomzelle*. Biochem. Z., 1924. **152**: p. 319-344.

101. Zheng, J., *Energy metabolism of cancer: Glycolysis versus oxidative phosphorylation (Review)*. Oncol Lett, 2012. **4**(6): p. 1151-1157.

102. Marie, S.K. and S.M. Shinjo, *Metabolism and brain cancer*. Clinics (Sao Paulo), 2011. **66 Suppl 1**: p. 33-43.

103. Lu, H., R.A. Forbes, and A. Verma, *Hypoxia-inducible factor 1 activation by aerobic glycolysis implicates the Warburg effect in carcinogenesis*. J Biol Chem, 2002. **277**(26): p. 23111-5.

104. Duran, R.V., et al., *HIF-independent role of prolyl hydroxylases in the cellular response to amino acids*. Oncogene, 2013. **32**(38): p. 4549-56.

105. Qutub, A.A. and C.A. Hunt, *Glucose transport to the brain: a systems model*. Brain Res Brain Res Rev, 2005. **49**(3): p. 595-617.

106. Chen, C., et al., *Regulation of glut1 mRNA by hypoxia-inducible factor-1. Interaction between H-ras and hypoxia*. J Biol Chem, 2001. **276**(12): p. 9519-25.

107. Maxwell, P.H., et al., *Hypoxia-inducible factor-1 modulates gene expression in solid tumors and influences both angiogenesis and tumor growth*. Proc Natl Acad Sci U S A, 1997. **94**(15): p. 8104-9.

108. Kim, J.W., et al., *HIF-1-mediated expression of pyruvate dehydrogenase kinase: a metabolic switch required for cellular adaptation to hypoxia*. Cell Metab, 2006. **3**(3): p. 177-85.

109. Fantin, V.R., J. St-Pierre, and P. Leder, *Attenuation of LDH-A expression uncovers a link between glycolysis, mitochondrial physiology, and tumor maintenance*. Cancer Cell, 2006. **9**(6): p. 425-34.

110. Swietach, P., R.D. Vaughan-Jones, and A.L. Harris, *Regulation of tumor pH and the role of carbonic anhydrase 9*. Cancer Metastasis Rev, 2007. **26**(2): p. 299-310.

111. Ullah, M.S., A.J. Davies, and A.P. Halestrap, *The plasma membrane lactate transporter MCT4, but not MCT1, is up-regulated by hypoxia through a HIF-1alpha-dependent mechanism*. J Biol Chem, 2006. **281**(14): p. 9030-7.

112. Shimoda, L.A., et al., *HIF-1 regulates hypoxic induction of NHE1 expression and alkalinization of intracellular pH in pulmonary arterial myocytes.* Am J Physiol Lung Cell Mol Physiol, 2006. **291**(5): p. L941-9.

113. Ivanov, S., et al., *Expression of hypoxia-inducible cell-surface transmembrane carbonic anhydrases in human cancer.* Am J Pathol, 2001. **158**(3): p. 905-19.

114. McCawley, L.J. and L.M. Matrisian, *Matrix metalloproteinases: multifunctional contributors to tumor progression.* Mol Med Today, 2000. **6**(4): p. 149-56.

115. Egeblad, M. and Z. Werb, *New functions for the matrix metalloproteinases in cancer progression.* Nat Rev Cancer, 2002. **2**(3): p. 161-74.

116. Muñoz-Nájar, U.M., et al., *Hypoxia stimulates breast carcinoma cell invasion through MT1-MMP and MMP-2 activation.* Oncogene, 2006. **25**(16): p. 2379-92.

117. Müller, A., et al., *Involvement of chemokine receptors in breast cancer metastasis.* Nature, 2001. **410**(6824): p. 50-6.

118. Staller, P., et al., *Chemokine receptor CXCR4 downregulated by von Hippel-Lindau tumour suppressor pVHL.* Nature, 2003. **425**(6955): p. 307-11.

119. Rempel, S.A., et al., *Identification and localization of the cytokine SDF1 and its receptor, CXC chemokine receptor 4, to regions of necrosis and angiogenesis in human glioblastoma.* Clin Cancer Res, 2000. **6**(1): p. 102-11.

120. Esencay, M., E.W. Newcomb, and D. Zagzag, *HGF upregulates CXCR4 expression in gliomas via NF-kappaB: implications for glioma cell migration.* J Neurooncol, 2010. **99**(1): p. 33-40.

121. Squier, M.K. and J.J. Cohen, *Cell-mediated cytotoxic mechanisms.* Curr Opin Immunol, 1994. **6**(3): p. 447-52.

122. Novack, D.V. and S.J. Korsmeyer, *Bcl-2 protein expression during murine development.* Am J Pathol, 1994. **145**(1): p. 61-73.

123. von Boehmer, H., *Positive selection of lymphocytes.* Cell, 1994. **76**(2): p. 219-28.

124. Jain, M.V., et al., *Interconnections between apoptotic, autophagic and necrotic pathways: implications for cancer therapy development.* J Cell Mol Med, 2013. **17**(1): p. 12-29.

125. Harris, A.L., *Hypoxia--a key regulatory factor in tumour growth*. Nat Rev Cancer, 2002. **2**(1): p. 38-47.

126. Steinbach, J.P. and M. Weller, *Apoptosis in gliomas: molecular mechanisms and therapeutic implications*. J Neurooncol, 2004. **70**(2): p. 245-54.

127. Papandreou, I., et al., *Anoxia is necessary for tumor cell toxicity caused by a low-oxygen environment*. Cancer Res, 2005. **65**(8): p. 3171-8.

128. Carmeliet, P., et al., *Role of HIF-1alpha in hypoxia-mediated apoptosis, cell proliferation and tumour angiogenesis*. Nature, 1998. **394**(6692): p. 485-90.

129. Reynolds, T.Y., S. Rockwell, and P.M. Glazer, *Genetic instability induced by the tumor microenvironment*. Cancer Res, 1996. **56**(24): p. 5754-7.

130. Greijer, A.E. and E. van der Wall, *The role of hypoxia inducible factor 1 (HIF-1) in hypoxia induced apoptosis*. J Clin Pathol, 2004. **57**(10): p. 1009-14.

131. Graeber, T.G., et al., *Hypoxia induces accumulation of p53 protein, but activation of a G1-phase checkpoint by low-oxygen conditions is independent of p53 status*. Mol Cell Biol, 1994. **14**(9): p. 6264-77.

132. Hollstein, M., et al., *p53 mutations in human cancers*. Science, 1991. **253**(5015): p. 49-53.

133. Vogelstein, B. and K.W. Kinzler, *p53 function and dysfunction*. Cell, 1992. **70**(4): p. 523-6.

134. Kastan, M.B., et al., *Participation of p53 protein in the cellular response to DNA damage*. Cancer Res, 1991. **51**(23 Pt 1): p. 6304-11.

135. Berra, E., et al., *HIF-1-dependent transcriptional activity is required for oxygen-mediated HIF-1alpha degradation*. FEBS Lett, 2001. **491**(1-2): p. 85-90.

136. Schmid, T., et al., *p300 relieves p53-evoked transcriptional repression of hypoxia-inducible factor-1 (HIF-1)*. Biochem J, 2004. **380**(Pt 1): p. 289-95.

137. Chen, D., et al., *Direct interactions between HIF-1 alpha and Mdm2 modulate p53 function*. J Biol Chem, 2003. **278**(16): p. 13595-8.

138. Raza, S.M., et al., *Necrosis and glioblastoma: a friend or a foe? A review and a hypothesis*. Neurosurgery, 2002. **51**(1): p. 2-12; discussion 12-3.

139. Sowter, H.M., et al., *HIF-1-dependent regulation of hypoxic induction of the cell death factors BNIP3 and NIX in human tumors.* Cancer Res, 2001. **61**(18): p. 6669-73.

140. Vande Velde, C., et al., *BNIP3 and genetic control of necrosis-like cell death through the mitochondrial permeability transition pore.* Mol Cell Biol, 2000. **20**(15): p. 5454-68.

141. Shimizu, S., et al., *Prevention of hypoxia-induced cell death by Bcl-2 and Bcl-xL.* Nature, 1995. **374**(6525): p. 811-3.

142. Nicotera, P. and G. Melino, *Regulation of the apoptosis-necrosis switch.* Oncogene, 2004. **23**(16): p. 2757-65.

143. Steinbach, J.P., et al., *Hypoxia-induced cell death in human malignant glioma cells: energy deprivation promotes decoupling of mitochondrial cytochrome c release from caspase processing and necrotic cell death.* Cell Death Differ, 2003. **10**(7): p. 823-32.

144. Semenza, G.L., *Targeting HIF-1 for cancer therapy.* Nat Rev Cancer, 2003. **3**(10): p. 721-32.

145. Laughner, E., et al., *HER2 (neu) signaling increases the rate of hypoxia-inducible factor 1alpha (HIF-1alpha) synthesis: novel mechanism for HIF-1-mediated vascular endothelial growth factor expression.* Mol Cell Biol, 2001. **21**(12): p. 3995-4004.

146. Stiehl, D.P., et al., *Normoxic induction of the hypoxia-inducible factor 1alpha by insulin and interleukin-1beta involves the phosphatidylinositol 3-kinase pathway.* FEBS Lett, 2002. **512**(1-3): p. 157-62.

147. Zhong, H., et al., *Modulation of hypoxia-inducible factor 1alpha expression by the epidermal growth factor/phosphatidylinositol 3-kinase/PTEN/AKT/FRAP pathway in human prostate cancer cells: implications for tumor angiogenesis and therapeutics.* Cancer Res, 2000. **60**(6): p. 1541-5.

148. Maxwell, P.H., et al., *The tumour suppressor protein VHL targets hypoxia-inducible factors for oxygen-dependent proteolysis.* Nature, 1999. **399**(6733): p. 271-5.

149. Zhao, S., et al., *Glioma-derived mutations in IDH1 dominantly inhibit IDH1 catalytic activity and induce HIF-1alpha.* Science, 2009. **324**(5924): p. 261-5.

150. Ravi, R., et al., *Regulation of tumor angiogenesis by p53-induced degradation of hypoxia-inducible factor 1alpha.* Genes Dev, 2000. **14**(1): p. 34-44.

151. Zundel, W., et al., *Loss of PTEN facilitates HIF-1-mediated gene expression.* Genes Dev, 2000. **14**(4): p. 391-6.

152. Meijer, T.W., et al., *Targeting hypoxia, HIF-1, and tumor glucose metabolism to improve radiotherapy efficacy.* Clin Cancer Res, 2012. **18**(20): p. 5585-94.

153. Ali, M.M., et al., *Changes in vascular permeability and expression of different angiogenic factors following anti-angiogenic treatment in rat glioma.* PLoS One, 2010. **5**(1): p. e8727.

154. Bao, S., et al., *Stem cell-like glioma cells promote tumor angiogenesis through vascular endothelial growth factor.* Cancer Res, 2006. **66**(16): p. 7843-8.

155. Lu, K.V., et al., *VEGF inhibits tumor cell invasion and mesenchymal transition through a MET/VEGFR2 complex.* Cancer Cell, 2012. **22**(1): p. 21-35.

156. Fujiwara, S., et al., *Silencing hypoxia-inducible factor-1alpha inhibits cell migration and invasion under hypoxic environment in malignant gliomas.* Int J Oncol, 2007. **30**(4): p. 793-802.

157. Li, Z., et al., *Hypoxia-inducible factors regulate tumorigenic capacity of glioma stem cells.* Cancer Cell, 2009. **15**(6): p. 501-13.

158. Méndez, O., et al., *Knock down of HIF-1alpha in glioma cells reduces migration in vitro and invasion in vivo and impairs their ability to form tumor spheres.* Mol Cancer, 2010. **9**: p. 133.

159. Gillespie, D.L., et al., *Silencing of hypoxia inducible factor-1alpha by RNA interference attenuates human glioma cell growth in vivo.* Clin Cancer Res, 2007. **13**(8): p. 2441-8.

160. Kong, D., et al., *Echinomycin, a small-molecule inhibitor of hypoxia-inducible factor-1 DNA-binding activity.* Cancer Res, 2005. **65**(19): p. 9047-55.

161. Lee, K., et al., *LW6, a novel HIF-1 inhibitor, promotes proteasomal degradation of HIF-1alpha via upregulation of VHL in a colon cancer cell line.* Biochem Pharmacol, 2010. **80**(7): p. 982-9.

162. Kung, A.L., et al., *Small molecule blockade of transcriptional coactivation of the hypoxia-inducible factor pathway.* Cancer Cell, 2004. **6**(1): p. 33-43.

163. Rapisarda, A., et al., *Topoisomerase I-mediated inhibition of hypoxia-inducible factor 1: mechanism and therapeutic implications*. Cancer Res, 2004. **64**(4): p. 1475-82.

164. Jensen, R.L., *Brain tumor hypoxia: tumorigenesis, angiogenesis, imaging, pseudoprogression, and as a therapeutic target*. J Neurooncol, 2009. **92**(3): p. 317-35.

165. Storey, P., *Introduction to magnetic resonance imaging and spectroscopy*. Methods Mol Med, 2006. **124**: p. 3-57.

166. Rudin, M., *Molecular Imaging: Basic Principles and Applications in Biomedical Research*. 1st ed. 2005: Imperial College Press.

167. Huettel, S., A.W. Song, and G. McCarthy, *Functional Magnetic Resonance Imaging*. 2nd ed. 2009: Sinauer Associates, Inc.

168. Weissleder, R., *Scaling down imaging: molecular mapping of cancer in mice*. Nat Rev Cancer, 2002. **2**(1): p. 11-8.

169. Hawighorst, H., et al., *Macroscopic tumor volume of malignant glioma determined by contrast-enhanced magnetic resonance imaging with and without magnetization transfer contrast*. Magn Reson Imaging, 1996. **14**(10): p. 1119-26.

170. Beaumont, M., et al., *Characterization of tumor angiogenesis in rat brain using iron-based vessel size index MRI in combination with gadolinium-based dynamic contrast-enhanced MRI*. J Cereb Blood Flow Metab, 2009. **29**(10): p. 1714-26.

171. Roberts, H.C., et al., *Quantitative measurement of microvascular permeability in human brain tumors achieved using dynamic contrast-enhanced MR imaging: correlation with histologic grade*. AJNR Am J Neuroradiol, 2000. **21**(5): p. 891-9.

172. Blokland, J.A., et al., *Positron emission tomography: a technical introduction for clinicians*. Eur J Radiol, 2002. **44**(1): p. 70-5.

173. Kelloff, G.J., et al., *Progress and promise of FDG-PET imaging for cancer patient management and oncologic drug development*. Clin Cancer Res, 2005. **11**(8): p. 2785-808.

174. Luker, G.D. and K.E. Luker, *Optical imaging: current applications and future directions*. J Nucl Med, 2008. **49**(1): p. 1-4.

175. Hilderbrand, S.A. and R. Weissleder, *Near-infrared fluorescence: application to in vivo molecular imaging*. Curr Opin Chem Biol, 2010. **14**(1): p. 71-9.

176. Keyaerts, M., V. Caveliers, and T. Lahoutte, *Bioluminescence imaging: looking beyond the light*. Trends Mol Med, 2012. **18**(3): p. 164-72.

177. Weissleder, R., *A clearer vision for in vivo imaging*. Nat Biotechnol, 2001. **19**(4): p. 316-7.

178. Wilson, T. and J.W. Hastings, *Bioluminescence*. Annu Rev Cell Dev Biol, 1998. **14**: p. 197-230.

179. Rehemtulla, A., et al., *Rapid and quantitative assessment of cancer treatment response using in vivo bioluminescence imaging*. Neoplasia, 2000. **2**(6): p. 491-5.

180. Sato, A., B. Klaunberg, and R. Tolwani, *In vivo bioluminescence imaging*. Comp Med, 2004. **54**(6): p. 631-4.

181. Contag, C.H., et al., *Use of reporter genes for optical measurements of neoplastic disease in vivo*. Neoplasia, 2000. **2**(1-2): p. 41-52.

182. Badr, C.E. and B.A. Tannous, *Bioluminescence imaging: progress and applications*. Trends Biotechnol, 2011. **29**(12): p. 624-33.

183. Paroo, Z., et al., *Validating bioluminescence imaging as a high-throughput, quantitative modality for assessing tumor burden*. Mol Imaging, 2004. **3**(2): p. 117-24.

184. Moriyama, E.H., et al., *The influence of hypoxia on bioluminescence in luciferase-transfected gliosarcoma tumor cells in vitro*. Photochem Photobiol Sci, 2008. **7**(6): p. 675-80.

185. Shaner, N.C., P.A. Steinbach, and R.Y. Tsien, *A guide to choosing fluorescent proteins*. Nat Methods, 2005. **2**(12): p. 905-9.

186. Mullins, J.M., *Overview of fluorophores*. Methods Mol Biol, 1994. **34**: p. 107-16.

187. Cao, Y., et al., *Observation of incipient tumor angiogenesis that is independent of hypoxia and hypoxia inducible factor-1 activation*. Cancer Res, 2005. **65**(13): p. 5498-505.

188. Weissleder, R. and M.J. Pittet, *Imaging in the era of molecular oncology*. Nature, 2008. **452**(7187): p. 580-9.

189. Vakoc, B.J., et al., *Three-dimensional microscopy of the tumor microenvironment in vivo using optical frequency domain imaging.* Nat Med, 2009. **15**(10): p. 1219-23.

190. Lehmann, S., et al., *Longitudinal and multimodal in vivo imaging of tumor hypoxia and its downstream molecular events.* Proc Natl Acad Sci U S A, 2009. **106**(33): p. 14004-9.

191. Lo Dico, A., et al., *Validation of an engineered cell model for in vitro and in vivo HIF-1alpha evaluation by different imaging modalities.* Mol Imaging Biol, 2014. **16**(2): p. 210-23.

192. Sambrook, J. and D.W. Russell, *SDS-Polyacrylamide Gel Electrophoresis of Proteins.* CSH Protoc, 2006. **2006**(4).

193. Raleigh, J.A. and C.J. Koch, *Importance of thiols in the reductive binding of 2-nitroimidazoles to macromolecules.* Biochem Pharmacol, 1990. **40**(11): p. 2457-64.

194. Mayer, A., et al., *Lack of correlation between expression of HIF-1alpha protein and oxygenation status in identical tissue areas of squamous cell carcinomas of the uterine cervix.* Cancer Res, 2004. **64**(16): p. 5876-81.

195. Vordermark, D. and J.M. Brown, *Evaluation of hypoxia-inducible factor-1alpha (HIF-1alpha) as an intrinsic marker of tumor hypoxia in U87 MG human glioblastoma: in vitro and xenograft studies.* Int J Radiat Oncol Biol Phys, 2003. **56**(4): p. 1184-93.

196. Vordermark, D. and J.M. Brown, *Endogenous markers of tumor hypoxia predictors of clinical radiation resistance?* Strahlenther Onkol, 2003. **179**(12): p. 801-11.

197. Rademakers, S.E., et al., *Metabolic markers in relation to hypoxia; staining patterns and colocalization of pimonidazole, HIF-1alpha, CAIX, LDH-5, GLUT-1, MCT1 and MCT4.* BMC Cancer, 2011. **11**: p. 167.

198. Beasley, N.J., et al., *Carbonic anhydrase IX, an endogenous hypoxia marker, expression in head and neck squamous cell carcinoma and its relationship to hypoxia, necrosis, and microvessel density.* Cancer Res, 2001. **61**(13): p. 5262-7.

199. Brown, R.S. and R.L. Wahl, *Overexpression of Glut-1 glucose transporter in human breast cancer. An immunohistochemical study.* Cancer, 1993. **72**(10): p. 2979-85.

200. Gorin, F., et al., *Perinecrotic glioma proliferation and metabolic profile within an intracerebral tumor xenograft.* Acta Neuropathol, 2004. **107**(3): p. 235-44.

201. Tran, B. and M.A. Rosenthal, *Survival comparison between glioblastoma multiforme and other incurable cancers.* J Clin Neurosci, 2010. **17**(4): p. 417-21.

202. Kaur, B., et al., *Hypoxia and the hypoxia-inducible-factor pathway in glioma growth and angiogenesis.* Neuro Oncol, 2005. **7**(2): p. 134-53.

203. Yang, L., et al., *Hypoxia and hypoxia-inducible factors in glioblastoma multiforme progression and therapeutic implications.* Exp Cell Res, 2012. **318**(19): p. 2417-26.

204. Harada, H., et al., *The combination of hypoxia-response enhancers and an oxygen-dependent proteolytic motif enables real-time imaging of absolute HIF-1 activity in tumor xenografts.* Biochem Biophys Res Commun, 2007. **360**(4): p. 791-6.

205. Moroz, E., et al., *Real-time imaging of HIF-1alpha stabilization and degradation.* PLoS One, 2009. **4**(4): p. e5077.

206. Shibata, T., A.J. Giaccia, and J.M. Brown, *Development of a hypoxia-responsive vector for tumor-specific gene therapy.* Gene Ther, 2000. **7**(6): p. 493-8.

207. Viola, R.J., et al., *In vivo bioluminescence imaging monitoring of hypoxia-inducible factor 1alpha, a promoter that protects cells, in response to chemotherapy.* AJR Am J Roentgenol, 2008. **191**(6): p. 1779-84.

208. Cecic, I., et al., *Oxygen sensitivity of reporter genes: implications for preclinical imaging of tumor hypoxia.* Mol Imaging, 2007. **6**(4): p. 219-28.

209. Keyaerts, M., et al., *Dynamic bioluminescence imaging for quantitative tumour burden assessment using IV or IP administration of D: -luciferin: effect on intensity, time kinetics and repeatability of photon emission.* Eur J Nucl Med Mol Imaging, 2008. **35**(5): p. 999-1007.

210. Kim, T.K. and J.H. Eberwine, *Mammalian cell transfection: the present and the future.* Anal Bioanal Chem, 2010. **397**(8): p. 3173-8.

211. Luo, D. and W.M. Saltzman, *Synthetic DNA delivery systems.* Nat Biotechnol, 2000. **18**(1): p. 33-7.

212. Fomchenko, E.I. and E.C. Holland, *Mouse models of brain tumors and their applications in preclinical trials.* Clin Cancer Res, 2006. **12**(18): p. 5288-97.

213. Post, D.E., et al., *Cancer therapy with a replicating oncolytic adenovirus targeting the hypoxic microenvironment of tumors.* Clin Cancer Res, 2004. **10**(24): p. 8603-12.

214. Friese, M.A., et al., *RNA interference targeting transforming growth factor-beta enhances NKG2D-mediated antiglioma immune response, inhibits glioma cell migration and invasiveness, and abrogates tumorigenicity in vivo*. Cancer Res, 2004. **64**(20): p. 7596-603.

215. Kapitonov, D., et al., *Targeting sphingosine kinase 1 inhibits Akt signaling, induces apoptosis, and suppresses growth of human glioblastoma cells and xenografts*. Cancer Res, 2009. **69**(17): p. 6915-23.

216. Liu, W. and C. Shou, *Mycoplasma hyorhinis and Mycoplasma fermentans induce cell apoptosis and changes in gene expression profiles of 32D cells*. Biol Res, 2011. **44**(4): p. 383-91.

217. Takaku, H., et al., *Anti-tumor activity of arginine deiminase from Mycoplasma argini and its growth-inhibitory mechanism*. Jpn J Cancer Res, 1995. **86**(9): p. 840-6.

218. Barker, F.G., 2nd, et al., *Necrosis as a prognostic factor in glioblastoma multiforme*. Cancer, 1996. **77**(6): p. 1161-6.

219. Li, X.F., et al., *Visualization of hypoxia in microscopic tumors by immunofluorescent microscopy*. Cancer Res, 2007. **67**(16): p. 7646-53.

220. Chun, Y.S., M.S. Kim, and J.W. Park, *Oxygen-dependent and -independent regulation of HIF-1alpha*. J Korean Med Sci, 2002. **17**(5): p. 581-8.

221. Stroka, D.M., et al., *HIF-1 is expressed in normoxic tissue and displays an organ-specific regulation under systemic hypoxia*. Faseb J, 2001. **15**(13): p. 2445-53.

222. Cher, L.M., et al., *Correlation of hypoxic cell fraction and angiogenesis with glucose metabolic rate in gliomas using 18F-fluoromisonidazole, 18F-FDG PET, and immunohistochemical studies*. J Nucl Med, 2006. **47**(3): p. 410-8.

223. Friedman, H.S., S.C. Schold, Jr., and D.D. Bigner, *Chemotherapy of subcutaneous and intracranial human medulloblastoma xenografts in athymic nude mice*. Cancer Res, 1986. **46**(1): p. 224-8.

224. Groothuis, D.R., et al., *Permeability of different experimental brain tumor models to horseradish peroxidase*. J Neuropathol Exp Neurol, 1982. **41**(2): p. 164-85.

225. Blasberg, R., et al., *Regional measurements of [14C]misonidazole distribution and blood flow in subcutaneous RT-9 experimental tumors.* Cancer Res, 1985. **45**(4): p. 1692-701.

226. Hirota, K. and G.L. Semenza, *Regulation of angiogenesis by hypoxia-inducible factor 1.* Crit Rev Oncol Hematol, 2006. **59**(1): p. 15-26.

227. Vakoc, B.J., et al., *Cancer imaging by optical coherence tomography: preclinical progress and clinical potential.* Nat Rev Cancer, 2012. **12**(5): p. 363-8.

228. Chen, W., et al., *Imaging proliferation in brain tumors with 18F-FLT PET: comparison with 18F-FDG.* J Nucl Med, 2005. **46**(6): p. 945-52.

229. Wu, C., et al., *PET imaging of inflammation biomarkers.* Theranostics, 2013. **3**(7): p. 448-66.

230. Leung, A.H., et al., *Inflammation targeted gd(3+)-based MRI contrast agents imaging tumor and rheumatoid arthritis models.* Bioconjug Chem, 2014. **25**(6): p. 1112-23.

231. Kuil, J., T. Buckle, and F.W. van Leeuwen, *Imaging agents for the chemokine receptor 4 (CXCR4).* Chem Soc Rev, 2012. **41**(15): p. 5239-61.

232. Liu, Y., et al., *PET imaging of chemokine receptors in vascular injury-accelerated atherosclerosis.* J Nucl Med, 2013. **54**(7): p. 1135-41.

233. Weissleder, R., et al., *In vivo imaging of tumors with protease-activated near-infrared fluorescent probes.* Nat Biotechnol, 1999. **17**(4): p. 375-8.

234. Breyholz, H.J., et al., *A 18F-radiolabeled analogue of CGS 27023A as a potential agent for assessment of matrix-metalloproteinase activity in vivo.* Q J Nucl Med Mol Imaging, 2007. **51**(1): p. 24-32.

235. Gillies, R.J., D. Verduzco, and R.A. Gatenby, *Evolutionary dynamics of carcinogenesis and why targeted therapy does not work.* Nat Rev Cancer, 2012. **12**(7): p. 487-93.

236. Huang, L.E., et al., *Hypoxia-induced genetic instability--a calculated mechanism underlying tumor progression.* J Mol Med (Berl), 2007. **85**(2): p. 139-48.

237. Franovic, A., et al., *Translational up-regulation of the EGFR by tumor hypoxia provides a nonmutational explanation for its overexpression in human cancer.* Proc Natl Acad Sci U S A, 2007. **104**(32): p. 13092-7.

238. Stuker, F., et al., *Hybrid small animal imaging system combining magnetic resonance imaging with fluorescence tomography using single photon avalanche diode detectors*. IEEE Trans Med Imaging, 2011. **30**(6): p. 1265-73.

239. Maguire, C.A., et al., *Triple bioluminescence imaging for in vivo monitoring of cellular processes*. Mol Ther Nucleic Acids, 2013. **2**: p. e99.

240. Wendt, M.K., et al., *In vivo dual substrate bioluminescent imaging*. J Vis Exp, 2011(56).

241. Burton, N.C., et al., *Multispectral opto-acoustic tomography (MSOT) of the brain and glioblastoma characterization*. Neuroimage, 2013. **65**: p. 522-8.

242. Cuddapah, V.A., et al., *A neurocentric perspective on glioma invasion*. Nat Rev Neurosci, 2014. **15**(7): p. 455-65.

243. Giese, A., et al., *Dichotomy of astrocytoma migration and proliferation*. Int J Cancer, 1996. **67**(2): p. 275-82.

244. Price, S.J. and J.H. Gillard, *Imaging biomarkers of brain tumour margin and tumour invasion*. Br J Radiol, 2011. **84 Spec No 2**: p. S159-67.

245. Bao, B., et al., *In vivo imaging and quantification of carbonic anhydrase IX expression as an endogenous biomarker of tumor hypoxia*. PLoS One, 2012. **7**(11): p. e50860.

246. Jaakkola, P., et al., *Targeting of HIF-alpha to the von Hippel-Lindau ubiquitylation complex by O2-regulated prolyl hydroxylation*. Science., 2001. **292**(5516): p. 468-72.

247. Scholzen, T., and J. Gerdes, *The Ki-67 protein: from the known and unknown*. J Cell Physiol., 2000. **182**(3): p. 311-22.

248. Witz, I., *Tumor-Microenvironment interactions: dangerous liaisons*. Adv Cancer Res., 2008. **100**: p. 203-29.

6 Acknowledgment

I would like to thank:

My supervisor Prof. *Markus Rudin* who gave me the opportunity to do this thesis and supported me throughout this work.

My committee members Prof. *Wilhelm Krek* and Prof *Michael Weller* for their ideas and suggestions recording this work.

Ruth Keist for teaching me new methods and assisting in my experimental proceedings in stressful times.

Debora Häfeli for her patience and organization of the animal housing of my mice.

Dr. *Steven Proulx* for supporting me in the organizing of the IVIS measurements for my glioma experiments at the campus Hönggerberg.

Prof. *Burkhard Becher* and Prof. *Michael Detmar* giving me the opportunity to use their IVIS system for my experiments.

My PhD colleague *Aline Seuwen* for her time and assistance in MRI experiments and her help in the theoretical part of MRI.

Dr. *Johannes vom Berg* for teaching me the orthotopic surgery and transfecting an important cell line for me.

Dr. *Sandrine Joly* for helping me with software problems, ideas to overcome them and simplify time consuming processes, and for interesting discussions.

Markus Küpfer and *Stefan Weber* for helping me to solve technical problems for the procedure of my experimental problems.

Dr. *Roland Dürr* for his advices on statistical analysis and my PhD colleague *Joanes Grandjean* for performing an advanced statistical analysis for my manuscript.

The group of Prof. *Michael Weller* for providing me the glioma cell lines.

Prof. *Roland Wenger* who that gave me the opportunity to use their luminometer for testing my cells.

Michelle Meier for her assistance in improving the analysis procedure and for her effort in supporting me in my writing process.

My husband *Porfirio Montemayor* for his patience and assistance in discussing scientific matters and for the motivation he gave me to bring this thesis to an end.

And finally to *my parents* that supported me during my whole life and believed in me that I can make my dreams come true.